Semiconductor nonlinear optical waveguides

Lambkin, Paul Martin

Award date:
1990

Awarding institution:
University of Bath

Semiconductor Nonlinear Optical Waveguides

submitted by Paul Martin Lambkin
for the degree of PhD
of the University of Bath
July 1990

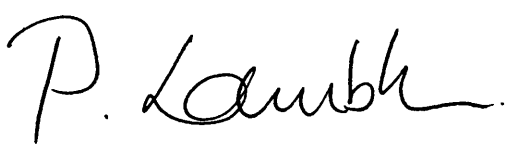

ProQuest LLC
789 East Eisenhower Parkway
P.O. Box 1346
Ann Arbor, MI 48106-1346

Summary

This thesis is an investigation of the properties of semiconductor, nonlinear, optical waveguides. The origin of nonlinearities in semiconductors is discussed and subsequent emphasis is given to the intensity dependent (Kerr-type) nonlinearity arising from band filling. Jacobi elliptic functions are introduced as the solution to the nonlinear wave equation governing electromagnetic propagation in media displaying such an intensity dependent nonlinearity. A detailed analysis of nonlinear guided waves in a planar structure is presented. This analysis is used to investigate two dimensional structures, for the first time, using a self consistent effective index approach. Finite nonlinear multilayer structures are examined with an emphasis on Bragg waveguiding configurations. These guides are shown to support nonlinear guided modes that have no linear counterpart. Finally, it is concluded that analytic solutions provide a straightforward and efficient method by which preliminary studies of nonlinear guided waves can be made.

To my mother and father

All persons in this book are real and none is fictitious even in part.

"Mollycules is a very intricate theorem and can be worked out with algebra but you would want to take it by degrees with rulers and cosines and familiar other instruments and then at the wind-up not believe what you had proved at all. If that happened you would have to go back over it till you got to a place where you believe your own facts and figures as exactly delineated from Hall and Knight's Algebra and then go on again from that particular place till you had the whole pancake properly believed and not have bits of it half-believed or a doubt in your head hurting you like when you lose a stud of your shirt in the middle of the bed.

- Very true, Mick decided to say."

Flan O'Brien, The Dalkey Archive.

Acknowledgements

I would like to express my sincere thanks to Dr. K. A. Shore for his excellent supervision throughout the course of this work - diolch!

Thanks also to Drs. Mike Adams, Dave Mace and Mike Fisher of BTRL for their help and advice.

I am very grateful for the help and good humour of the Bath University electronics group past and present. This includes John Kot, Martin McCall, Rob Norcross, Rob Noyes, Ian Middlemast, and Nigel Pennington. In particular, I thank Dr. J. Sarma for many helpful discussions that seldom failed to leave me with a sense of wonder, and thanks to Alice Bailey for helping with the layou$_t$ and speling. I feel that the computer officer, C. S. Chang, deserves special mention, not only for his inexaustable patience in the face of computing ignorance, but also for his creditable attempts to preserve South American rain forests.

I am indebted to Jane, my landlady, not only for feeding me on numerous occasions, but for letting me watch the World Cup on the colour telly. Finally, I should like to thank my family for all their support.

Contents

Chapter One

Nonlinear Semiconductor Optoelectronics

1.1 Introduction

In electronics a rich variety of phenomena, including rectification, modulation, harmonic generation, and heterodyning, arise from the nonlinear response of electronic processes. In the 1960's the invention of the laser also enabled nonlinear responses to be obtained from optical processes. Nonlinear optics is concerned with the phenomena, some of which have analogues in electronics, that can subsequently arise. In principle, devices based on optical nonlinearity would achieve large bandwidths as a result of the high operating frequencies. This feature has motivated a great deal of interest in all-optical devices especially in the tele-communications industry where optics is already well established.

1.2 Optical Nonlinearity

Optical nonlinearity is manifested by changes in the properties of a medium subject to optical illumination. The fact that intense electric and magnetic fields are capable of inducing optical changes in a medium has been known for some time. Faraday discovered that the plane of polarisation of a light beam propagating in glass can be rotated by an applied magnetic field. This is known as the Faraday effect. Kerr, in a complementary experiment, showed that by applying a strong electric field in glass, light undergoes double refraction. This is known as the Kerr effect. From these results it is reasonable to suppose that if the electric and magnetic fields of a light beam are sufficiently strong, the beam itself will optically alter its ambient medium which in turn will affect propagation of the light beam. Such beams only became available with development of the laser. The high degree of coherence of the laser not only allowed the focusing of light on to small areas, but also enabled the weak contributions of nonlinear interactions from widely separated parts of a medium to be combined to produce an appreciable resultant.

Two general categories of optical nonlinearity can be distinguished. *Intrinsic* nonlinear phenomena can be described as violations of the principle of superposition arising from the nonlinear response of individual atoms, molecules,

or unit cells to incident waves. In general, this involves the conversion of input photons at a given frequency to output photons of different frequency, generated during interactions with polarisable material. This accounts for such phenomena as second harmonic generation and sum and difference frequency generation. *Extrinsic* nonlinearity is a change of properties which is directly related to changes in composition of the medium resulting from the absorption or emission of light. Intensity dependent refractive index is an important phenomenon that falls into this latter category. There is now a formidable body of literature devoted to these categories. An excellent overview is provided in the proceedings of the International School of Materials Science and Technology (Flytzanis and Oudar, 1985) (Boardman, 1989).

1.3 Nonlinear Optical Waveguides

In order to maintain high intensities and make efficient use of any nonlinearities present, guided wave geometries are used to confine the optical beams. For example the coherent coupler (Jensen, 1982) relies on the intensity dependent coupling between adjacent guides sharing a nonlinear coupling region. A comprehensive review of nonlinear interactions in guided wave geometries is given by Stegeman and Seaton (1985). Guided propagation is also essential to integrated optics which is based on the concept of combining different components in a single device. In the the now well established area of optical communications, sources and detectors are implemented using the semiconductor materials gallium arsenide (GaAs) and indium phosphide (InP). Integration would obviously be made easier if other devices were also fabricated in the same material system. Nonlinearity in semiconductors and the waveguide geometries in which they might be employed are thus of great importance. It is to these areas of interest that this work is directed.

1.4 Structure of the Thesis

In chapter two the origins of nonlinearities in semiconductors are discussed along with the restrictions subsequently implied for device design. That chapter concludes with a description of a refractive index measurement experiment performed to assess the feasibility of directly measuring nonlinear changes in refractive index . Elliptic functions, and particularly Jacobi elliptic functions are introduced in chapter three. They are shown to be the solution of a second order nonlinear differential equation. This equation is subsequently derived in chapter four as the governing equation for electromagnetic propagation in media

displaying an intensity dependent refractive index. A detailed analysis of nonlinear guided waves in a planar structure is then presented and a connection made with previous work in this field. In chapter five a two dimensional structure is analysed for the first time using a self consistent effective index approach. Finite nonlinear multilayer structures are treated in chapter six with an emphasis on Bragg waveguiding configurations. Finally, in chapter seven some conclusions are drawn concerning the role of analytic solutions in the analysis of nonlinear guided waves.

1.5 References

A. D. Boardman and T. Twardowski, (editors), "Nonlinear Optics: Materials and Devices," Proceedings of the International School of Materials Science and Technology, Erice, Sicily, 1989, to be published.

C. Flytanis and J. L. Oudar, (editors), "Nonlinear Optics: Materials and Devices," Proceedings of the International School of Materials Science and Technology, Erice, Sicily, (1985).

S. M Jensen,"The nonlinear coherent coupler," IEEE J. Quantum. Electron., vol. QE-18, pp. 1580-1583, (1982).

G. I. Stegeman and C. T. Seaton,"Nonlinear integrated optics," J. Appl. Phys. vol. 58, pp. R57-R78, (1985).

Chapter Two

Semiconductor Optical Nonlinearities

2.1 Introduction

Optical nonlinearity in semiconductors has attracted considerable attention since the invention of lasers. The large nonlinear effects and compatibility with sources and detectors make integrated nonlinear optical devices a practical possibility. This has provided the motivation for what has become a large and sophisticated field of investigation. In this thesis emphasis is placed on the exploitation of nonlinear effects and so their origins are only given in outline. A more extensive explanation is given by Haug (1988) and Klingshirn (1990). This chapter thus gives a brief description of the origins of nonlinearities in semiconductors and indicates the extent to which they have been measured and employed in all-optical devices. The chapter concludes with details of a series of experiments undertaken to measure the complex refractive index of semiconductors.

2.2 The Electron Oscillator

When an electric field **E** is applied to dielectric medium the bound charges are displaced against restoring forces. This creates internal dipole moments adding to the electric flux density. The sum of the internal dipole moments induced per unit volume is termed the polarisation **P**. The total flux density is thus:

$$\mathbf{D} = \varepsilon_0 \mathbf{E} + \mathbf{P}, \tag{2.1}$$

where the polarisation is related to the applied field by:

$$\mathbf{P} = \chi \varepsilon_0 \mathbf{E}. \tag{2.2}$$

The total flux density then becomes:

$$\mathbf{D} = \varepsilon_0 (1 + \chi) \mathbf{E}. \tag{2.3}$$

The dimensionless ratio χ, known as the dielectric susceptibility, contains the essential optical properties of the material. It describes the various light / matter interactions and so its complexity determines to what degree these phenomena are

taken into account. Alternatively the relative permittivity can be defined as:

$$\varepsilon = (1 + \chi), \tag{2.4}$$

and the refractive index n as $\sqrt{\varepsilon}$.

An important optical characteristic is the frequency dependence, or dispersion, of the relative permittivity. Dispersive effects are greatest at certain frequencies resonant with atomic transitions. When the frequency ω of the applied field is tuned close to that of a transition, the atoms acquire large dipole moments that oscillate at ω. The total field is then the sum of the incident wave and the field radiated by the dipoles. Since the radiated field is not in phase with the incident one, the effect is to change the phase velocity of the incident wave, or equivalently, to change the real part of the permittivity.

The calculation of the dipole moments of an atom can be treated within a sophisticated quantum mechanical formalism. More simply, an electron oscillating in a harmonic potential well can be used to empirically model the dipole moment. If the potential well is anharmonic the permittivity becomes field dependent and the medium exhibits intrinsic nonlinearity. Such a nonlinear optical response gives rise to numerous interesting phenomena (Stegeman, 1985) including second harmonic generation and Raman scattering.

2.3 Defocusing Nonlinearity in Semiconductors

Up to now it has been assumed that an optical system reacts instantaneously to the amplitudes of the incident electromagnetic fields. In extrinsic nonlinear processes the incident light generates species, such as excitons, electron-hole pairs, or phonons, that have finite lifetimes. The susceptibility will thus depend on their density at any given time . Since these excited particles usually undergo scattering during their lifetime, extrinsic processes are incoherent.

State or band filling is an example of such a process. The effect relies on Pauli's exclusion principle which states that no two electrons in a crystal can be placed in the same quantum state. If an electron undergoes a given transition it blocks others from making the same transition. When a semiconductor is irradiated by an optical field close in frequency to that of the band gap, excited carriers fill the bands and reduce the number of initial and final states available for absorption. When the band is filled from the bottom up to the energy of excitation, the material becomes virtually transparent so that the absorption is fully saturated.

This negative change in the absorption affects the refractive index through the Kramers-Kronig relations:

$$\Delta n(E) = \frac{E}{\pi} \int_0^\infty \frac{\Delta\alpha(E')}{(E')^2 - (E)^2} dE', \tag{2.5}$$

where E is the energy of the incident field and α is the absorption coefficient. As the bands fill, the interactions with the incident radiation become fewer and the effect is to reduce the refractive index as the local field intensity I increases. The negative change in refractive index means the nonlinearity is termed *defocusing*. The studies undertaken in this work are concerned with such defocusing nonlinearity. This is in contrast to much of the previous work on nonlinear guiding that has concentrated on the lithium niobate material system.

An early study of band gap resonant nonlinearity by Miller (1981) measured $n_I \equiv \frac{dn}{dI}$, the nonlinear refraction coefficient, as $-1.10^{-3} cm^2/W$ for InSb at 77K. Measurements on GaAs / GaAlAs multiple quantum wells (MQW's) (Miller, 1982) at room temperature showed the resonant effect to be very high; $n_I \approx -2.10^{-5} cm^2/W$, and lead to heightened interest in bulk semiconductors and MQW's as promising passive optical materials.

2.4 Modelling the Nonlinearity

The optical properties of laser excited semiconductors are determined by the interactions between electron-hole pairs. Whilst the phenomenon can be accurately modelled by a quantum mechanical Greens function formalism, such a procedure is numerically intensive. Banyai and Koch (1986) developed a less sophisticated, partly phenomenological, description which was shown to be in good agreement with experimental data. In Figure 2.1(a-d) a comparison between theory and experiment, reproduced from Lee (1986), is given which clearly illustrates the relationship between intensity and absorption and the extent to which it has been successfully modeled. The top curve in Figure 2.1(a) is the low intensity absorption spectrum for bulk GaAs at room temperature whilst the subsequent curves show the spectra for increasing intensity. The resulting changes in refractive index, calculated using the Kramers-Kronig transformation, are given in Figure 2.1(b). Corresponding spectra calculated from the Banyai and Koch

plasma theory are given in Figure 2.1(e) and Figure 2.1(d).

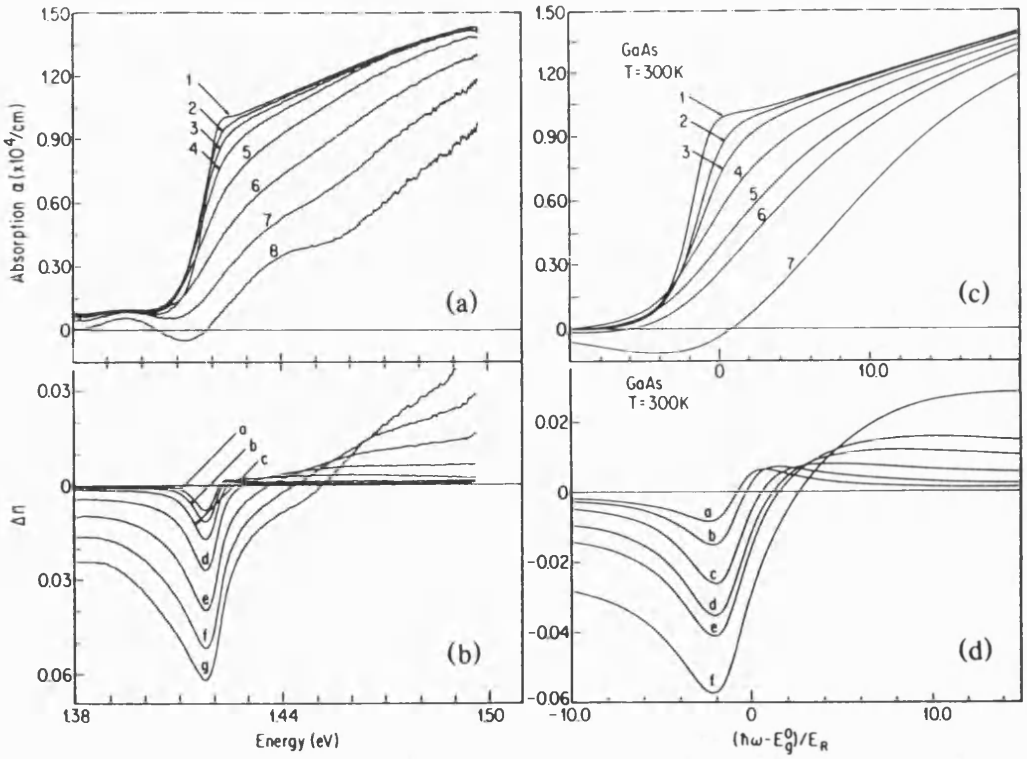

Figure 2.1 Room temperature bulk GaAs optical nonlinearities: experiment and theory. (a) Experimental absorption spectra for different excitation powers P: (1) 0, (2) 0.2, (3) 0.5, (4) 1.3, (5) 3.2, (6) 8, (7) 20, (8) 50 mW on a 15 μm diameter spot. (b) Nonlinear refractive index changes corresponding to the measured absorption spectra. Curves a - g are obtained by the Kramers-Kronig transformation of the corresponding experimental data (2) - (8) in (a). (c) Calculated absorption spectra for different electron-hole pair densities N: (1) 10^{15}, (2) 8×10^{16}, (3) 2×10^{17}, (4) 5×10^{17}, (6) 10^{18}, (7) 1.5×10^{18} cm^{-3}. $E_g^0 = 1.420\,eV$ and $E_R = 4.2\,meV$. (d) Calculated nonlinear refractive index changes. Curves a - f are obtained from curves (2) - (7) in (c), respectively.

2.5 A Simple Band Filling Model

A simpler model than that of the previous section can be derived using a rate equation approach. Simplicity is achieved by relying on fitting free parameters. The density of electron-hole pairs N is governed by the following equation:

$$\frac{\partial N}{\partial t} = -\frac{N}{\tau} + \frac{\alpha(\omega,N)}{E} I. \qquad (2.6)$$

Here τ is the recombination time and E is the energy associated with the incident

light. Assuming steady state gives:

$$\frac{N}{\tau} = \frac{\alpha(\omega,N)}{E} I. \tag{2.7}$$

If the relationship between carrier density and absorption is assumed to be linear then it follows that the change in absorption can be written as:

$$\alpha = \alpha_0 + \sigma_{eh} N \tag{2.8}$$

Similarly the change in refractive index Δn is given as:

$$n = n_0 + \eta_{eh} N. \tag{2.9}$$

Using Eq. 2.8 in Eq. 2.7 gives:

$$\alpha = \frac{\alpha_0}{1 - I\frac{\tau\sigma_{eh}}{E}}, \tag{2.10}$$

where α_0 is the low intensity absorption coefficient. Defining a saturation intensity I_s gives:

$$\alpha = \frac{\alpha_0}{1 + \frac{I}{I_s}} \quad \text{where} \quad I_s = -\frac{E}{\sigma_{eh}\tau}. \tag{2.11}$$

Miller (1982) showed that this expression accurately described the variation of α with intensity for GaAs / GaAlAs MQW's. The variations were later successfully reproduced using the Banyai and Koch theory (1986). The change in refractive index can then be expressed as:

$$\Delta n = \frac{I\,\Delta n_{max}}{I_s(1 + \frac{I}{I_s})}, \tag{2.12}$$

where

$$\Delta n_{max} = -\frac{\alpha_0 \eta_{eh}}{\sigma_{eh}}. \tag{2.13}$$

This rate equation approach to band filling is thus completely characterised by the parameters Δn_{max} and I_s and has been used to duplicate measurements made on a GaInAs / InP MQW (Fisher 1989). A further simplification is to make a linear approximation to the variation of Δn with intensity. Thus a straight line,

coincident with the saturation curve at zero intensity and at the saturation intensity, is used to replace Eq. 2.12 and is written as:

$$\Delta n(I_s) = \frac{\Delta n_{max}}{2} = n_I I_s. \tag{2.14}$$

Finally the change in refractive index with intensity is given by:

$$n = n_0 + n_I I \tag{2.15}$$

where $n_I = \frac{\Delta n_{max}}{2I_s}$ and n_0 is the low intensity, linear refractive index. This form of nonlinearity is said to be *Kerr-like* and has the considerable merit of permitting analytical solutions to the wave equation to be obtained.

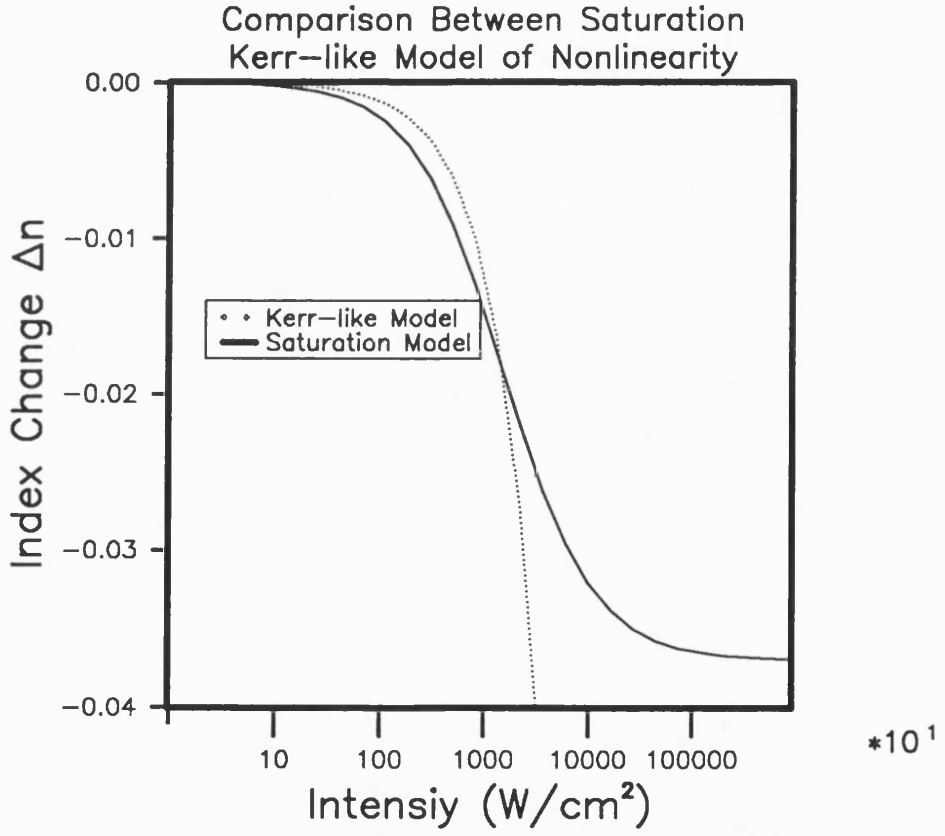

Figure 2.2 The Kerr-like and saturation models of band-filling nonlinearity.

A comparison between the saturation and Kerr-like models for the change in refractive index is given in Figure 2.2 using a logarithmic scale for the intensity. The saturation curve is taken from (Fisher, 1990) where it was used to fit data obtained from experiments on a GaInAs / InP MQW. The linear approximation is coincident at the saturation intensity beyond which the model becomes invalid.

Eq. 2.15 is thus a simple constitutive relation describing the optical response of a semiconductor when it is excited by radiation close to that of the band gap. It is clear from Figure 2.2 that this representation of the band filling nonlinearity has obvious limitations, but in the right circumstances still provides a valid characterisation of the nonlinearity and obviates the need for an intensive numerical approach. This will be demonstrated in the next chapter.

2.6 Nonlinear Optical Waveguides

The utilisation of nonlinear effects in semiconductor waveguide geometries is of great interest. To date the waveguide devices that have received the greatest attention are nonlinear directional couplers (Jensen 1982). The linear coupler simply consists of two adjacent guides. The power propagating in the composite structure oscillates between the individual guides over the coupling length. This is a result of beating between the modes of the coupler. If a nonlinearity is present then the coupling length will become intensity dependent allowing control over the proportion of power carried by each branch at a given length. However, in a waveguiding structure the absorption α must be less than about $100cm^{-1}$ and as can be seen from Figure 2.2(a) the absorption associated with the band edge itself is of the order of $10^4 cm^{-1}$. Li Kam Wa (1985) pointed out that by operating off resonance an appreciable nonlinear response can be utilised without debilitating operating losses. Detuning by $30nm$ gave $n_I \approx -10^{-7} cm^2/W$ and $\alpha \approx 15\, cm^{-1}$ enabling partial switching due to variation of intensity to be observed between the coupled waveguides. A similar approach has lead to the observation of bi-stability and nonlinear coupling between modes in passive GaAs / GaAlAs MQW waveguides (Li Kam Wa and Robson, 1987) (Li Kam Wa, 1988).

An alternative to detuning is to place the nonlinearity in a less sensitive part of the guide. Cada (1986) adopted this idea in a nonlinear vertical coupler. Here the nonlinearity was restricted to the medium between lossless guides. In this structure most of the energy is confined to the lossless regions and so advantage could be taken of on-resonant effects in the absorbing coupling medium. The principle was successfully demonstrated both by Cada (1988) and Berger(1988). However, different regions of a bulk semiconductor guide cannot be arbitrarily designated as nonlinear. Light is usually guided in the semiconductor medium of highest index which normally means the medium of lowest band gap. When the guide is excited by light of energy slightly below this gap (to obtain the nonlinear effect with small absorption) lower index regions will be non-absorptive and

hence linear. To move to shorter wavelengths would be to risk crippling pandemic absorption.

Finally, it is noted that the band edge nonlinearity can be enhanced by prolonging the carrier lifetime. This can be achieved in n-i-p-i structures by spatially separating the electrons and holes (Kobayashi, 1988). Very large nonlinearities can be induced with $n_I \approx 0.05 cm^2/W$ giving lifetimes typically of the order of a *ms* (Kost, 1988).

2.7 Measurement of Refractive Index Nonlinearity

2.7.1 Techniques

Measurements of the nonlinear response of semiconductor materials have predominantly been undertaken using transmission experiments. This normally involves a pump and probe arrangement to obtain a series of transmission spectra in the region of the band edge for various pump intensities. The change in absorption can then be related to the change in refractive index by the Kramers Kronig relationship Eq. 2.5 . This was the approach adopted by Miller and Chemla (1982). Even more indirect routes are possible such as four wave mixing experiments (Miller, 1983) and the Mach Zehnder interferometer arrangement used by Li Kam Wa (1985).

Whilst the transmission experiments furnish relative changes in refractive index via absorption measurements, it would be useful to make direct measurements of the complex refractive index itself. A technique that might accomplish this and that has experienced a renaissance with the advent of the personal computer is *ellipsometry.* The next section describes a number of experiments using ellipsometry to measure the refractive index of some semiconductor substrates. These were performed at the British Telecom Research Laboratories in part fulfillment of the requirements of a SERC CASE award. These preliminary measurements were made to assess the technique as a suitable method for measuring nonlinear refractive indices.

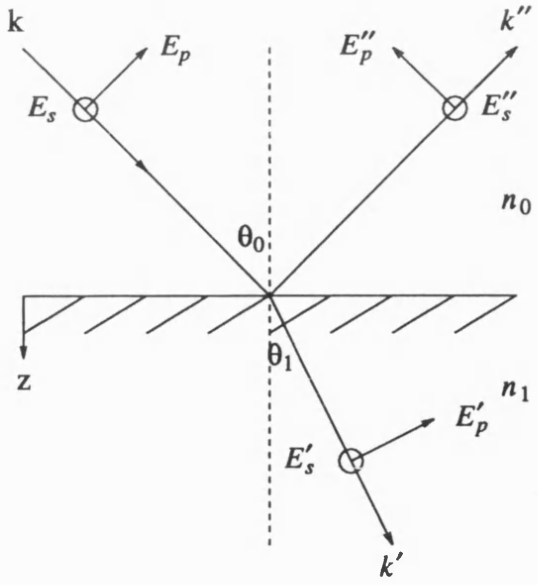

Figure 2.3 Plane wave reflection at a smooth boundary.

2.7.2 Ellipsometry

The complex Fresnel amplitude reflection coefficients for a single interface are defined according to Figure 2.3 as:

$$r_s \equiv \frac{|E_s''|}{|E_s|} \quad \text{and} \quad r_p \equiv \frac{|E_p''|}{|E_p|}. \tag{2.16}$$

The plane wave is decomposed into the s - component of polarisation, in which the plane of vibration of the E vector is perpendicular to the plane of incidence (ie, the plane of the paper), and the p - component, where the vibration is parallel to the plane of incidence. The complex reflectance ratio given by:

$$\rho = \frac{r_p}{r_s}, \tag{2.17}$$

then characterises the interface with respect to an incident plane wave. Ellipsometry seeks to measure ρ, from which the complex dielectric function can be calculated, by comparing the polarisation state of the reflected wave with the known polarisation state of an incident wave.

2.7.3 Measurement Configuration

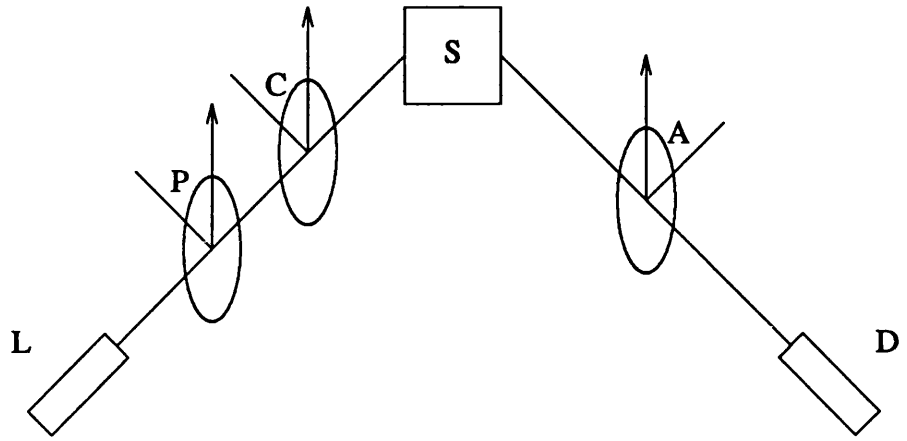

Figure 2.4 A rotating-analyser ellipsometer (RAE) consisting of a light source L, polariser P, compensator C, system S, rotating analyser A, and detector D.

The system utilised in this work is the standard Polariser, Compensator, Sample, Analyser (PCSA) ellipsometer, which falls into the class of rotating analyser ellipsometers (RAE's). The setup is shown in Figure 2.4 . Without the use of the compensator it is not possible to measure thin film or complex refractive indices by means of an RAE. The azimuth angles of the polariser, compensator fast axis, and analyser, are P, C, and A respectively and are measured clockwise from the plane of incidence. The phase retardation of the compensator is δ_c . If the elements P and C are set and the analyser is rotated about the beam axis at a constant angular velocity, then the detected signal I has the form (Aspnes, 1974) :

$$I = I_{av} + I_c \cos(2A) + I_s \sin(2A), \tag{2.18}$$

where I_{av} is the average flux incident at the detector. The experimentally determined quantities in an RAE system are the relative amplitudes:

$$\alpha = \frac{I_c}{I_{av}} \quad \text{and} \quad \beta = \frac{I_s}{I_{av}}. \tag{2.19}$$

Here, I_{av}, I_c, and I_s are determined from N sample values $I_v (v = 1, 2, 3, ..., N)$ of the incident flux taken at equal intervals over one cycle of the sinusoidal component according to the following expressions:

$$I_{av} = \frac{1}{N}\sum_{v=1}^{N} I_v, \tag{2.20}$$

$$I_c = \frac{2}{N}\sum_{v=1}^{N} I_v \cos(\theta_v), \tag{2.21}$$

$$I_s = \frac{2}{N}\sum_{v=1}^{N} I_v \sin(\theta_v), \tag{2.22}$$

where

$$\theta_v = 2\pi\frac{(v-1)}{N}. \tag{2.23}$$

The complex reflectance ratio is then given by (Azzam and Bashara, 1977) :

$$\rho = \tan\psi e^{i\Delta} = \frac{1+\alpha}{[\beta \pm i(1-\alpha^2-\beta^2)^{\frac{1}{2}}]} \times \frac{\tan C + \rho_c \tan(P-C)}{1-\rho_c \tan C \tan(P-C)}, \tag{2.24}$$

where

$$\rho_c = e^{i\delta_c}. \tag{2.25}$$

The complex reflectance and the complex dielectric constant $\varepsilon = \varepsilon_1 + i\varepsilon_2$ of a uniform, isotropic, reflecting surface in contact with an ambient medium whose dielectric constant is ε_a are related by (Aspnes, 1974) :

$$\frac{\varepsilon}{\varepsilon_a} = [(1-\rho)/(1+\rho)]^2 \sin^2\phi_i \tan^2\phi_i + \sin^2\phi_i, \tag{2.26}$$

where ϕ_i is the angle of incidence. For real samples the above two-phase model (ambient and substrate) is not realistic, but it is useful to assume perfection and use the measured ρ to derive a "pseudodielectric function" $\langle\varepsilon\rangle$ using Eqs. 2.24,and 2.26 . The pseudodielectric function thus represents an average of the dielectric responses of the substrates and any overlayers (oxide layers etc.). In the experiments the compensator angle C was set to zero enabling the relative amplitude and phase shift of the p and s components of the incident flux to be determined independently by P and δ_c respectively.

Aspnes (1974) has derived the conditions for which measurements are of maximum precision. The optimum value of δ_c satisfies:

$$\cos(\Delta - \delta_c) = 0, \tag{2.27}$$

and so results in the $\sin(2A)$ component in the detected flux vanishing. In this preliminary study transparent materials were first considered for which $\Delta = 0$, giving an optimum retardation $\delta_c = 90^o$. The compensator was therefore adjusted to this value. Aspnes (1974) also showed that the optimum polariser angle P_{opt} will occur for:

$$P_{opt} = \psi \tag{2.28}$$

When this condition is met the $\cos(2A)$ component in the detected flux will also vanish. The highest precision measurements are therefore made when circularly polarised light is incident on the detector which produces a constant output signal. It is possible to iterate towards the optimum conditions by resetting the polariser angle to a value based on a previously measured value of ψ. This scheme was adopted here in order to approach the situation where $\alpha = \beta = 0$.

2.7.4 Results

Using a semiconductor laser source operating at $1.582\ \mu m$ and an automated data logging system, refractive index measurements were made on three different samples:

S_1	Si	Doped substrate, roughened back surface,
S_2	InP	Doped substrate, roughened back surface,
S_3	InP	Undoped substrate, etched back surface,

with $C = 0$, $\delta_c = 90^o$ and $\phi = 57.4^o$. Results are summarised in Tables 2.1, 2.2 and 2.3 where n and k refer to the real and imaginary parts of the refractive index respectively. An example trace corresponding to experiment S.2.2 is given in Figure 2.5. Superimposed on the data is the Fourier fit associated with Eqs. 2.20 - 2.23.

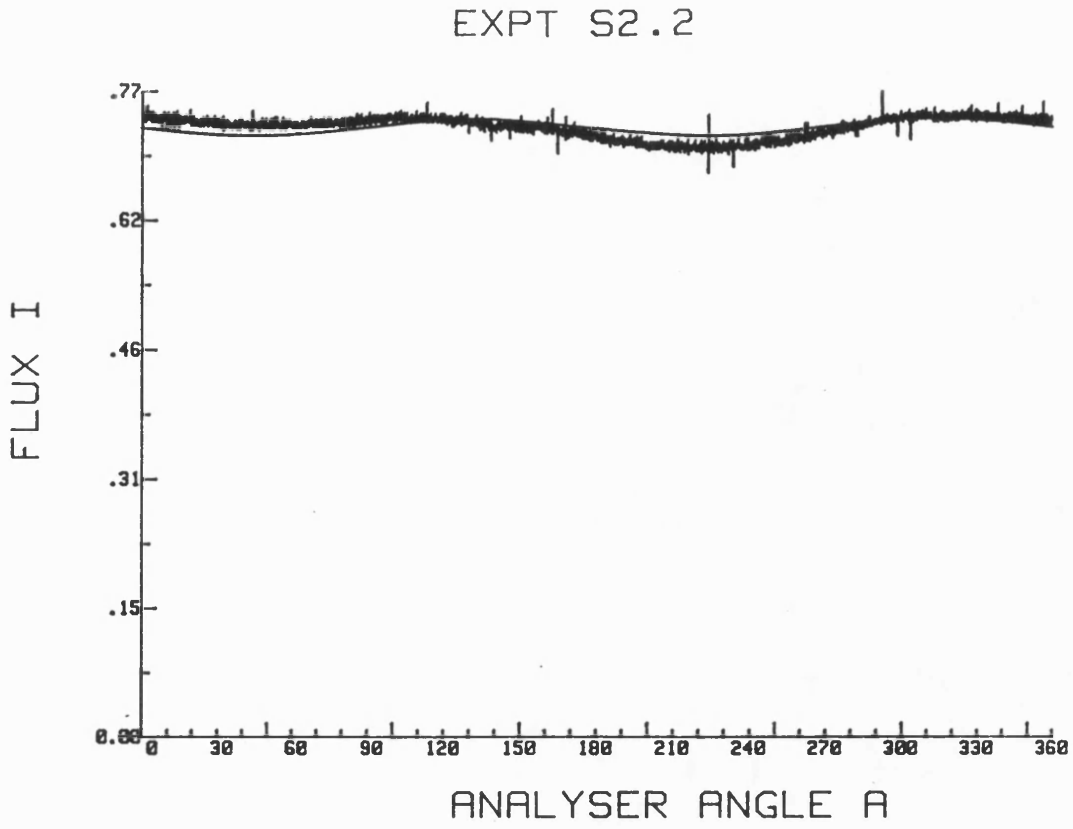

Figure 2.5 Detected signal for experiment S.2.2 .

Sample S_1 Silicon				
Experiment	P^o	n	k	P^o_{opt}
S1.1	24.17	3.515	-0.072	23.90
S1.2	23.90	3.516	-0.070	23.91
S1.3	23.91	3.514	-0.068	23.89

TABLE 2.1

Sample S_2 Indium Phosphide (doped)				
Experiment	P^o	n	k	P^o_{opt}
S2.1	21.26	3.173	-0.044	21.71
S2.2	21.71	3.171	-0.040	21.69

TABLE 2.2

Sample S_3 Indium Phosphide (undoped)				
Experiment	P^o	n	k	P^o_{opt}
S3.1	21.71	3.229	-0.101	22.21
S3.2	21.12	3.224	-0.098	22.09
S3.3	22.09	3.225	-0.100	22.02

TABLE 2.3

The ellipsometric values can be compared to those taken from Willardson and Beer (1967).

Silicon		
Wavelength μm	n	k
1.532	3.4784	-
1.6	3.4710	-

Indium Phosphide		
Wavelength μm	n	k
1.500	3.172	-
1.549	3.167	-
1.600	3.161	-
1.653	3.156	-

2.7.5 Accuracy

The degree to which the pseudodielectric function $\langle\varepsilon\rangle$ represents ε will obviously depend on the extent to which the ideal two-phase model accurately describes the sample configuration. Semiconductor substrates exposed to atmosphere will form oxide overlayers and hence alter the dielectric function. For example, the rate of film growth during the atmospheric oxidation of Si after a HF rinse has been measured (Azzam and Bashara, 1977) as 6.86Å/ decade of time in seconds. A more complicated three-phase model (substrate - overlayer - ambient) can be used in this situation corresponding to Figure 2.6, but requires additional measurements to determine the extra parameters. At around $1.5\mu m$ the overlayers are nominally transparent oxides. This means that only the thickness and ordinary refractive index of the overlayer need be determined. If the substrate is also transparent then ψ and Δ become independent with ψ being only a function of ε_1. Thus ε_1 can be obtained directly with no interference from the overlayer. Even with these simplifications more effort is required to obtain ε_2.

The most direct approach is to measure the film thickness d independently. Alternatively, measurements can be made at different angles of incidence. If, as in Figure 2.6, an 20Å silicon oxide layer is assumed to be present, then the complex refractive index can be calculated as :

$$n = 3.470,\ k = -0.046\,.$$

This does not compare favourably with the result from experiment S1.3 which gave:

$$n = 3.514,\ k = -0.068\,.$$

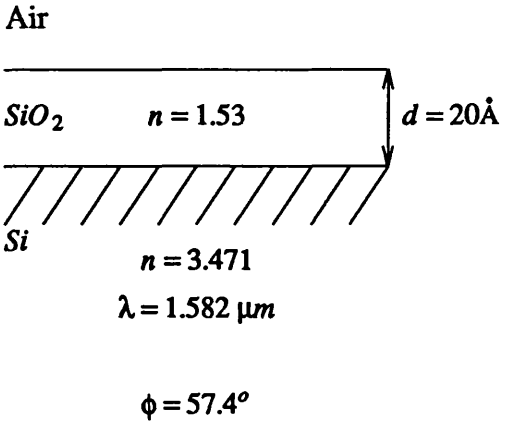

Figure 2.6 A three-phase system.

Some indication of the sensitivity to the errors in the azimuth angles can be given by recalculating the dielectric function assuming a 1^o error in retardation δ_c and a 0.3^o error in the fast axis angle C. This gives the following result:

$$n = 3.461,\ k = -0.093\,.$$

Whilst azimuth errors cannot wholly account for the inaccuracies of S1.3, they could make a significant contribution. The lack of symmetry in the flux trace will also lead to inaccuracies and is indicative of poor alignment or poor quality polarisers.

It has thus been demonstrated that the absolute measurement of the refractive index of a semiconductor at optical wavelengths is not straightforward. As it stands, the experiment requires considerable improvement to obtain accurate results. In an effort to establish whether relative changes could be reliably detected, a number of measurements were repeated with and without re-mounting the sample. Example results are given below in Tables 2.4 and 2.5:

Sample S_2 Indium Phosphide (doped)				
Experiment	Comment	P^o	n	k
S2.2	First measurement	21.71	3.171	-0.040
S2.2.1	Repeat, sample not moved	21.71	3.170	-0.038
S2.2.2	Repeat, sample remounted	21.71	3.171	-0.039

TABLE 2.4

Sample S_3 Indium Phosphide (undoped)				
Experiment	Comment	P^o	n	k
S3.3	First measurement	22.09	3.225	-0.100
S3.3.1	Repeat, sample remounted	22.09	3.216	-0.080

TABLE 2.5

These show that results are reproducible to within ~ 0.02 when a sample has been moved, with an order of magnitude improvement if the sample is undisturbed. The difference in result for the doped and undoped InP samples is most likely a function of their back surfaces. The doping levels involved would not produce a change in dielectric function detectable by this experiment.

2.7.6 Conclusions

It has been established that accurate refractive index measurements were unobtainable with the experimental arrangement used. However, results were reproducible on a run-to-run basis making the detection of relative changes a possibility. Whether band filling induced index changes are resolvable by the present system can be determined by considering transmission measurements made on a GaInAs / InP MQW (Fisher, 1990). Here the maximum change in absorption was $\sim 4000 cm^{-1}$ which corresponds, via the Kramers-Kronig relations, to a change in the real part of the refractive index of ~ 0.04. The change in the imaginary part can then be approximated by using:

$$\frac{\alpha}{2} = \frac{2\pi}{\lambda} k, \tag{2.29}$$

which gives $(\Delta k)_{max} \sim 0.05$. This is indeed resolvable provided the sample is not disturbed between measurements. Despite ellipsometry being, in general, a powerful technique, transmission experiments would seem to provide a quicker and simpler method for measuring nonlinear intensity dependent refractive indices.

2.8 References

D. E. Aspnes, "Optimizing precision of rotating-analyzer ellipsometers," J. Opt. Soc. Am., vol. 64, pp. 639-646, (1974).

L. Banyai and S. W. Koch, "A simple theory for the effects of plasma screening on the optical spectra of highly excited semiconductors," Z. Phys. B, vol. 63, pp. 283-291, (1986).

R. M. A. Azzam and N. M. Bashara, "Ellipsometry and polarized light," North-Holland publishing company, pp. 257-268, (1977).

P. R. Berger, Yi Chen, P. Bhattacharya and J. Pamulapati, "Demonstration of all optical modulation in a vertical guided-wave nonlinear coupler, " Appl. Phys. Lett., vol. 52, pp. 1125-1127, (1988).

M. Cada, R. C. Gauthier, B. E. Paton, J. Chrowstowski, "Nonlinear guided waves coupled nonlinearly in a planar GaAs/GaAlAs multiple quantum well structure," Appl. Phys. Lett., vol. 49, pp. 755-757, (1986).

M. Cada, B. P. Keyworth, J. M. Glinski, A. J. Springthorpe, and P. Mandeville, "Experiment with multiple-quantum-well waveguide switching element," J. Opt. Soc. Am. B, vol. 5, pp. 462-466, (1988).

M. A. Fisher, "Measurements of the nonlinear refractive index of a GaAlAs/InP multiple quantum well,"J. Appl. Phys. vol. 67, pp. 543-545, (1990).

H. Haug, " *Optical nonlinearities and instabilities in semiconductors,*" Academic Press, (1988).

C. Klingshirn, "Non-linear optical properties of semiconductors," Semicond. Sci. Technol., vol. 5, pp. 457-469, (1990).

A. Kost, E. Garmire, A. Danner and P. D. Dapkus, "Large optical nonlinearities in a GaAs/AlGaAs hetero n-i-p-i structure, " Appl. Phys. Lett., vol. 52, pp. 637-639, (1988).

H. Kobayashi, Y. Yamanchi and H. Ando, "Nonlinear optical absorption in an n-InGaAsP/p-InP heterodoping superlattice, " Appl. Phy. Lett., vol. 52, pp. 359-361, (1988).

Y. H. Lee, A. Chavez-Pirson, S. W. Koch, H. M. Gibbs, S. H. Park, J. Morhange, A. Jeffery, N. Peyghambarian, L. Banyai, A. C. Gossard, and W. Wiegmann, "Room-temperature optical nonlinearities in GaAs," Phys. Rev. Lett., vol. 57, pp. 2446-2449, (1986).

P. Li Kam Wa, J. E. Sitch, N. J. Mason, J. S. Roberts, P. N. Robson, "All optical multiple quantum well waveguide switch," Electron. Lett., vol. 21, pp. 26-27, (1985).

P. Li Kam Wa and P. N. Robson, "Optical nonlinearities in a passive GaAs/GaAlAs multiple quantum well strain-induced waveguide," IEEE J. Quantum Electron., vol. QE-23, (1987).

P. Li Kam Wa, P. N. Roberts, J. S. Roberts, M. A. Pate, and J. P. R. David, "All optical switching between modes of a GaAs/GaAlAs multiple quantum well waveguide," Appl. Phys. Lett., vol. 52, pp. 2013-2014, (1988).

D. A. B. Miller, C. T. Seaton, M. E. Price, and S.D. Smith, "Band-gap resonant nonlinear refraction in III-V semiconductors," Phys. Rev. Lett., vol. 47, pp. 197-200, (1981).

D. A. B. Miller, D. S. Chemla, D. J. Eilenberger, and P. W. Smith, A. C. Gossard, and W. T. Tsang, "Large room-temperature optical nonlinearity in GaAs/ $Ga_{1-x}Al_xAs$ multiple quantum well structures," Appl. Phys. Lett., vol. 41, pp. 676-681, (1982).

D. A. B. Miller, D. S. Chemla, D. J. Eilenberger, P. W. Smith, A. C. Gossard and W. Wiegmann, " Degenerate four-wave mixing in GaAs / GaAlAs multiple quantum well structures," Appl. Phys. Lett., vol. 42, pp. 925-927, (1983).

G. I. Stegeman, C. T. Seaton, W. Hetherington, A. D. Boardman, and P. Egan, "Nonlinear guided waves," Proceedings of the international school of material science and technology, Erice, Sicily, July 1-14, 1985, pp. 31-64.

R. K. Willardson, A. C. Beer, (editors), " *Semiconductors and Semimetals, volume 3, optical properties of III-V compounds* ," Academic press, (1967).

Chapter Three

Elliptic Jacobi Functions

3.1 Introduction

One cannot proceed very far in the theory of nonlinear differential equations before encountering solutions expressed in terms of elliptic integrals or elliptic functions. In chapter four a nonlinear differential equation will be derived that governs electromagnetic propagation in a medium characterised by a Kerr-like nonlinearity. Jacobi functions are solutions to this nonlinear differential equation. They are the natural generalisations of the inverse circular and direct circular functions and are so called because they arose as a special example in the rectification of the arc of an ellipse. Since elliptic functions, and more particularly Jacobi functions, are relatively unfamiliar it is considered worthwhile to outline some of their properties here. The elliptic functions of Jacobi are derived in terms of theta functions which provide a method for their numerical evaluation. An alternative scheme of evaluation suitable for a purely real analysis is also outlined. Finally, the nonlinear differential equation whose solution is in terms of Jacobi functions is derived.

3.2 Doubly Periodic Functions and Elliptic Functions

Suppose that the function $f(z)$, where z is in general complex, has two distinct periods $2\omega_1$ and $2\omega_2$ so that:

$$f(z+2\omega_1)=f(z) \tag{3.1}$$

$$f(z+2\omega_2)=f(z) \tag{3.2}$$

Further, let the periods have a complex ratio $\frac{\omega_1}{\omega_2}$ so that there exists a network of period parallelograms, or meshes, as shown in Figure 3.1. The period parallelograms are called *fundamental* if they are the smallest such meshes for the function $f(z)$. The values of $f(z)$ in any parallelogram P are repeated in each of the other parallelograms as indicated by Eqs. 3.1 and 3.2 . Doubly periodic functions are a natural extension of the simply periodic trigonometric functions of

elementary mathematics. If a doubly periodic analytic function $f(z)$ has, in the finite plane, no singular points other than poles, then $f(z)$ is called an *elliptic* function.

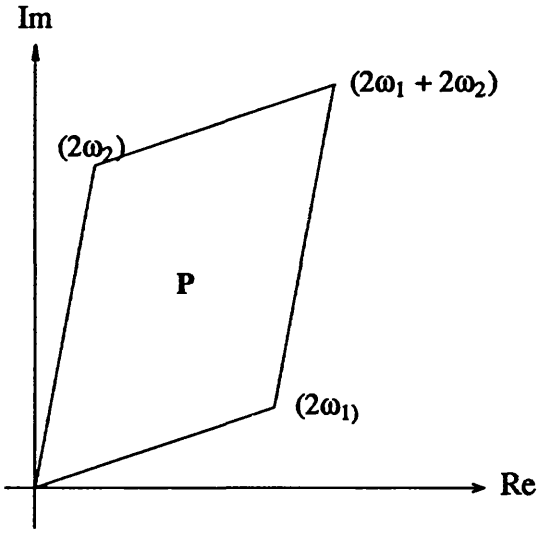

Figure 3.1 The Period Parallelogram

3.3 Theta Functions

Theta functions were first developed systematically by C. G. J. Jacobi in his treatise *Fundamenta nova theori functionum ellipticarum 1829*. Four principal theta functions have been recognised and are defined by means of the following (Rainville, 1960) :

$$\theta_1(z,q) = 2\sum_{n=0}^{\infty}(-1)^n q^{(n+\frac{1}{2})^2} \sin(2n+1)z\,, \tag{3.3}$$

$$\theta_2(z,q) = 2\sum_{n=0}^{\infty} q^{(n+\frac{1}{2})^2} \cos(2n+1)z\,, \tag{3.4}$$

$$\theta_3(z,q) = 1 + 2\sum_{n=1}^{\infty} q^{n^2} \cos(2nz)\,, \tag{3.5}$$

$$\theta_4 = 1 + 2\sum_{n=0}^{\infty}(-1)^n q^{n^2} \cos(2nz)\,. \tag{3.6}$$

The only requirement on these functions is that $|q| < 1$. It can be represented conventionally in the form:

$$q = \exp(\pi i \tau), \tag{3.7}$$

where τ is a complex number of the form $\tau = r + si$, in which $s > 0$.

It can be shown that $\theta_3(z)$ and $\theta_4(z)$ have the common period π and that θ_1 and θ_2 have the common period 2π, which reflects the periodicity of the sine and cosine functions. Another period might be expected in relation to the exponential $q = \exp(\pi i \tau)$ since:

$$\exp(u + 2\pi i) = \exp(u). \tag{3.8}$$

It turns out that the theta functions are not doubly periodic, however, it is possible to use the theta functions to construct functions which are doubly periodic. Such functions are the elliptic Jacobi functions.

3.4 The Elliptic Functions of Jacobi

Dropping the q dependence of the theta functions and introducing a new independent variable u, known as the argument, by $z = \dfrac{u}{\theta_3^2(0)}$ three Jacobi elliptic functions may be defined by:

$$sn(u) = \frac{\theta_3(0)}{\theta_2(0)} \frac{\theta_1(\theta_3^{-2}(u))}{\theta_4(\theta_3^{-2}(u))}, \tag{3.9}$$

$$cn(u) = \frac{\theta_4(0)}{\theta_2(0)} \frac{\theta_2(\theta_3^{-2}(u))}{\theta_4(\theta_3^{-2}(u))}, \tag{3.10}$$

$$dn(u) = \frac{\theta_4(0)}{\theta_2(0)} \frac{\theta_3(\theta_3^{-2}(u))}{\theta_4(\theta_3^{-2}(u))}, \tag{3.11}$$

where the parameter

$$k = \frac{\theta_2^2(0)}{\theta_3^2(0)}, \tag{3.12}$$

is known as the modulus and may sometimes be dropped from the functional notation. The periodicity properties of the functions $sn(u)$, $cn(u)$, and $dn(u)$ may be written as follows:

$$sn(u+4K)=sn(u+2iK')=sn(u), \tag{3.13}$$

$$cn(u+4K)=cn(u+2K+2iK')=cn(u), \tag{3.14}$$

$$dn(u+4K)=dn(u+4iK')=dn(u), \tag{3.15}$$

where

$$K=\frac{1}{2}\pi\,\theta_3^2(0), \tag{3.16}$$

and

$$K'=-\frac{1}{2}i\pi\tau\,\theta_3^2(0). \tag{3.17}$$

It can therefore be seen that $2K$ and $K'i$ play roles similar to π in the theory of the circular functions and πi in the theory of the hyperbolic functions. The Jacobi elliptic functions are consequently rich in special values and identity relationships (Byrd and Friedman, 1953).

3.4.1 Representation of Jacobi Elliptic Functions as Fourier Series.

Since $\theta_3^2(0)=\frac{2K}{\pi}$, it follows that $\frac{u}{\theta_3^2(0)}=\frac{\pi u}{2K}$, and so the following notation shall be adopted:

$$v=\frac{\pi}{2K}u, \tag{3.18}$$

giving

$$sn(u,k)=\frac{\theta_3(0)\theta_1(v)}{\theta_2(0)\theta_4(v)}, \tag{3.19}$$

$$cn(u,k)=\frac{\theta_4(0)\theta_2(v)}{\theta_2(0)\theta_4(v)}, \tag{3.20}$$

$$dn(u,k)=\frac{\theta_4(0)\theta_3(v)}{\theta_3(0)\theta_4(v)}. \tag{3.21}$$

The expansions of the theta functions will result in the Jacobi functions being represented as the ratios of Fourier series and hence introduces the possibility of representing them as single Fourier series. This is indeed possible and the

expansions are as follows (Davis, 1960) :

$$sn(u,k)=2\frac{\pi}{Kk}\sum_{n=0}^{\infty}\frac{q^{n+\frac{1}{2}}}{1-q^{2n+1}}\sin(2n+1)v, \tag{3.22}$$

$$cn(u,k)=2\frac{\pi}{Kk}\sum_{n=0}^{\infty}\frac{q^{n+\frac{1}{2}}}{1-q^{2n+1}}\cos(2n+1)v, \tag{3.23}$$

$$dn(u,k)=\frac{\pi}{2K}+2\frac{\pi}{K}\sum_{n=1}^{\infty}\frac{q^{n}}{1+q^{2n}}\cos(2nv). \tag{3.24}$$

If $v=x+iy$ and $\tau=r+si,\ s>0$, then the series will converge for all values of v within the strip $|y|<\frac{1}{2}\pi s$, and represent the functions there. The only obstacle to evaluating the Fourier series is computing q when k is given. A practical method makes use of the following:

$$l=\frac{1}{2}\left[\frac{1-\sqrt{k'}}{1+\sqrt{k'}}\right], \tag{3.25}$$

where

$$k'=\sqrt{1-k^2}, \tag{3.26}$$

is known as the complementary modulus. Eq. 3.25 can be written as:

$$l=\frac{1}{2}\left[\frac{\theta_2(0,q^4)}{\theta_3(0,q^4)}\right]=\frac{q+q^9+q^{25}+q^{49}+q^{81}+\cdots}{1+2q^4+2q^{16}+2q^{36}+2q^{64}+\cdots}, \tag{3.27}$$

which is now inverted and q obtained as the following series in l :

$$q=l+2l^5+15l^9+150l^{13}+1{,}707l^{17}+20{,}910l^{21}+268{,}616l^{25}+\cdots, \tag{3.28}$$

which converges rapidly for values of l less than $\frac{1}{2}$. If l is close to $\frac{1}{2}$, then the convergence of Eq. 3.28 may be improved by using k instead of k' in Eq. 3.25 and computing q' instead of q. The value of q is then given by:

$$ln(q).ln(q')=\pi^2. \tag{3.29}$$

Values correct to 15 decimal places can thus be computed without prohibitive labour. This method was also used (Spencely and Spencely, 1947) to construct tables of elliptic functions to this accuracy. An example of the variation of the

Jacobi functions in the complex plane is given in Figures 3.2, 3.3, and 3.4, and is taken from (Jahnke and Emde, 1960).

3.4.2 Jacobi Functions with Real or Imaginary Arguments and Moduli

The evaluation method for the Jacobi functions given in the previous section is quite general and so it is valid for complex arguments and moduli. The evaluation can be simplified provided the argument and modulus are either real or imaginary. This is accomplished by the use of various transformation formulae (Byrd, 1953) which express a function with one modulus and argument in terms of those with a new modulus and argument. Once in canonical form the modulus can be reduced by successive application of Gauss' transformation (Byrd, 1953) until a trigonometric approximation is valid. Reversing the "descending" transformation will then yield the desired value of the Jacobi function.

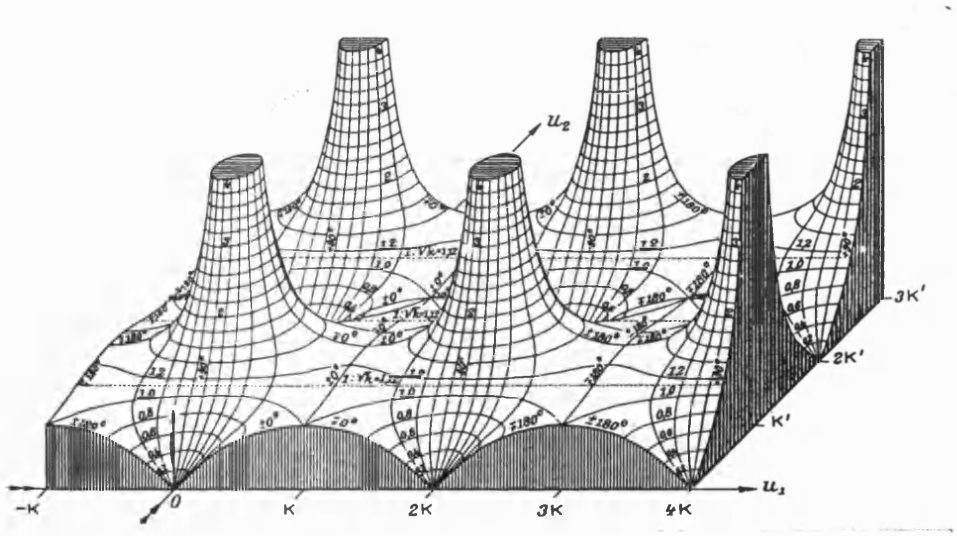

Figure 3.2 Relief of the doubly periodic function $sn(u)$ for $k = 0.8$ ($u = u_1 + iu_2$)

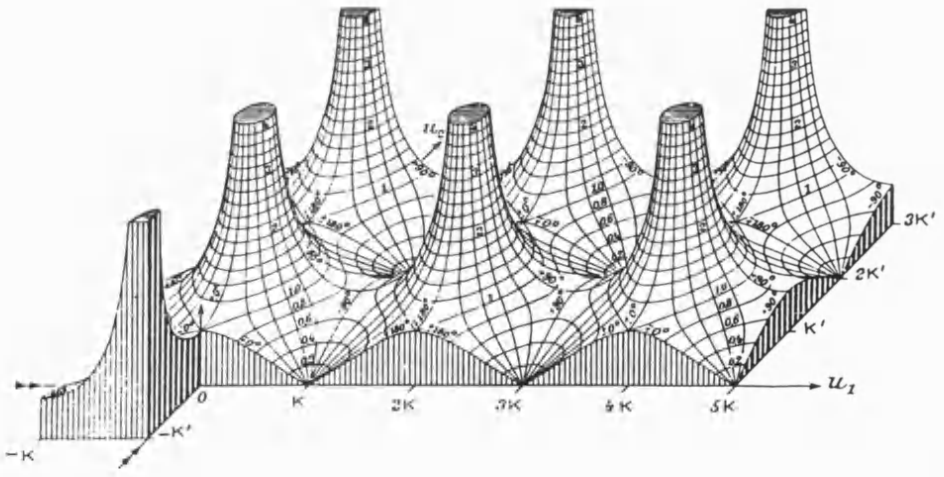

Figure 3.3 Relief of the doubly periodic function $cn(u)$ for $k = 0.8$ ($u = u_1 + iu_2$)

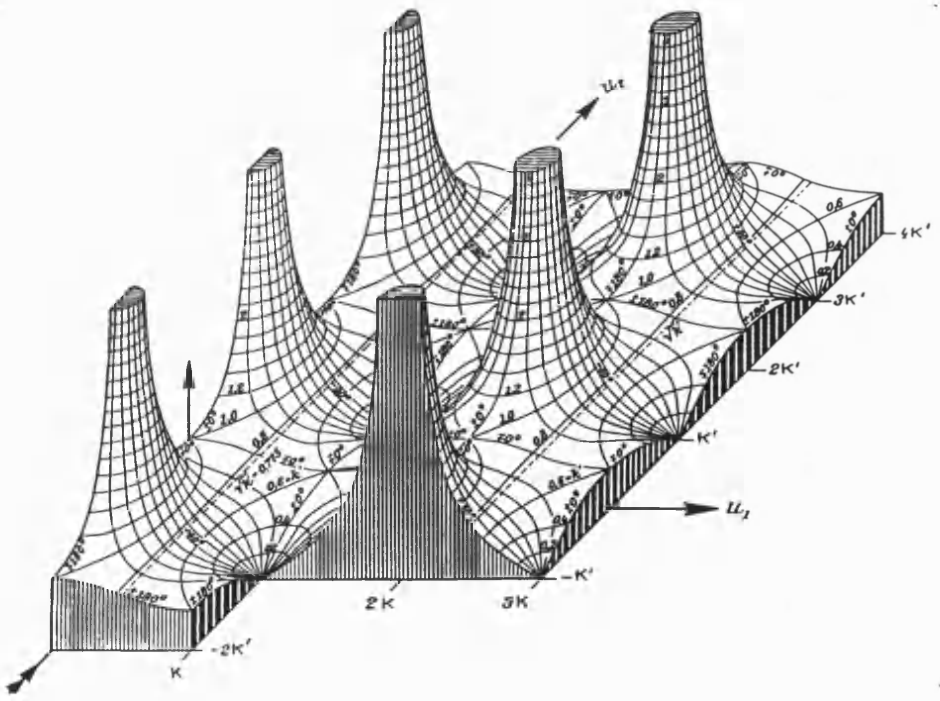

Figure 3.4 Relief of the doubly periodic function $dn(u)$ for $k = 0.8$ ($u = u_1 + iu_2$)

3.4.3 A Differential Equation Involving Jacobi Functions

The second derivative of the cn elliptic function can be written as:

$$\frac{d^2 cn(u)}{du^2} = (2k^2 - 1)cn(u) - 2k^2 cn^3(u). \tag{3.30}$$

If a general solution is written as:

$$y = C\ cn(\lambda(x - x_0), k), \tag{3.31}$$

where λ and x_0 are arbitrary constants, then it is possible to write:

$$\frac{d^2 y}{dx^2} = \lambda^2(2k^2 - 1)y - \frac{2k^2\lambda^2}{C^2}y^3, \tag{3.32}$$

or

$$\frac{d^2 y}{dx^2} = Ay + By^3, \tag{3.33}$$

where

$$k^2 = \frac{(\lambda^2 + A)}{2\lambda^2} \quad \text{and} \quad C^2 = -\frac{(\lambda^2 + A)}{B}. \tag{3.34}$$

The other Jacobi functions are also solutions to the second order nonlinear differential equation described by Eq. 3.33 .

The nonlinear differential equation Eq. 3.33 originates in a number of natural phenomena. For example, it describes the oscillations of a simple pendulum when the small angle approximation is no longer valid. In chapter four it will be shown that electromagnetic propagation in a medium characterised by a Kerr-like nonlinearity is also governed by Eq. 3.33 and hence has solutions in terms of elliptic Jacobi function.

3.5 References

Paul F. Byrd and Morris D. Friedman, " *Handbook of Elliptic Integrals for Engineers and Physicists,*" Springer - Verlag, (1954).

Harold T. Davis, " *Introduction to Nonlinear Differential and Integral Equations,*" Dover publications, Inc., 2nd Ed., (1962).

E. Jahnke, F. Emde, and Lösch, " *Tables of higher functions,*" McGraw-Hill book company Inc., New York, (1960).

Earl D. Rainville, " *Special Functions,*" The Macmillan Company, 1st. Ed.,(1960).

G. W. and R. M. Spencely, " *Smithsonian Elliptic Functions Tables,*" The Smithsonian Institute, (1947).

Chapter Four

Planar Nonlinear Semiconductor Optical Waveguides

4.1 Introduction

The general requirement for an electromagnetic waveguide is to confine the energy flow along the guiding structure and not perpendicular to it. This usually involves fields being confined to a high refractive index region by surrounding low index material. A simple optical waveguide that confines energy in one direction only is the planar or slab guide shown in Figure 4.1 . It consists of a slab of high index material bounded by semi-infinite, low index regions. Not only is it a practical and frequently employed design, it can be solved analytically and so provides a unique physical insight into the nature of guided wave propagation. The linear slab guide, treated in many texts eg. (Yariv, 1985), represents a "building block" in the understanding of more complicated structures and so the intention here is to study its nonlinear counter-part in some detail.

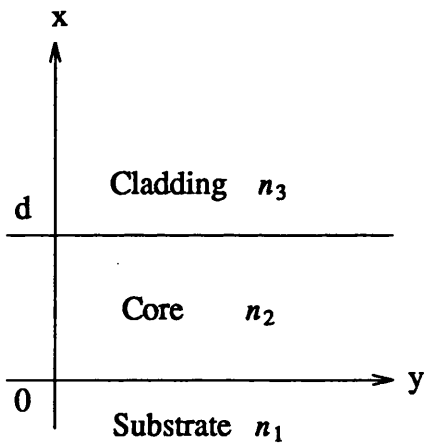

$n_2 > n_1 > n_3$

Figure 4.1 A slab dielectric waveguide. Propagation in the z direction out of the paper.

4.2 Maxwell's Equations

An electromagnetic field in space is described classically by two field vectors , **E** and **H** called the electric vector and the magnetic vector respectively. The effects of matter on the field are introduced via a second set of vectors **D** and **B** called the electric displacement and the magnetic induction . These vectors are related by Maxwell's equations:

$$\nabla\times\mathbf{E}+\frac{\partial\mathbf{B}}{\partial t}=0, \tag{4.1}$$

$$\nabla\times\mathbf{H}-\frac{\partial\mathbf{D}}{\partial t}=\mathbf{J}, \tag{4.2}$$

$$\nabla.\mathbf{D}=\rho, \tag{4.3}$$

$$\nabla.\mathbf{B}=0, \tag{4.4}$$

where **J** is the explicit source term (amperes / square metre) and ρ is the electric charge density (coulombs / cubic metre). These equations are the basic laws of electricity and magnetism in differential form and fully describe the propagation of electromagnetic radiation in any medium. In studying optics it is usual to consider radiation far away from any electromagnetic sources and hence **J** and ρ are zero.

To describe the effects that the material and fields have on each other Maxwell's equations must be supplemented by the constitutive equations given by:

$$\mathbf{D}=\tilde{\varepsilon}\mathbf{E}=\varepsilon_0\mathbf{E}+\mathbf{P}, \tag{4.5}$$

$$\mathbf{B}=\mu_0\mathbf{H}, \tag{4.6}$$

where the parameter $\tilde{\varepsilon}$ is, in general, a tensor known as the dielectric tensor (or permittivity). **P** is the electric polarisation and ε_0 and μ_0 are the permittivity and permeability of vacuum respectively. These equations represent a model of the material system interacting with electromagnetic radiation. The sophistication of the model is mirrored by the complexity of the dielectric tensor. For example, if the material is isotropic, the tensor reduces to a scalar. If the quantity $\tilde{\varepsilon}$ can be assumed to be independent of the field strengths - the material is linear. If this is not so then the material is classified as nonlinear. In chapter two the origin of the polarisation **P** was described and a constitutive relation derived for

semiconductors irradiated by light close in energy to that of the material's band gap. It expressed the relative permittivity in terms of optical field intensity I ,

$$\varepsilon(I) = \varepsilon_{nl} = (n_0 + n_I I)^2 . \tag{4.7}$$

Boundary conditions relating the field vectors **E, H, D,** and **B** either side of an interface between two media can be directly derived from Maxwell's equations. For the situation when there is no free charge and no surface currents, the boundary conditions require that the components of **D** and **B** normal to the bounding surface, and the components of **E** and **H** parallel to the surface, are continuous across the boundary.

4.3 The Wave Equation

From Maxwell's equations it is possible to write an equation governing the propagation of the electric field vector in a medium.

$$\nabla^2 \mathbf{E}(\mathbf{r}, t) + \nabla(\mathbf{E}.\frac{\nabla\varepsilon(\mathbf{r})}{\varepsilon(\mathbf{r})}) - \mu_0\varepsilon_0\varepsilon(\mathbf{r})\frac{\partial^2}{\partial t^2}\mathbf{E}(\mathbf{r}, t) = 0, \tag{4.8}$$

where **r** is a space co-ordinate and t is time. If the variation of the dielectric constant is small in distances of the order of a wavelength little error is introduced if $\frac{1}{\varepsilon}\nabla\varepsilon$ is neglected. The propagation equation becomes:

$$\nabla^2 \mathbf{E}(\mathbf{r}, t) - \mu_0\varepsilon_0\varepsilon(\mathbf{r})\frac{\partial^2}{\partial t^2}\mathbf{E}(\mathbf{r}, t) = 0. \tag{4.9}$$

Any function of the form $f(\mathbf{r} \pm vt)$ will satisfy this equation where v is the velocity of propagation given by:

$$v = \frac{c}{\sqrt{\varepsilon}}, \tag{4.10}$$

and c is the velocity of light in vacuum:

$$c = \frac{1}{\sqrt{\varepsilon_0\mu_0}}. \tag{4.11}$$

Here a harmonic solution is assumed such that :

$$\mathbf{E}(\mathbf{r}, t) = \mathbf{E}(x, y)\, exp(i(\omega t - k_z z)), \tag{4.12}$$

which describes propagation in the z direction. Using this expression in Eq. 4.8 and introducing the the time variation first gives:

$$\nabla^2 \mathbf{E}(\mathbf{r}) + k_0^2 \varepsilon(\mathbf{r}) \mathbf{E}(\mathbf{r}) = 0, \tag{4.13}$$

where

$$k_0^2 = \omega^2 \mu_0 \varepsilon_0, \tag{4.14}$$

is the free space propagation constant. Now introducing the z dependence for a rectangular co-ordinate system:

$$\left(\frac{\partial^2}{\partial x^2} + \frac{\partial^2}{\partial y^2} \right) \mathbf{E}(x, y) + [k_0^2 \varepsilon(\mathbf{r}) - k_z^2] \mathbf{E}(x, y) = 0. \tag{4.15}$$

A solution to this equation that satisfies the boundary conditions is called a *mode* of the waveguide. In linear analysis a general solution to a one dimensional guide can be represented as a linear sum of two polarisations, the transverse electric (TE) and the transverse magnetic (TM) modes with respect to the x-axis. Given that $\frac{\partial}{\partial y} = 0$ the TE mode contains only the E_y, H_x, and H_z components where the electric field is restricted to the transverse plane. In this case, the electric field E_y and $\nabla\varepsilon$ will be orthogonal so $\mathbf{E}.\nabla\varepsilon = 0$ and the reduction of Eqn. 4.8 to Eqn. 4.9 will be exact. In contrast, the TM mode contains only the H_y, E_x, and E_z components where the magnetic field is restricted to the transverse plane. Here $\mathbf{E}.\nabla\varepsilon \neq 0$ and Eqn 4.9 relies on the approximation $\frac{1}{\varepsilon}\nabla\varepsilon \simeq 0$. Any linear combination of the modes will be a solution of the waveguide. This property is known as orthogonality. Although for the nonlinear guide a linear sum of modes will not generally be a solution, the TE / TM analysis is still retained. A theory is first developed for the TE mode.

4.4 Nonlinear Waveguides

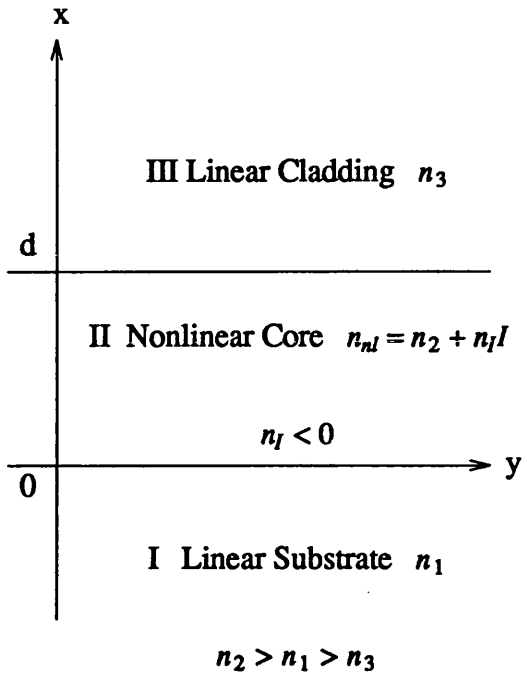

Figure 4.2 A nonlinear dielectric slab waveguide.

Essentially, the use of nonlinear material in a guide structure allows the guide parameters to be altered or modulated by the incident light, thereby changing the field profiles in some useful manner, eg nonlinear directional couplers (Jensen, 1982). In the present work the origin of the defocusing nonlinearity is the absorption associated with the band edge of semiconductor material. This, as was indicated in chapter two, has an important implication in the guide design; namely, the nonlinearity will be present only in the high index core. With this consideration a suitable guide geometry is shown in Figure 4.2 .

The TE mode is considered first for which the only electric field component present is $E_y(x)$. Since the slab guide is considered to be infinite in extent, there is no field variation in the y direction and so $\frac{\partial}{\partial y} = 0$. The equations governing the electric field in the substrate and cladding are then written as:

$$\text{Region I} \quad \frac{d^2E_y}{dx^2} + k_1^2 E_y = 0, \tag{4.16}$$

$$\text{Region III} \quad \frac{d^2E_y}{dx^2} + k_3^2 E_y = 0. \tag{4.17}$$

Here the transverse propagation constants are introduced as:

$$k_1^2 = k_0^2 n_1 - k_z^2 \quad \text{and} \quad k_3^2 = k_0^2 n_3 - k_z^2 , \tag{4.18}$$

which represent conservation equations for the substrate and cladding. The solutions to Eqs. 4.16 and 4.17 will be of the form:

$$\text{Region I} \quad E_y = E_0 \exp(ik_1 x) , \tag{4.19}$$

$$\text{Region III} \quad E_y = E_d \exp(ik_3 (d - x)) . \tag{4.20}$$

E_0 is the field amplitude at the interface between the nonlinear core and the linear cladding, whilst E_d is the field amplitude at the opposite interface. In line with the requirement to confine energy in the core region (Region II), the fields in Regions I and III must decay exponentially. This will be achieved by satisfying the following $k_z^2 > k_0^2 n_1$, given that $n_1 > n_3$. Modes that fulfill this condition are referred to as confined or guided.

Attention is now turned to the core layer. From Eq 4.7 the dielectric constant is given as:

$$\varepsilon(I) = \varepsilon_{nl} = (n_l + n_I I)^2 \tag{4.21}$$

Expanding the square and replacing n_l by n_2 gives:

$$\varepsilon_{nl} = n_{nl}^2 = n_2^2 + 2n_2 n_I I + n_I^2 I^2 . \tag{4.22}$$

The term $n_I^2 I^2$ may be neglected provided $| n_I | I \ll 2n_2$. The intensity I is given by the Poynting vector which for the TE mode is:

$$I = \frac{1}{2} \frac{k_z}{\omega \mu_0} | E_y |^2 . \tag{4.23}$$

Substituting and writing in terms of permittivity:

$$\varepsilon_{nl} = \varepsilon_2 + n_2 \frac{n_I k_z}{\omega \mu_0} | E_y |^2 , \tag{4.24}$$

hence

$$\varepsilon_{nl} = \varepsilon_2 + \alpha_{nl} \mid E_y \mid^2, \tag{4.25}$$

where

$$\alpha_{nl} = \frac{n_2 n_I k_z}{\omega \mu_0} = \frac{k_z}{k_0} \frac{n_2 n_I}{\mu_0 c} \approx \frac{n_2^2 n_I}{\mu_0 c}. \tag{4.26}$$

Where the approximation $\frac{k_z}{k_0} \approx n_2$ is valid for guides with a small dielctric step. When this expression is used in Eq.4.15 the following nonlinear wave equation is obtained:

$$\frac{d^2 E_y}{d x^2} + [k_0^2(\varepsilon_2 + \alpha_{nl} \mid E_y \mid^2) - k_z^2] E_y = 0, \tag{4.27}$$

and for purely real fields

$$\frac{d^2 E_y}{d x^2} + k_2^2 E_y + \alpha_{nl} k_0^2 E_y^3 = 0, \tag{4.28}$$

where

$$k_2^2 = k_0^2 \varepsilon_2 - k_z^2. \tag{4.29}$$

The nonlinear differential equation described by Eq. 4.28 is recognised as being of the same form as the differential equation introduced in Section 3.4.3 and whose solutions were in terms of Jacobi elliptic functions, viz:

$$\frac{d^2 y}{d x^2} + Ay + By^3 = 0. \tag{4.30}$$

This was first pointed out by Akmediev (1982).

4.4.1 Analytical Solutions

Following Boardman and Egan (1986) a first integral of Eq. 4.28 is obtained as:

$$\left(\frac{dE_y}{d x}\right)^2 + \left(k_2^2 + \frac{k_0^2 \alpha_{nl}}{2} E_y^2\right) E_y^2 = C, \tag{4.31}$$

where the constant of integration C can be written in terms of the boundary fields, $E_0 = E_y(x = 0)$ and $E_d = E_y(x = d)$, as:

$$C = k_0^2 E_0^2 \, (\varepsilon_2 - \varepsilon_1 + \frac{\alpha_{nl} E_0^2}{2}) ,$$

$$= k_0^2 E_d^2 \, (\varepsilon_2 - \varepsilon_3 + \frac{\alpha_{nl} E_d^2}{2}) . \qquad (4.32)$$

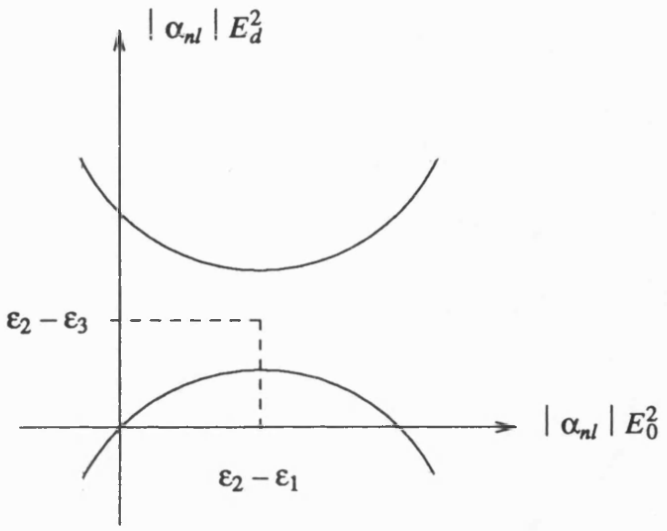

Figure 4.3 The hyperbolic relationship between the optical intensities at each of the core interfaces. The portion of the curve falling inside the boxed region corresponds to guided modes.

Eq. 4.32 defines a hyperbolic relationship between the boundary field intensities as shown in Figure 4.3 . Real fields will be restricted to the positive quadrant and for guided modes the following must also be true:

$$\varepsilon_2 - | \alpha_{nl} | E_0^2 > \varepsilon_1 \quad \text{and} \quad \varepsilon_2 - | \alpha_{nl} | E_d^2 > \varepsilon_3 . \qquad (4.33)$$

For the structure considered here, where $\alpha_{nl} < 0$, only the portion of the curves falling within the boxed region indicated will give guided type solutions. A second integration of the nonlinear differential equation yields the Jacobi function solutions:

$$E_y = P\ cn(q(x + x_0), m)\,. \tag{4.34}$$

Here cn is the Jacobi elliptic cosine function. The modulus is now designated m instead of the more usual k to avoid confusion with propagation constants. The parameter x_0 is an integration constant. A comparison of Eqs. 4.28 and 4.30 gives the following:

$$m^2 = \frac{q^2 - k_2^2}{2q^2}, \tag{4.35}$$

and

$$P^2 = \frac{q^2 - k_2^2}{k_0^2 \alpha_{nl}}, \tag{4.36}$$

with

$$q = (2k_0^2 \alpha_{nl} C + k_2^4)^{\frac{1}{4}}\,. \tag{4.37}$$

Applying continuity conditions to the E_y field and its derivative across the interfaces, produces an eigenvalue equation:

$$cn(qd, m) = \frac{2E_0 E_d (q^2 - k_1 k_3)}{k_1^2 E_0^2 + k_3^2 E_d^2 + q^2[E_0^2 + E_d^2] + \frac{\alpha_{nl} k_0^2}{2}[E_0^2 - E_d^2]^2}\,. \tag{4.38}$$

In the limit $\alpha_{nl} = 0$, corresponding to a linear asymmetric guide, the above equation reduces to the form appropriate to a linear asymmetric slab waveguide (Yariv, 1985).

4.5 TM Mode Solutions

The TM modes involve $\mathrm{E}(E_x, 0, E_z)$ and $\mathrm{H}(0, H_y, 0)$. For such modes propagating in a medium characterised by an intrinsic nonlinearity the permittivity will be a tensor with a dependence on both electric field components (Boardman and Egan, 1984). As a consequence, an analytical solution is no longer available and the resulting wave equation must be solved numerically (Ogusu, 1989). In contrast, the refractive index associated with the incoherent band filling nonlinearity remains simply dependent on the intensity and can be written as:

$$\varepsilon_{nl} = \varepsilon_2 + \alpha_{nl}^{TM} \mid H_y \mid^2, \tag{4.39}$$

where

$$\alpha_{nl}^{TM} = \frac{k_0 n_I}{\omega \varepsilon_0}. \tag{4.40}$$

An analytical solution, essentially similar to that of the TE mode, is still available and will be used in the next chapter to study two dimensional structures. The details of the TM nonlinearity, dispersion equation and the relationship between the fields at either boundary are given in Appendix 1 . The linear limit of the dispersion equation is also derived in the appendix and shown to be identical to that of the familiar linear TM eigenvalue equation.

4.6 Solution Technique

Returning to the TE analysis Eq. 4.32 describes the relationship between the field intensities at each interface. For a prescribed value of E_0^2 the value E_d^2 can be calculated with the sign of $\pm\sqrt{E_d}$ determining whether a solution will be even or odd. Values of E_0 and E_d can then be used in Eq. 4.38 and a numerical search made for values of k_z that will satisfy it. Since the eigenvalue equation must be solved numerically the method is sometimes referred to as being semi-analytic. The quantity k_z / k_0 relates the phase velocity of the mode to the phase velocity of a plane wave in free space and is thus, notionally, a refractive index. It is therefore known as the effective index n_{eff}. The eigenvalues k_z can be used in the field equations Eq. 4.19 and Eq. 4.20 for the substrate and cladding and also in the following equation for the field in the nonlinear core:

$$E_y = \frac{qE_0\left(qcn(qx) + k_1 sn(qx)dn(qx)\right)}{q^2 dn^2(qx) + k_0^2 \frac{\alpha_{nl}E_0^2}{2} sn^2(qx)}, \tag{4.41}$$

in which the dependence on the modulus has been suppressed.

Since no loss has been included in the analysis, the propagation constant k_z will be real and so the arguments and the moduli of the elliptic functions will be either purely real or imaginary. In such circumstances, as indicated in chapter three, the functions can be evaluated using transformations.

4.7 Guided Power

The power carried by the guided wave will be given by:

$$P_{tot} = k_z \left(\frac{\varepsilon_0}{\mu_0} \right)^{\frac{1}{2}} \frac{1}{k_0} \int_{-\infty}^{\infty} E_y^2 \, dx \, . \tag{4.42}$$

Substituting for the form of the fields in the substrate and cladding yields:

$$P_{tot} = k_z \left(\frac{\varepsilon_0}{\mu_0} \right)^{\frac{1}{2}} \frac{1}{k_0 \alpha_{nl}} \left[\frac{\alpha_{nl} E_0^2}{2} \frac{1}{k_1} + \frac{\alpha_{nl} E_d^2}{2} \frac{1}{k_3} + E_0^2 \int_0^d E_y^2 \, dx \right]. \tag{4.43}$$

The integral of the field in the core can be cast in terms of elliptic integrals, but here a simple quadrature was used to evaluate it.

Finally, a normalised power flow P_N can be introduced such that:

$$P_N = \frac{P_{tot}}{P_0}, \quad P_0 = \left(\frac{\varepsilon_0}{\mu_0} \right)^{\frac{1}{2}} \frac{1}{\alpha_{nl} k_0} \, . \tag{4.44}$$

Calculated results can therefore be quite general and applicable to a wide range of structures if distances occurring in the problem are normalised to the frequency using $X = k_0 x$. However, for the sake of definiteness, normalised results have not been quoted in the present work.

4.8 Verification of Programme

A computer code was written to perform the analysis outlined above to solve planar nonlinear waveguides. The programme was used to successfully reproduce results taken from (Boardman and Egan, 1986) and (Ogusu, 1986) where, in the latter, the special case of a symmetrical nonlinear waveguide was treated. Confident in the numerical integrity of the programme, the underlying theory could then be assessed.

4.9 Verification of Analytic Solution To Planar Guide

Here, in the absence of experimental data, results from the nonlinear planar waveguide programme are compared with those from a more elaborate treatment of the same problem (Gibbons and Sarid, 1987). In this way, it will be possible to highlight the present model's strengths and weaknesses.

Resonant electronic nonlinearity in a semiconductor slab waveguide was first treated by Gibbons and Sarid (1987) and included carrier diffusion effects across the guide. The approach solved two second order differential equations, the wave equation and the carrier diffusion equation, by using a numerical integration in a

self-consistent way. The nonlinearity was modeled by the plasma theory of Banyai and Koch (1987) and takes into account the finite fraction of the optical power carried by a guided mode that must be absorbed to give rise to the nonlinearity. Consequently, a complex propagation constant k_z gives all the information necessary to propagate the mode. Since absorption, and hence k_z, are carrier density dependent, it is necessary to recalculate k_z self-consistently for each propagation step along the guide.

The analysis was applied by Gibbons and Sarid to three symmetric GaAs slab waveguides with AlGaAs cladding and operating at a wavelength detuned from the GaAs band edge. The AlGaAs cladding contributes nothing to the nonlinearity since its band edge is at a higher energy than that of the bulk GaAs. These guides are illustrated in Figure 4.4 .

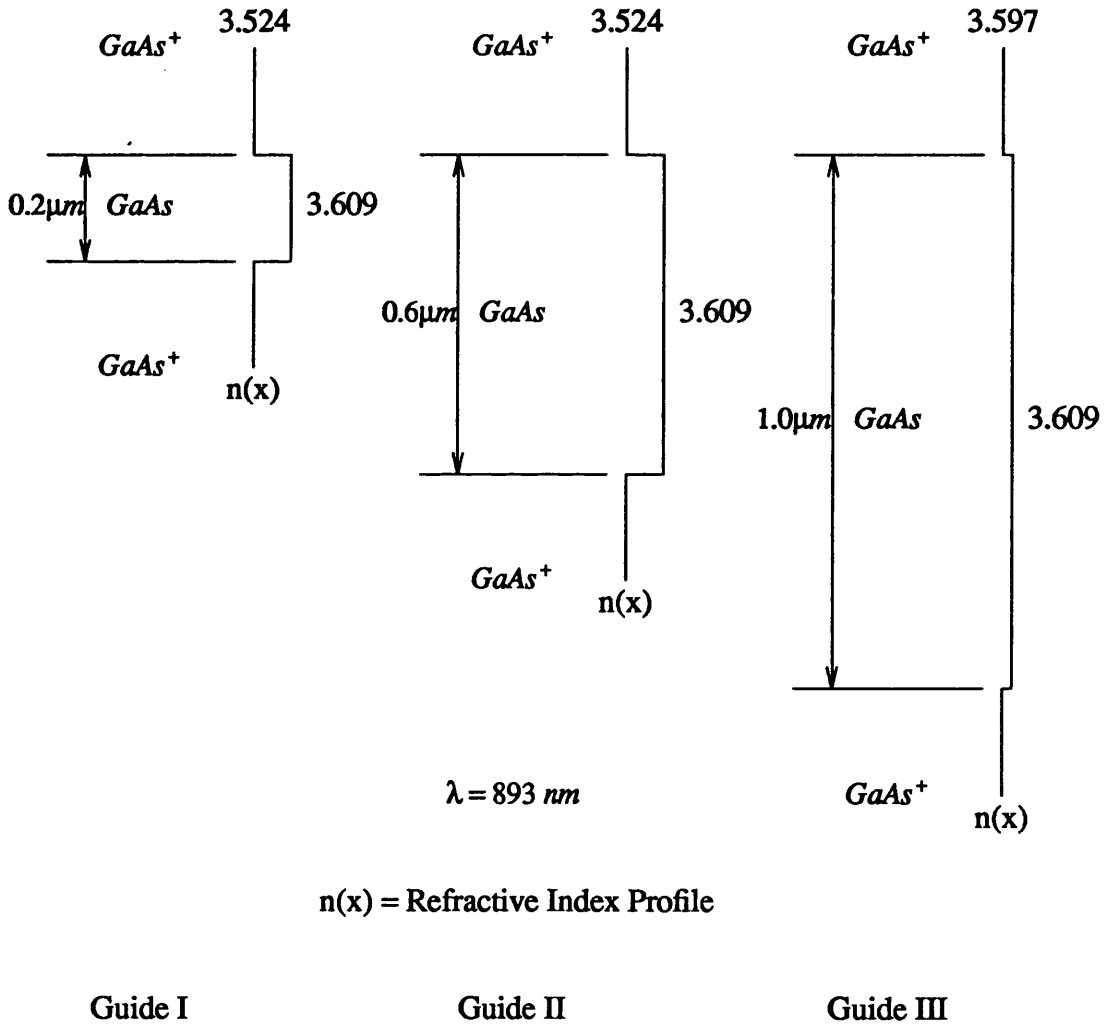

Figure 4.4 The three guides analysed by Gibbons and Sarid (1987)

For each guide the effective index was calculated as a function of power per unit length relative to the linear value. The results for the change in effective index Δn_{eff} , with $(L = 10\mu m)$ and without $(L = 0)$ carrier diffusion, are reproduced in Figures 4.5, 4.6, and 4.7 where L is the diffusion length. Gibbons and Sarid concluded that diffusion became significant in wide guides with relatively large core / cladding index steps. More significantly, for such structures the roll off in Δn_{eff} was a result of the nonlinearity saturating. This was not true of the third guide where the core / cladding index step was small. Here the mode broadening means the increase in power is accommodated in the linear cladding and produces a roll off in Δn_{eff} .

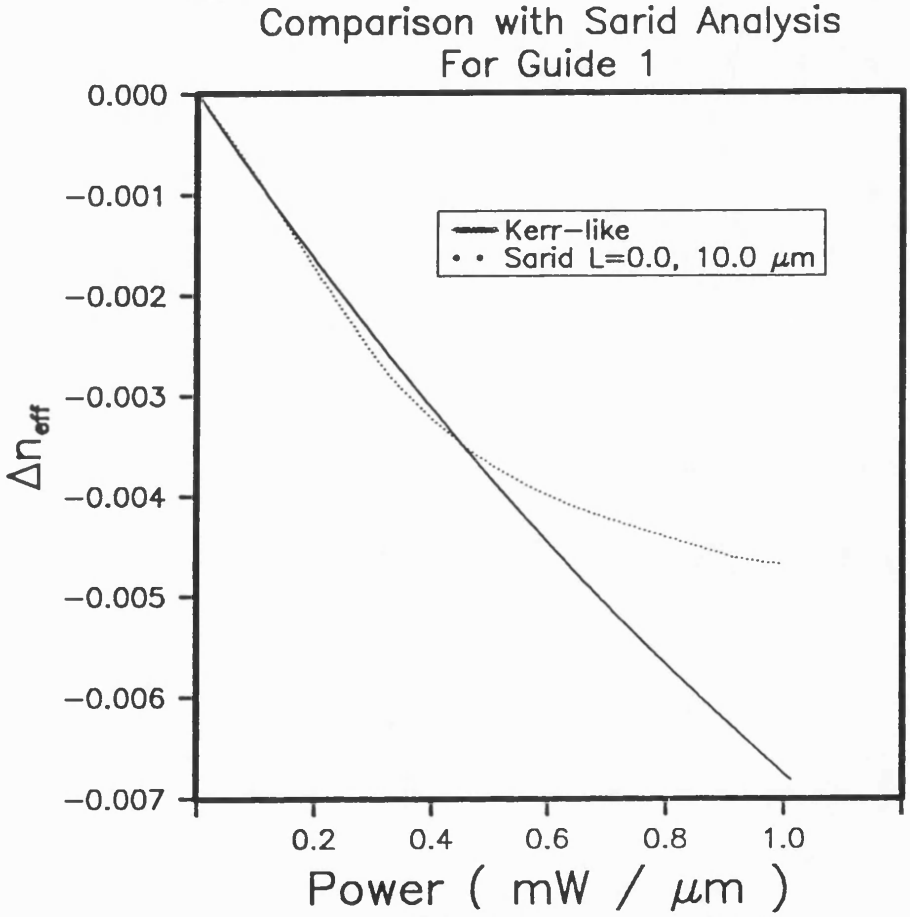

Figure 4.5 Comparison of results for Guide I between the Kerr-like model of semiconductor nonlinearity and the plasma theory used in the Gibbons and Sarid (1987) analysis.

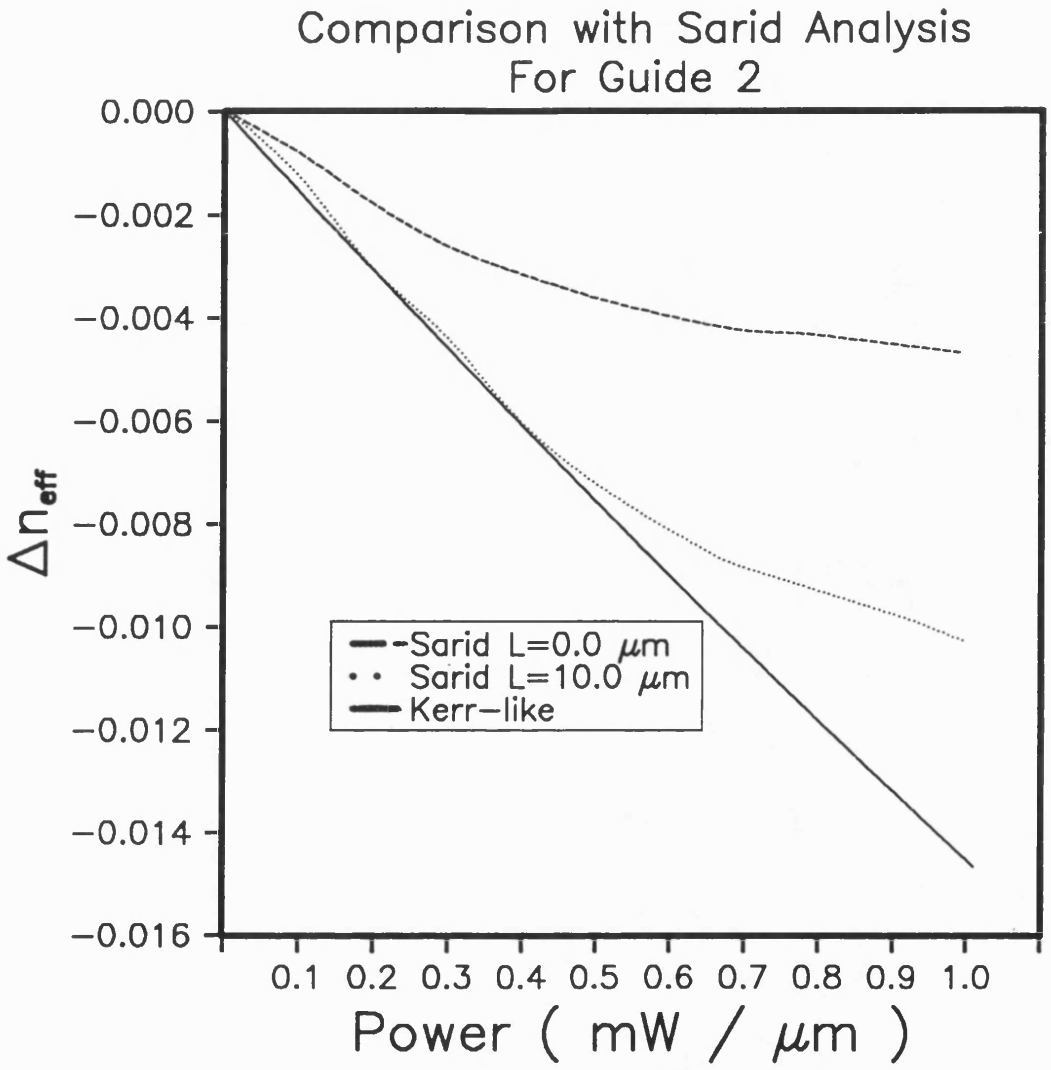

Figure 4.6 Comparison of results for Guide II between the Kerr-like model of semiconductor nonlinearity and the plasma theory used in the Sarid (1987) analysis.

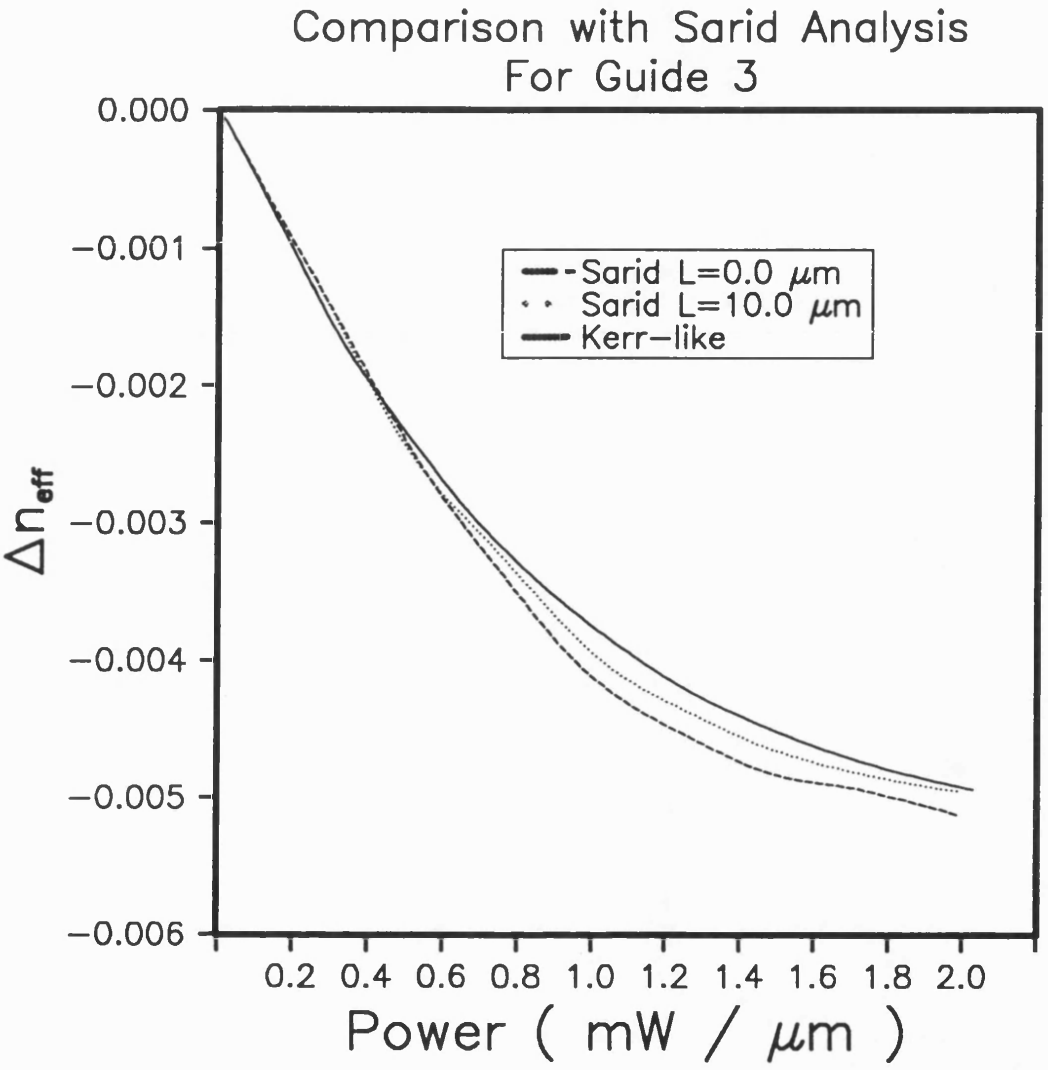

Figure 4.7 Comparison of results for Guide III between the Kerr-like model of semiconductor nonlinearity and the plasma theory used in the Sarid (1987) analysis.

Results calculated from the analytic solution of the nonlinear wave equation have been superimposed on the Gibbons and Sarid curves in Figures 4.5 - 4.7 . A value $n_I = -1.2\ 10^{-11}\ m^2/W$ was used for the nonlinear coefficient to obtain the analytic curves which provided a good match for guide III only. This value would seem reasonable and consistent with operating at a wavelength detuned from the exciton peak. For example, in an experimental demonstration of a GaAs / GaAlAs MQW waveguide switch (Li Kam Wa, 1985) the nonlinear coefficient was measured as $n_I \sim -10^{-11}\ m^2/W$. This was obtained for an operating wavelength of 850 *nm* and with an exciton line at 820 *nm* .

Figures 4.5 and 4.6 show that saturation and diffusion effects have become significant in guides I and II. Since neither effect is accounted for by the Kerr-like nonlinearity the match obtained for these guides is poor. However, it has been demonstrated that for a guide not limited by saturation or diffusion (ie. a guide with a small dielectric step) and using an experimentally consistent value of n_I , a nonlinear modal analysis provides a realistic description of the nonlinear waveguiding phenomena in a planar structure. Furthermore, this has been achieved with a fraction of the computational effort required for the intensive numerical approach of Gibbons and Sarid. The modal properties of such guides are now investigated.

4.10 Planar Asymmetric Nonlinear Waveguides

Most work on semiconductor nonlinearities to date has concentrated on the GaAs / AlGaAs material system at wavelengths around 850 *nm* . For telecommunications applications InP based materials are more attractive. They allow wavelengths close to 1.55 μm to be accessed which corresponds to the minimum absorption in fibres. In addition, the use of MQW structures allows independent tailoring of the band gap (and hence operating wavelength) and refractive index.

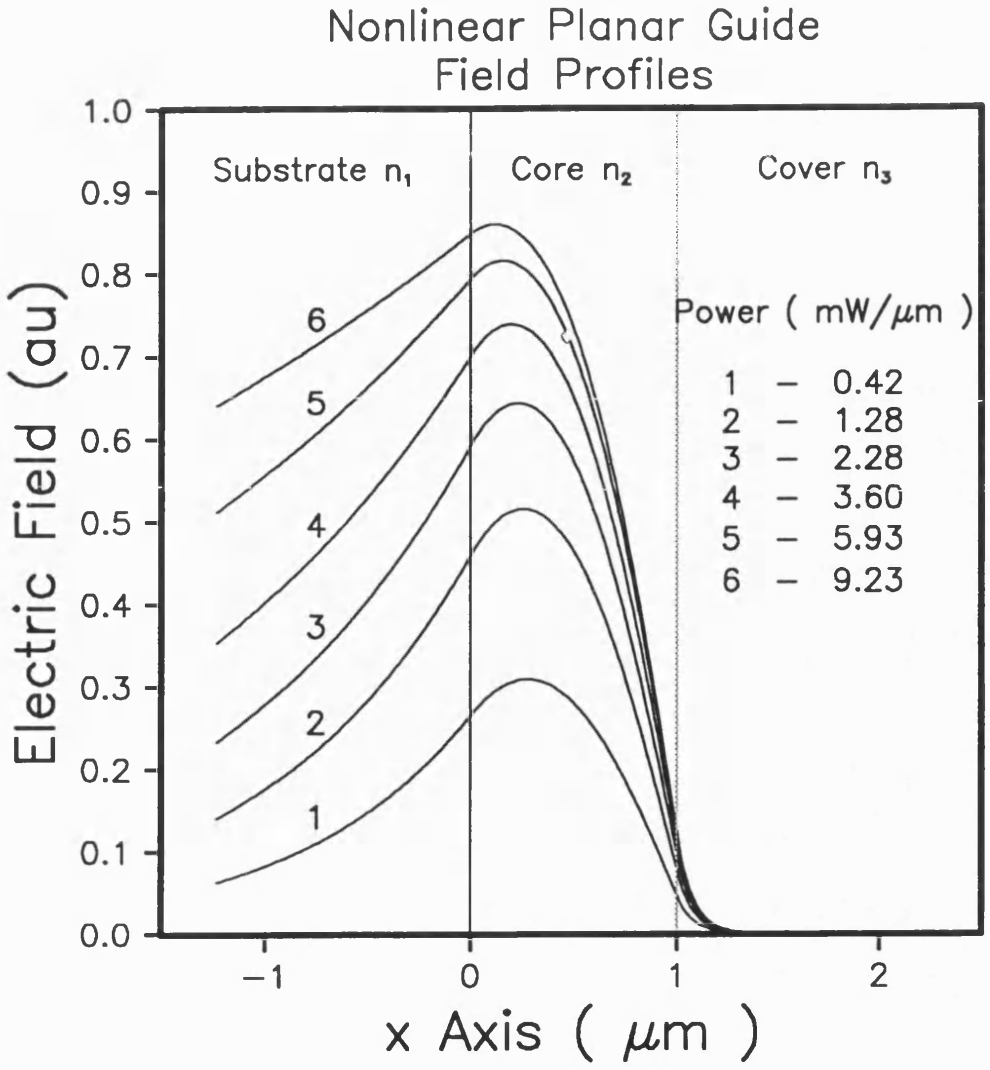

Figure 4.8 Mode profiles of a semiconductor, defocusing, nonlinear, slab waveguide as the power is increased.

Calculations have been performed for a waveguide fabricated in GaInAs / AlInAs MQW material, lattice matched to InP (Lambkin and Shore, 1988) corresponding to the structure of Figure 4.2 . The core was assumed to consist of 120 Å GaInAs wells and 30 Å AlInAs barriers, the cladding layer was taken to be formed with 60 Å GaInAs wells and 30 Å AlInAl wells. The structure is designed to have a band edge nonlinearity at around 1.55 μm .

The dielectric constant of the core layer at this wavelength was estimated, using a weighted mean (Streifer, 1979) of the dielectric constants of the constituent ternary materials (Afromowitz, 1974), (Broberg and Lindgren) to be 11.76 . Similarly, the dielectric constant of the cladding was established as 11.42 . The cover layer is taken to be air of unity dielectric constant and thus the waveguide structure is strongly asymmetric. Using a representative value for the

semiconductor nonlinearity, $n_I = -1\ 10^{-11}\ m^2 / W$, Figure 4.8 shows how the optical field profiles vary as the power is increased, whilst Figure 4.9 delineates the corresponding change in effective index. Since the the index difference between the core and substrate is reduced by the incident field, the effective index approaches the substrate index and the field begins to fill the semi-infinite region. Any additional power is thus expelled into a linear part of the guide and thus a limiting action is exhibited. This is illustrated in Figure 4.10 . In reality, if the guide index step is too great, the nonlinearity will saturate before the index difference has been washed out and the guide will not limit. By assuming a spot diameter of $1\ \mu m$ an estimate of the launched power to obtain the breakdown in guiding can be obtained as $10\ mW$.

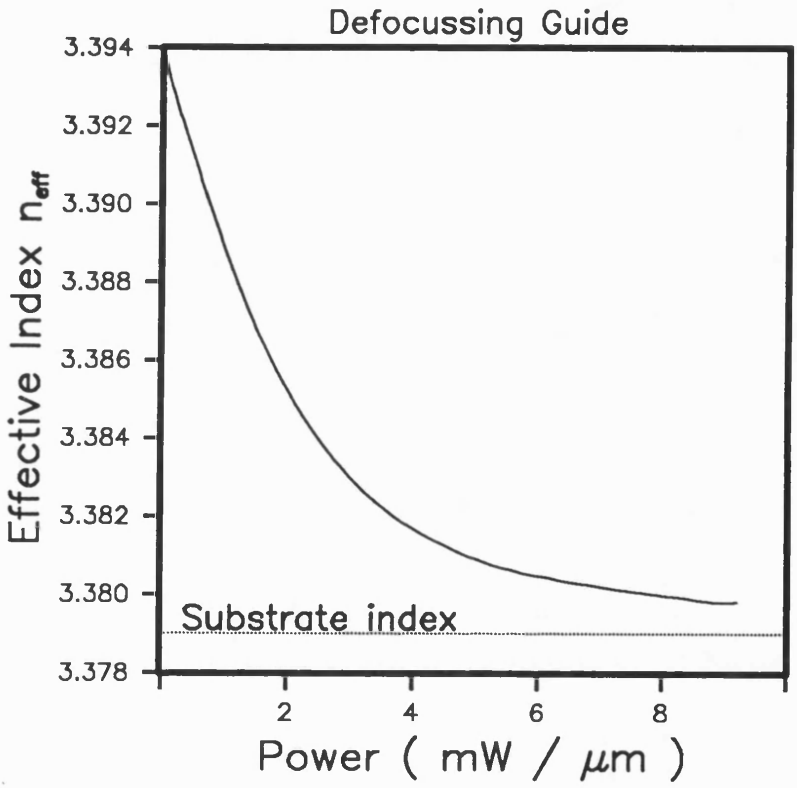

Figure 4.9 The power dispersion curve for a semiconductor, defocusing, nonlinear, slab waveguide.

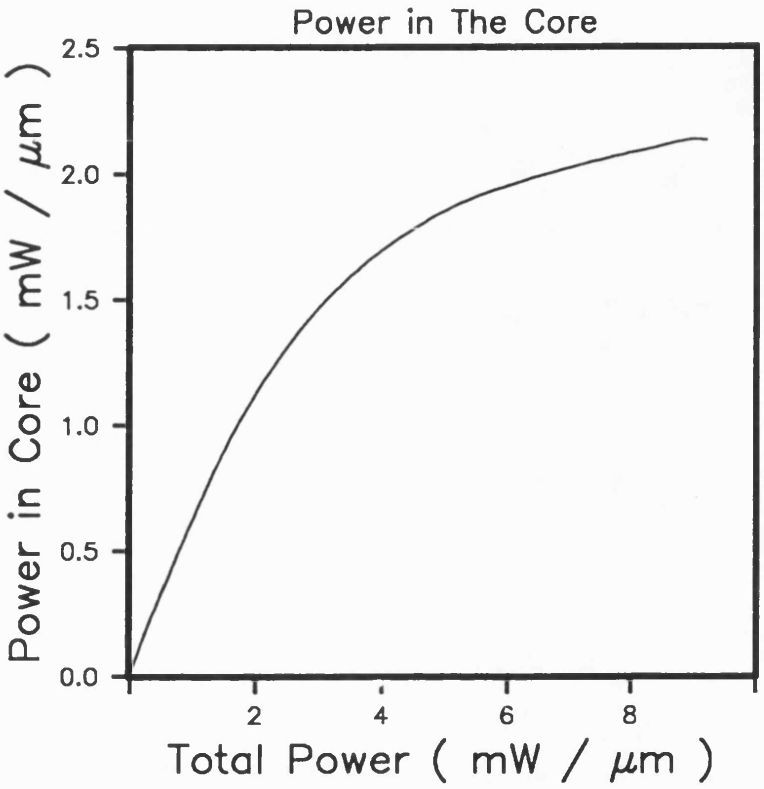

Figure 4.10 A plot of the power confined to the core as a function of the total power, indicating that the defocusing nonlinear waveguide behaves as an optical limiter.

4.11 References

M. A. Afromowitz, "Refractive index of $Ga_{1-x}Al_xAs$," Solid-State Commun., vol. 15, pp. 59-63, (1974).

N. N. Akmediev, K. O. Boltar and V. M. Eleonski, "Dielectric optical waveguide with nonlinear susceptibility. Asymmetric refractive-index profile," Opt. Spectrosc. (USSR), vol. 53, pp. 403-405, (1982).

A. D. Boardman and P. Egan, "Nonlinear surface and guided polaritons of a general layered dielectric structure," Journal de Physique, Colloque C5, Supplement no. 4, Tome 45, pp. 59-63, (1974).

A. D. Boardman and P. Egan, "Optically nonlinear waves in thin films," IEEE J. Quantum. Electron. vol. QE-22, pp. 319-324, (1986).

B. Broberg and S. Lindgren,"Refractive index of $In_{1-x}Ga_xAs_yP_{1-y}$ layers and InP in the transparent wavelength region," J. Appl. Phys., vol. 55, pp. 3376-3381, (1984).

W. M. Gibbons and D. Sarid, "Effects of carrier diffusion on the nonlinear response of optical waveguides," Opt. Lett., vol. 12, pp. 564-566, (1987).

P. M. Lambkin and K. A. Shore, " Asymmetric semiconductor waveguide with defocusing nonlinearity," IEEE J. Quantum. Electron., vol. 24, pp. 2046-2051, (1988).

K. Ogusu, "TE waves in a symmetric dielectric slab waveguide with a Kerr-like nonlinear permittivity," Opt. and Quantum Electron., vol. 19, pp. 73 - 77, (1987).

K. Ogusu, "TM waves guided by nonlinear planar waveguides," IEEE. Trans. Microwave Theory Tech., vol. 37, pp. 941 - 946, (1989).

W. Streifer, D. R. Scrifres, and R. D. Burnham,"Optical analysis of multiple-quantum-well lasers," Appl. Opt., vol. 18, pp. 3547-3548, (1979).

Li Kam Wa, J. E. Sitch, N. J. Mason, J. S. Roberts, P. N. Robson, "All optical multiple-quantum-well waveguide switch," Electron. Lett., vol. 21, pp. 26 - 27, (1985).

A. Yariv, "Optical Electronics," Holt, Rinehart and Winston, (1985).

Chapter Five

Nonlinear Rib Waveguides

5.1 Introduction

A natural extension of the one dimensional planar waveguide is the two dimensional channel waveguide. Here lateral confinement of optical energy is obtained by introducing a y-direction perturbation in the refractive index or effective index. This can be achieved in semiconductor waveguides, for example, by compositional changes, as in a buried heterostructure, or by dielectric loading (eg. the addition of a rib). The solutions of the wave equation for a slab waveguide can be expressed in terms of TE and TM modes each of which are described by three field components. This simple description is possible because the fields are assumed to be independent of y. Two-dimensional guides not only require additional field components but also impose additional boundary conditions. However, the extra field components are not a major concern since they are normally small relative to the respective components corresponding to a slab guide. The imposition of further boundary conditions is more problematic and, in general, only satisfied by hybrid TE and TM modes. Analytic solutions to this problem are not possible and so require the use of either approximate or numerical techniques. A comparison of a number of the available methods has been made (Working group I, COST 216, 1989) which includes an evaluation of the popular effective index (EI) method. This chapter briefly reviews the EI method before applying it in a self-consistent way to a nonlinear waveguide. Results are presented and finally polarisation effects are considered in MQW guides.

5.2 The Effective Index (EI) Method

A specific example of a channel waveguide is the rib guide illustrated in Figure 5.1, where the co-ordinate axes and dimensions are defined. The EI method establishes an "effective refractive index" for the region inside the rib (region I) by solving the problem of a one dimensional slab waveguide formed if the rib were infinitely wide. A similar procedure for the region outside the rib (region II) solves for the slab waveguide obtained as if the rib width were zero. These

effective indices are designated n_I and n_{II}, and define a further planar guide in the orthogonal direction (see Figure 5.1).

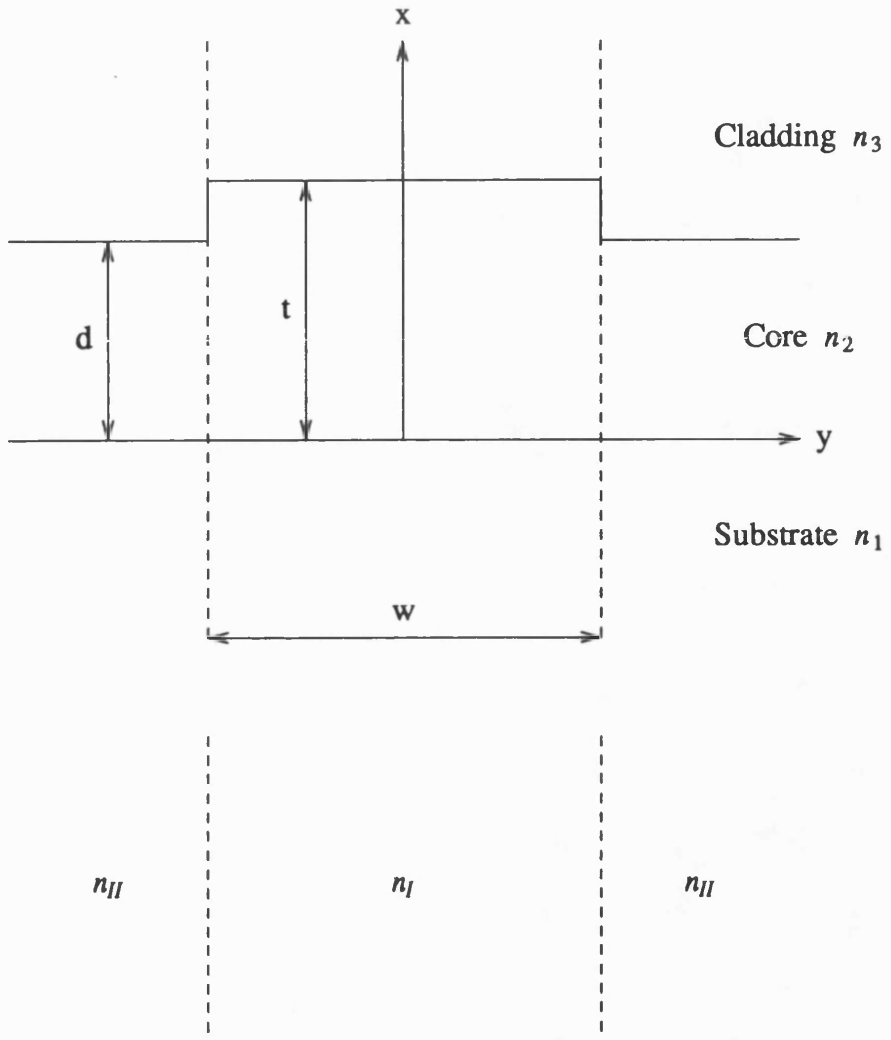

Figure 5.1 The rib-guide structure with the associated effective lateral guide.

The solution to this symmetric structure, with a core layer thickness w, can give a good approximation to the propagation constants of modes supported by the rib waveguide. If the transverse, x-direction, guides are solved for the TE mode, it is usual to solve the lateral, y-direction, effective guide for the TM mode and vice-versa. An optical field distribution can be derived as the product of the field profile given by the transverse calculation and the field profile given by the lateral calculation. The approximation inherent in this method is that by considering the waveguide initially as three distinct regions, field continuity has been ignored at the rib edges. The method is thus most accurate when the rib height is small, and the rib width is much greater than the height. In a nonlinear context these conditions are likely to be satisfied since the induced index perturbation should be

of the same order as the maximum nonlinear change in refractive index. The propagation constants calculated by this method are greater than the true values (Working group I, COST 216, 1989).

5.3 The Nonlinear Rib Waveguide Analysis

Nonlinear rib geometries have been used in a number of experiments to enhance nonlinear effects. Normandin and Houghton (1989) demonstrated an optical limiter for fibre optics using a channel waveguide. It consisted of a silicon thin film on a doped silicon substrate and relied on a defocusing, band filling nonlinearity at an operating wavelength of $1.06\,\mu m$. Incident light from a fibre determined the refractive index profile in the coupling region of the guide and the resultant waveguiding conditions were computed in view of this imposed index distribution. The theoretical treatment did not consider nonlinear guided modes and only took planar geometry into account. A modal analysis of a nonlinear rib guide has been given by Chrostowski and Chelkowski (1987), but this considered a self-focusing Kerr nonlinearity in the guide substrate.

The guide that will be treated here is the analogue of the guide illustrated in Figure 5.1, with the core considered to be nonlinear . The dimensions are chosen for monomode operation in the linear regime, a property that will be preserved with increasing power by the defocusing nature of the refractive index changes. In essence, the analysis combines a series of x-direction nonlinear slab waveguides with a y-direction multi-layer linear guide to give a propagation constant n_{rib} in the manner of an EI approximation.

It has already been established that the shape of the electric field and the value of the modal index in a nonlinear slab waveguide depend on the value of the field E_0 at the interface between the nonlinear core and substrate. In the rib guide E_0 is now a function of the y-co-ordinate. Consider the rib guide to be divided into N+2 regions, as in Figure 5.2 .

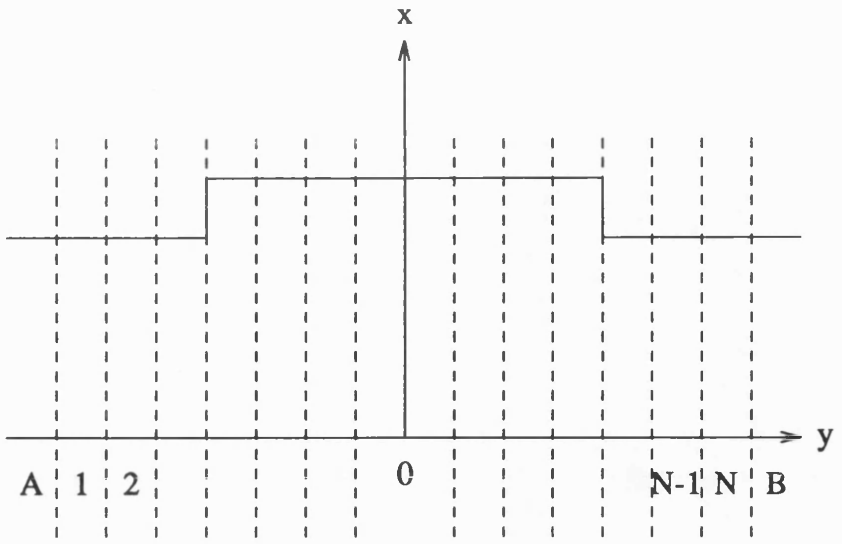

Figure 5.2 Self-consistent multilayer (N-layer) model

Each region is then treated as an infinitely wide nonlinear planar guide that can be solved for an interface intensity value based on an $E_0(y)$ distribution. This will give for the i'th region an effective index n_i. The regions A and B can be treated as linear planar guides given that they are sufficiently laterally displaced from the rib for the optical field to be negligible. Due to symmetry, the effective indices for these regions will be equal and so are designated n_A. The x-direction planar waveguide solutions can now be used to form an N layer, y-direction, linear waveguide. For a self consistent solution to the rib waveguide, the field associated with the multilayer solution n_{rib} should correspond exactly with the $E_0(y)$ distribution used to generate the effective multilayer guide. If the correspondence is not within a tolerance, a correction must be made and the process repeated. An initial $E_0(y)$ distribution is calculated assuming the guide to be entirely linear. In more detail the above technique involves the following steps:

1. Assign a value to $E_0^2(0)$ that will remain unaltered for the calculation.

2. By assuming the rib to be linear, calculate a lateral field distribution $\phi(y)$.

3. For the i'th region calculate a weighting factor w_i as follows:

$$w_i = \frac{\phi_i^2}{\phi_{\max}^2} \quad i = 1,N \,, \tag{5.1}$$

where ϕ_i^2 is the average intensity in the i'th region given by:

$$\phi_i^2 = \frac{\int_{y_i}^{y_i + \Delta y} \phi^2(y)\, dy}{\Delta y}, \qquad ((5.2)$$

and

$$\phi_{max}^2 = \text{maximum } (\phi_i^2) \;\; i = 1, N . \qquad (5.3)$$

4. In each region solve the x-direction nonlinear planar guides using an interface intensity given by $w_i E_0^2(0)$.

5. Recalculate $\phi(y)$ and compare with the previous distribution.

6. Return to step 3 if the required tolerance is not met.

The linear multilayer problem is solved via a transverse resonant method, details of which are given in the next chapter. The EI technique outlined here is capable of straightforward extension to other channel structures and can also take into account polarisation effects.

Some care must be taken when setting the number and width of the layers used in the y direction discretisation. To ensure that power calculations are realistic, the "window" over which the integrations are made must be large enough for the field to become negligible at the window edges. It is also useful to note that wider strips can be used in the shoulder regions of the rib guide where the changes in the field intensities, and hence the effective index profile, will be slower. Conversely, a high packing density can be used under the rib itself where the fastest changes occur. Figure 5.3 shows how, for a fixed intensity $E_0^2(0)$, the calculated total power varies as a function of the number of layers used to discretise the guide over a given width. The method converges for increasing N, but more importantly, converges for the relatively small value of ~30.

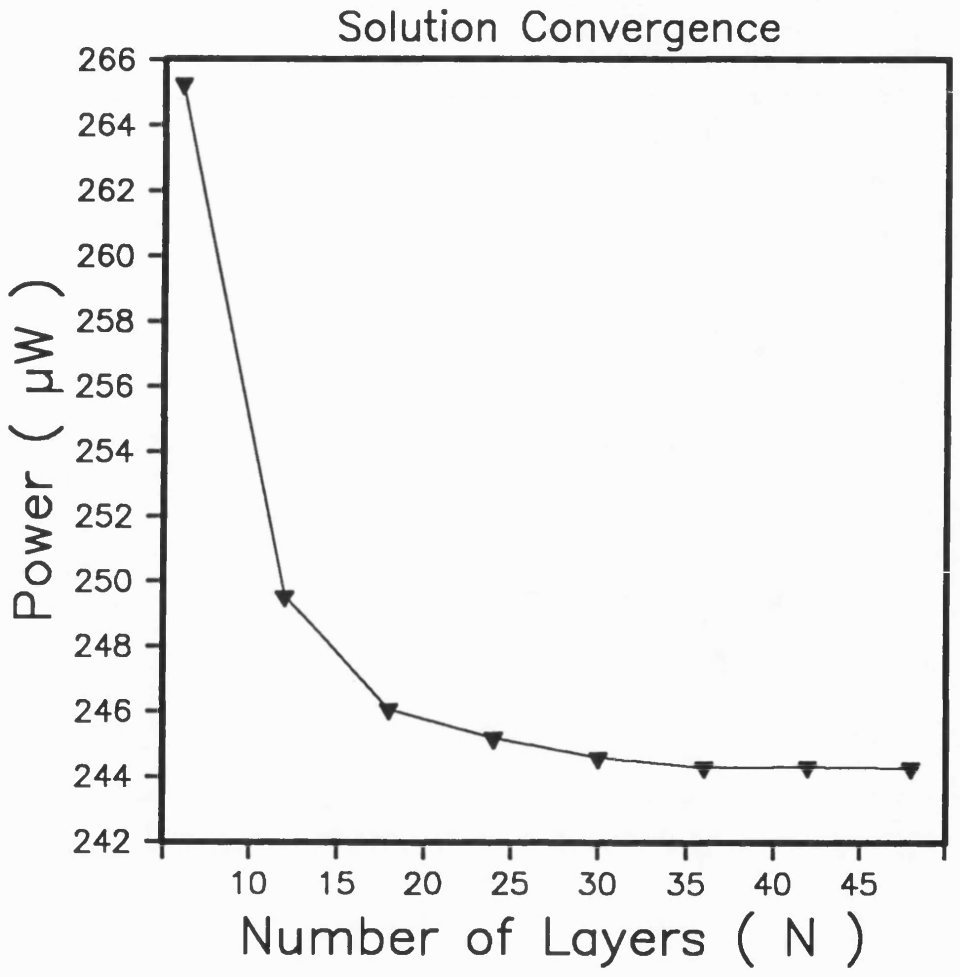

Figure 5.3 An example of the convergence of a solution of a nonlinear rib waveguide. N is the number of layers used in the discretisation of the lateral effective guide.

5.4 Results

Calculations have been performed (Lambkin and Shore, 1989) (Lambkin and Shore, 1988) for a guide fabricated with the same material parameters as the MQW, asymmetric, planar guide described in the previous chapter. The core is designed to exhibit a band edge nonlinearity at 1.55 μm and again a representative value of $n_I = 10^{-11}\ W/m$ is taken to model the nonlinearity. The shoulder thickness d is 1.0 μm whilst the rib itself is 3 μm wide and 1.3 μm high; this means the guide is single moded. All calculations have been performed using N=45.

Figure 5.4 shows how the effective index of the whole guide n_{rib} varies with total power. It also shows the variation with the power confined in the core below the rib, namely, the power in the channel. For completeness, results for a predominantly TM mode are also included. The behaviour can be explained in terms of the loss of lateral confinement as the optical field washes out the y-direction index perturbation. Lateral guiding is finally lost when $n_{rib} = n_A$. A limiting action can be observed by realising that the power in the channel is tending towards a constant, whilst the total power increases monotonically as the field spreads laterally. It is instructive to compare the effective index profiles for the low and high power solutions. In Figure 5.5 the depressed index profile, induced by the defocusing nonlinearity, is superimposed on the low power, linear profile. The fact that both coincide at the window edges indicates that the guide was considered over a sufficient width for the powers to be representative. The respective guide solutions have also been shown. The associated field intensity profiles are given in Figures 5.6, 5.7 . They are obtained by normalising the intensities to the value at the origin. If the guide were linear the distributions would therefore be identical for any power. In contrast, Figure 5.7 clearly shows that at the high power the lateral confinement is breaking down. The discontinuities in the contours represent errors induced by the EI method failing to satisfy the boundary conditions at the rib edge.

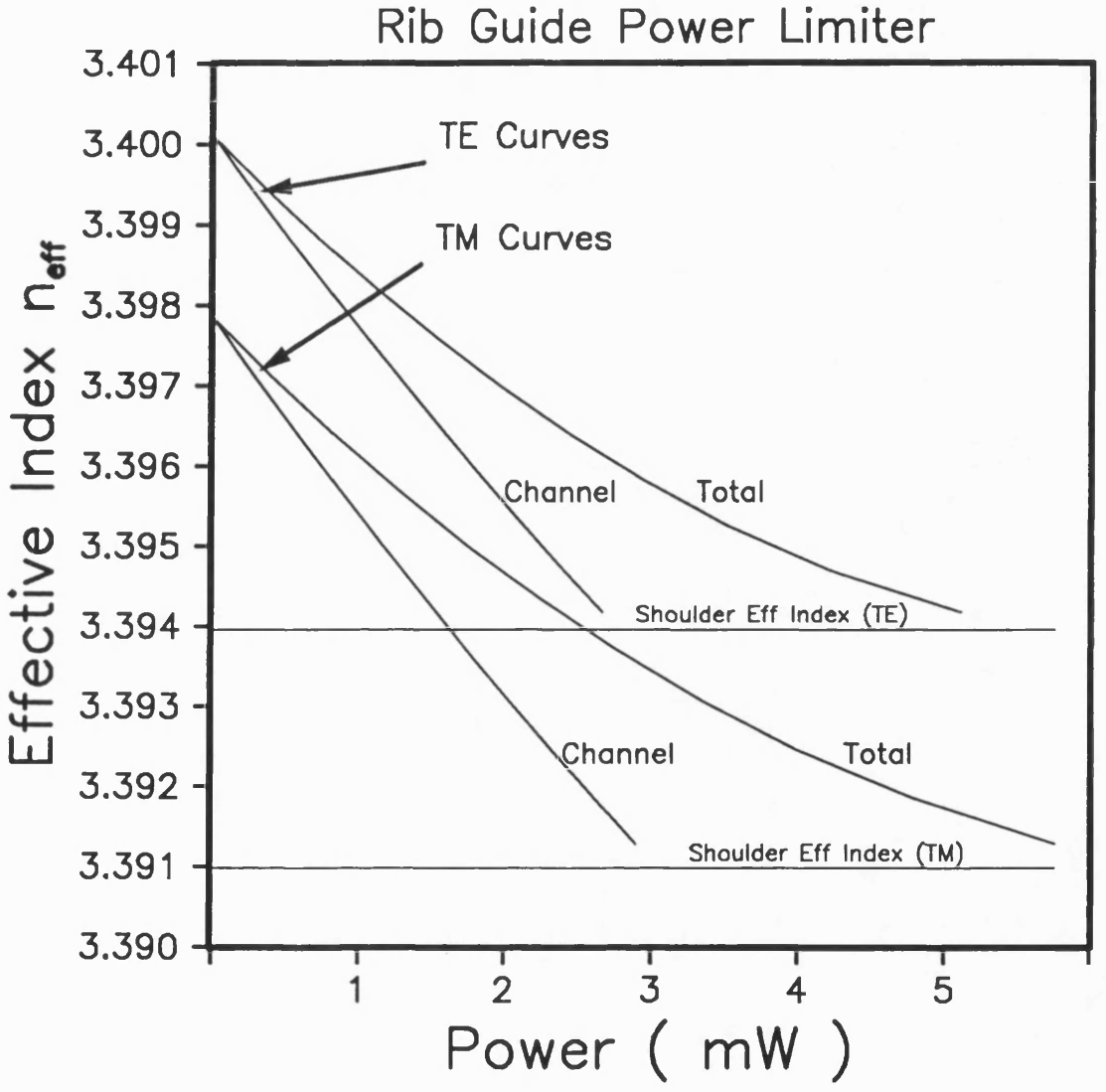

Figure 5.4 The power dispersion curves for the nonlinear semiconductor rib waveguide. Results are given for both TE and TM polarisations and the low power effective indices of the shoulder regions are also indicated. The curves labelled 'Channel' relate solutions to the power confined under the rib.

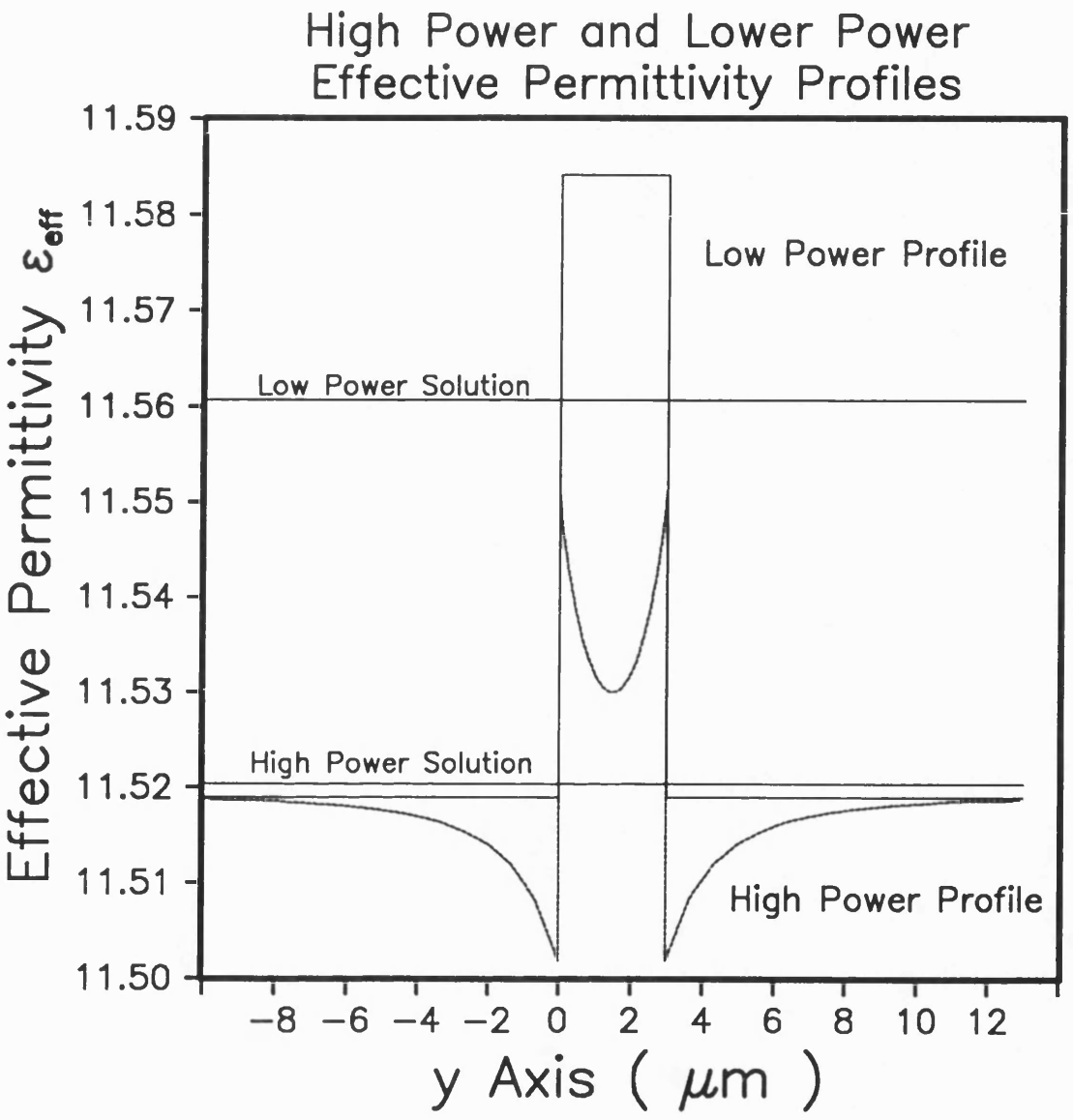

Figure 5.5 A nonlinear, high power, lateral permittivity profile associated with nonlinear semiconductor rib waveguide. The linear, low power, profile is also shown, as are the solutions corresponding to the two cases.

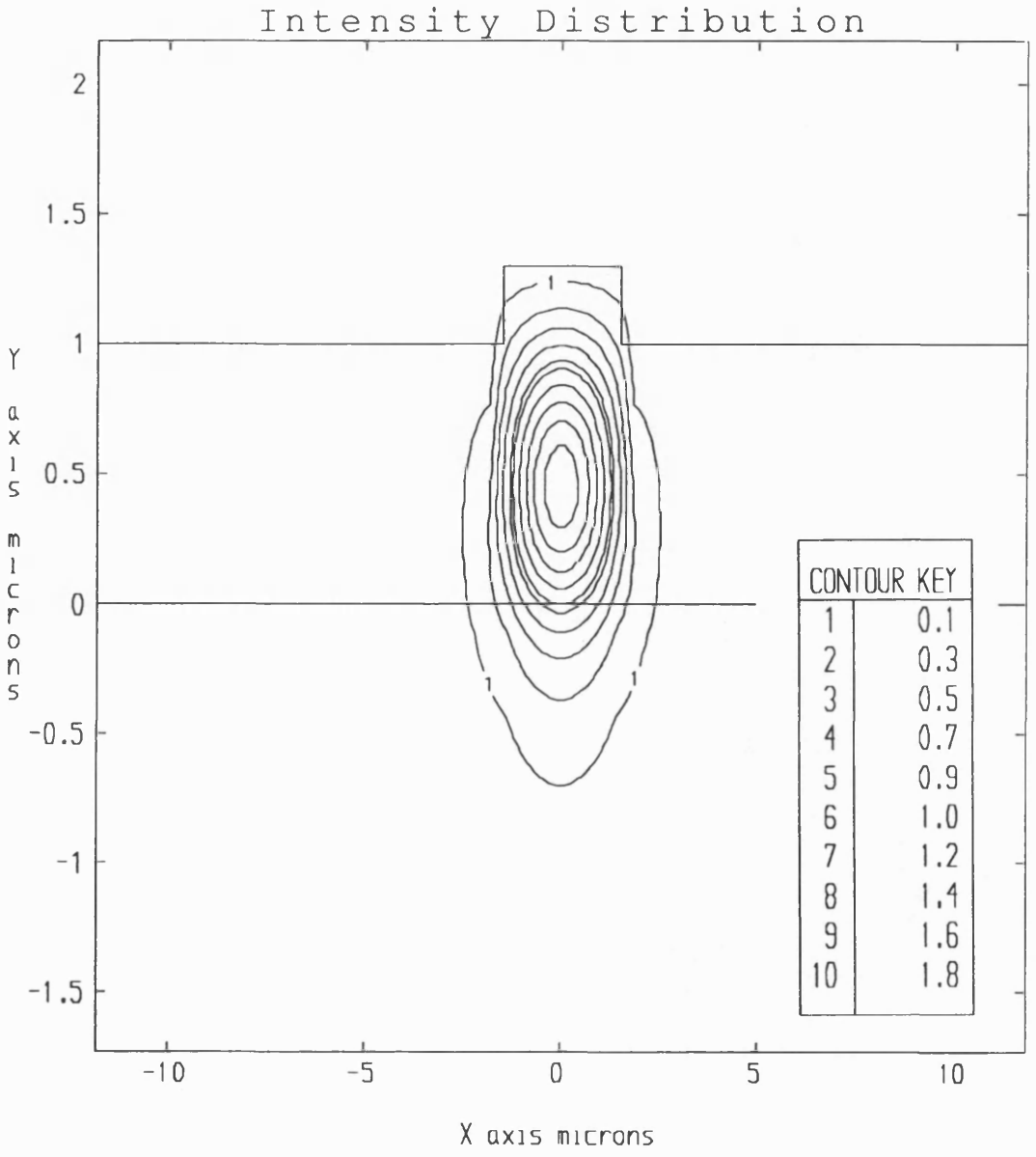

Figure 5.6 Normalised intensity distribution for a linear, low power mode.

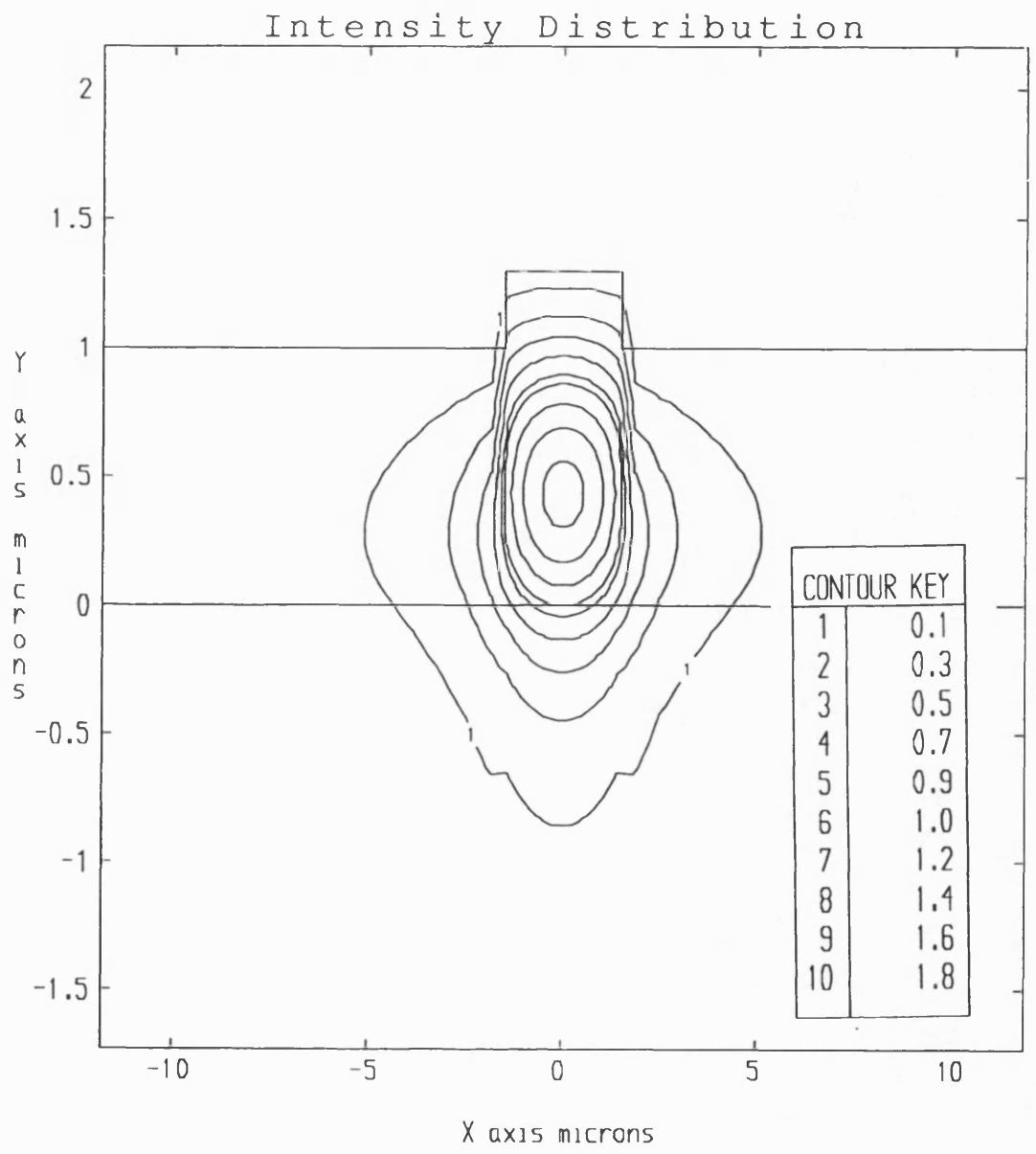

Figure 5.7 Normalised intensity distribution for a nonlinear, high powered mode.

It is immediately obvious from Figure 5.5 that the nonlinearity outside the rib mitigates against the suppression of a lateral index step. If the nonlinearity were confined to the rib only, then the limiting should occur at lower powers. This is confirmed in Figure 5.8 where calculations have been performed for such a structure and compared with the previous one. The more efficient use of the defocusing nonlinearity means that the limiting occurs for powers reduced by ~ 2/3. For approximately the same power represented in Figure 5.7, Figure 5.9 shows the permittivity profile for the modified structure. The lateral perturbation has almost vanished and as a result the lateral spreading of the intensity has greatly increased. This is illustrated in Figure 5.10.

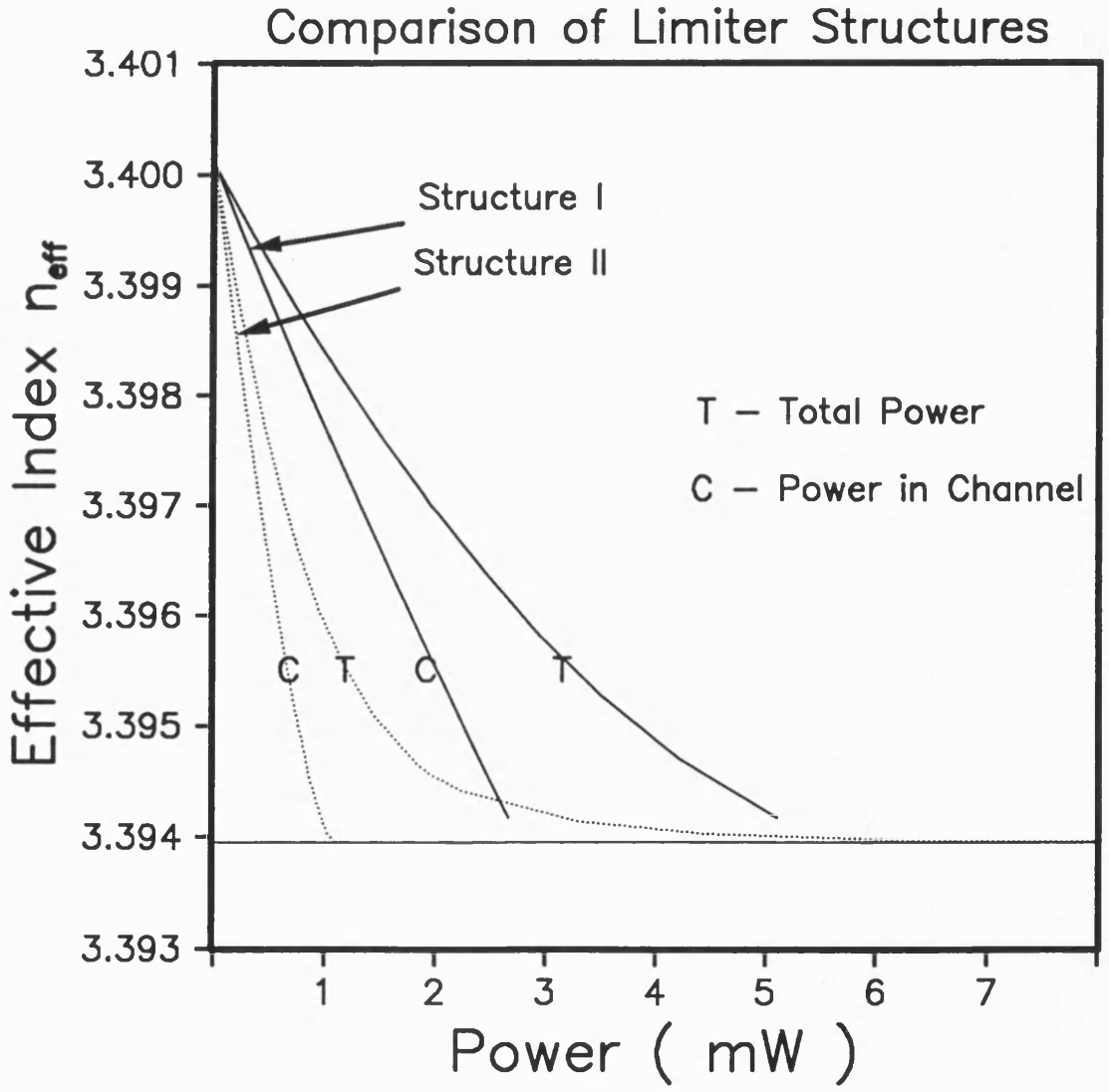

Figure 5.8 A comparison of power dispersion curves for Structure I - Nonlinearity present in rib and shoulder regions and Structure II - Nonlinearity under rib only.

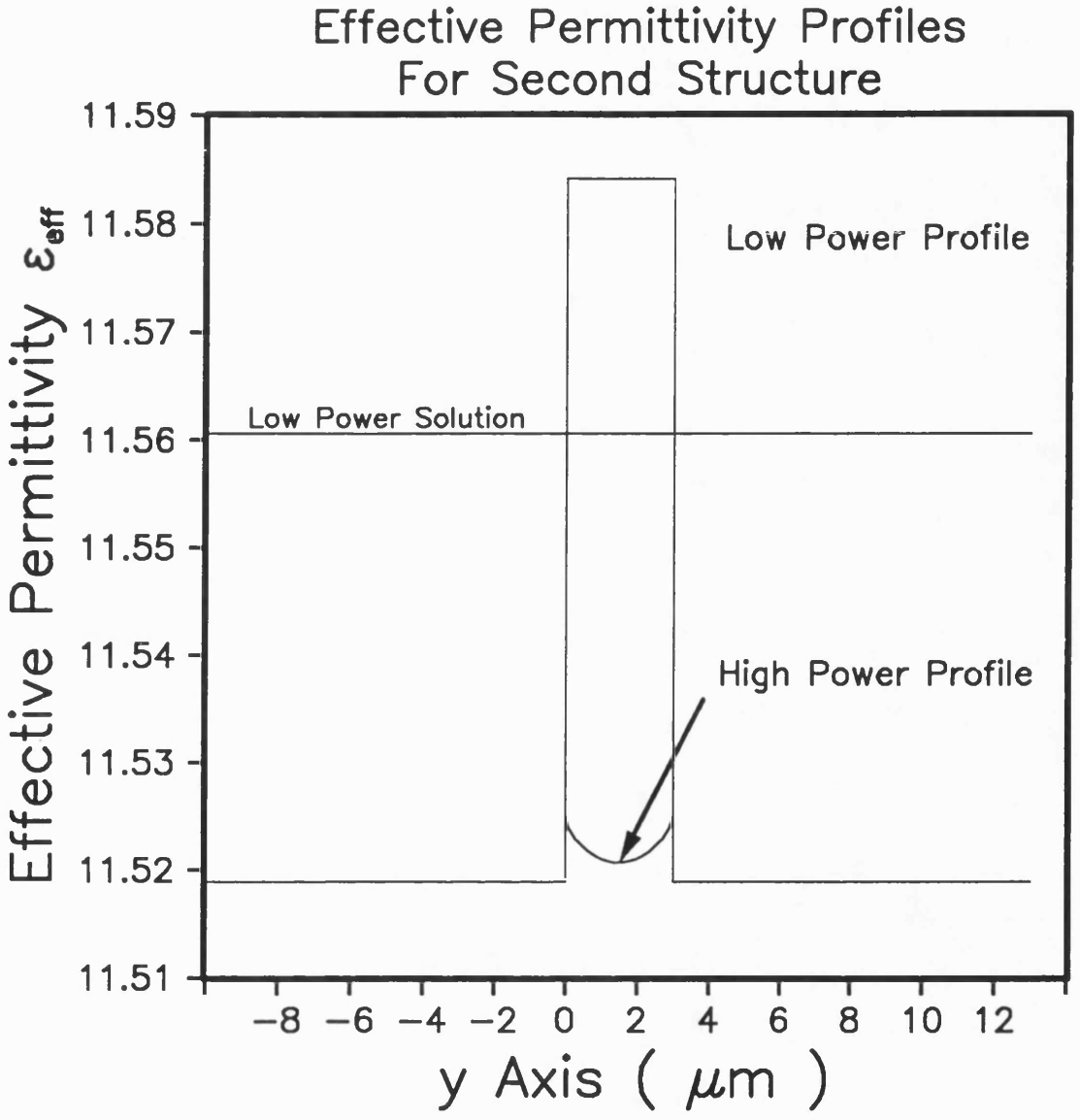

Figure 5.9 A nonlinear, high power, lateral permittivity profile associated with Structure II - Nonlinearity under rib only. The linear, low power profile is also shown.

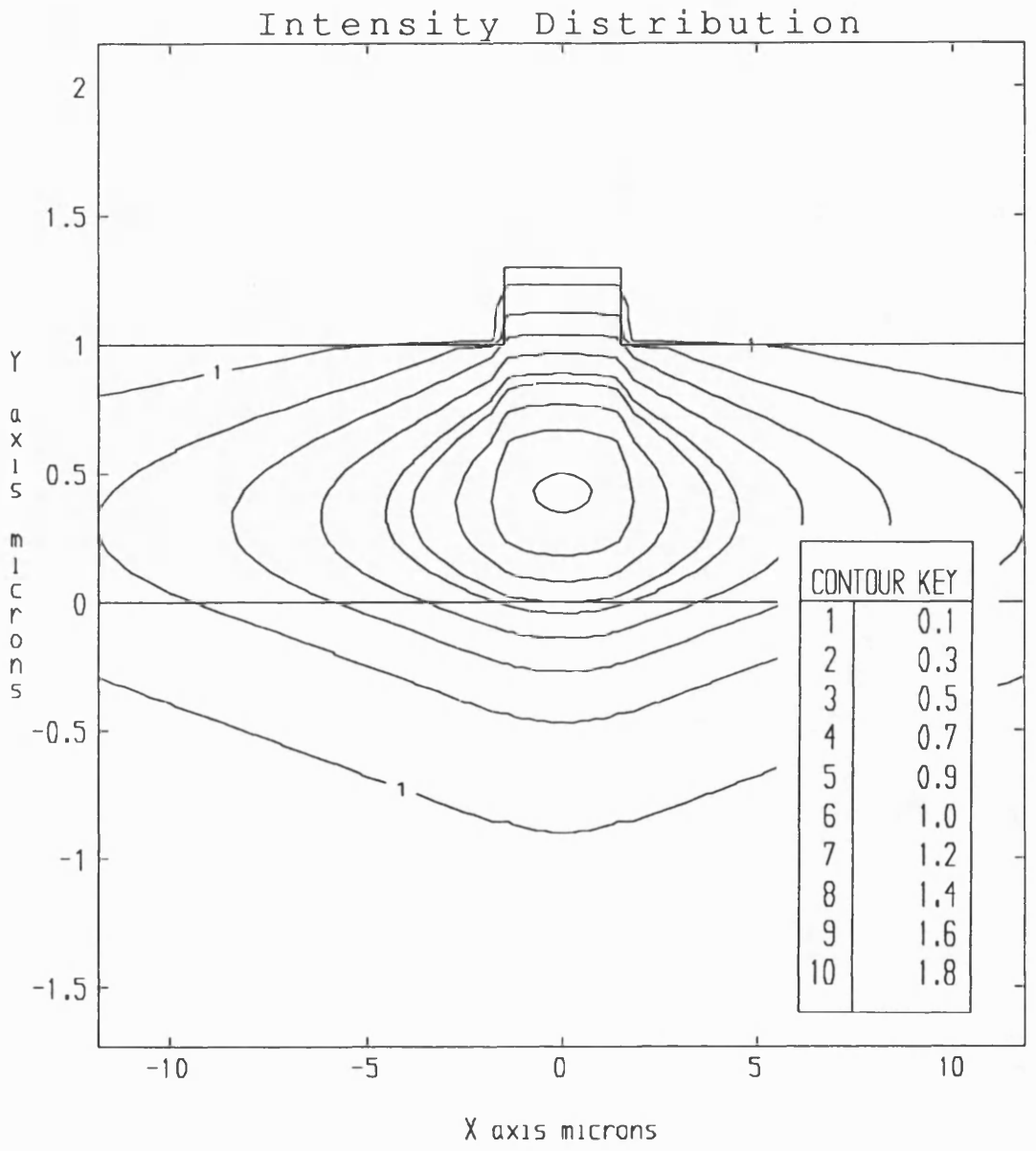

Figure 5.10 Normalised intensity distribution for a nonlinear, high powered mode. The nonlinearity is restricted to the region under the rib.

5.5 Polarisation Effects

For the calculations presented here it has been assumed that the nonlinearity corresponding to TE and TM modes will be equal. This is not likely to be the case for multiple quantum well waveguides. Absorption should be significantly reduced for light polarised perpendicular to the layers. This has been experimentally demonstrated both in a single quantum well waveguide (Weiner, 1985) and in a GaAs / AlGaAs MQW nonlinear directional coupler (Jin, 1988). In the latter experiment the excitonic resonances for the light polarised parallel and perpendicular were separated by approximately 6 nm. Weiner (1985) suggested that an additional degree of freedom in guide design would be introduced by this "strong linear and nonlinear dichroism". However, by operating away from the excitonic resonance, as in the guides considered here, the dichromatic effect will be greatly reduced.

5.6 Conclusions

A straightforward method of calculating the mode shapes of channel waveguides with a nonlinear film has been presented. The method should provide a good approximation to the exact solution given that:

(i) The rib width is sufficiently large with respect to the core thickness .

(ii) The film to substrate index step is relatively small.

This is confirmed by a comparison, presented in Appendix 2, between results from the semi-analytical approach given here and results from a numerical investigation using the Beam Propagation Method (BPM).

5.7 References

J. Chrostowski and S. Chelkowski, "Analysis of an optical rib waveguide with a nonlinear substrate," Opt. Lett., vol. 12, pp. 528 - 530, (1987).

R. Jin, C. L. Chuang, H. M. Gibbs, and S. W. Koch, J. N. Polky, G. A. Pubanz, "Picosecond all-optical switching in single-mode GaAs/AlGaAs strip-loaded nonlinear directional couplers," Appl. Phys. Lett., vol. 53, pp. 1791 - 1793, (1988).

P. M. Lambkin and K. A. Shore, "Non-linear semiconductor ridge waveguides," in IEE *Colloquium on Nonlinear Optical Waveguides* (Institution of Electrical Engineers, London, 1988), paper 12, (1988).

P. M. Lambkin and K. A. Shore, "Analysis of an optical rib waveguide with a nonlinear substrate," J. Opt. Soc. Soc. Am. B, vol. 6, pp. 669 - 674, (1989).

R. Normandin and D. C. Houghton, "Fully adjustable optical limiter for fiber optics using silicon films," Appl. Phys. Lett., vol. 54, pp. 1836 - 1838, (1989).

J. S. Weiner, D. S. Chelma, and D. A. B. Miller, H. Haus, A. C. Gossard and W. Wiegmann, C. A. Burrus, "Highly anisotropic optical properties of single quantum well waveguides," Appl. Phys. Lett., vol. 47, pp. 664 - 667, (1985).

Working group I, COST 216, "Comparison of different modelling techniques of longitudinally invariant integrated optical waveguides," IEE. Proc., vol. 136, Pt. J, pp. 273 - 280, (1989).

Chapter Six

Multilayer Guiding Structures

6.1 Introduction

Multilayer configurations occur frequently in optical device design eg. superlattices and MQW'S. The analysis of stratified media can also be applied to effective multilayers generated by replacing a continuous effective profile by a large number of homogeneous layers. This technique has been applied to the problem of bending losses in curved waveguides (Ghatak and Thyagarajan, 1989), and was used earlier in chapter five to study the mode profiles of nonlinear ridge guides.

This chapter firstly considers linear multilayer structures with particular emphasis placed on periodic structures and the phenomenon of Bragg reflection. The ideas of transmission matrices and transverse resonance are introduced using an equivalent transmission line analysis of linear structures. Analogous nonlinear structures are then considered and an analysis of a finite, nonlinear, Bragg reflection waveguide is presented.

6.2 Linear Multilayer Structures and Transverse Resonance

The structure whose guided modes are being sought is shown in Figure 6.1 . Only the TE modes will considered so the the electric and magnetic fields will be given by $\mathbf{E} = \mathbf{E}(0, E_y, 0)$ and $\mathbf{H} = \mathbf{H}(H_x, 0, H_z)$. Assuming harmonic solutions, the only non-zero electric field component is written as:

$$E_y(x, z, t) = E_y(x)\, exp\,(\, i\,(\omega t - k_z z))\,. \tag{6.1}$$

A mode will then be given by the solution of the scalar wave equation:

$$\frac{d^2 E_{yn}}{d\,x^2} + k_{xn}^2 E_{yn} = 0\,, \tag{6.2}$$

in each of the $N + 2$ layers where the transverse propagation constant is given by:

$$k_{xn}^2 = k_0^2 n_n^2 - k_z^2\,. \tag{6.3}$$

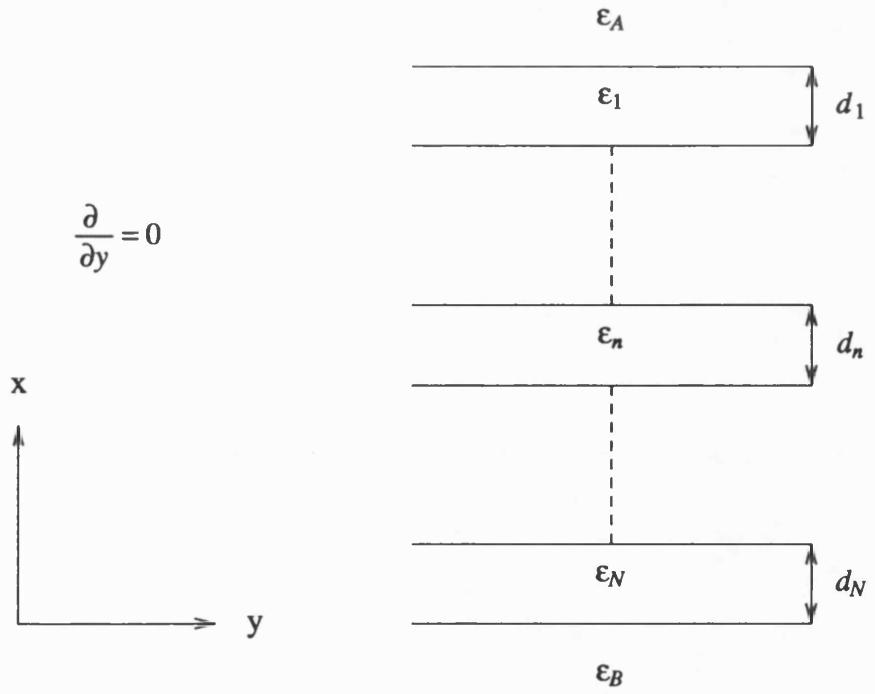

Figure 6.1 Multilayer Dielectric Guide

Similarly the equation governing the transverse magnetic field will be:

$$\frac{d^2 H_{zn}}{d x^2} + k_{xn}^2 H_{zn} = 0 , \tag{6.4}$$

The transverse wave Eqs. 6.2 and 6.4 governing E_y and H_z are exactly analogous to those governing the voltage V and current I on a transmission line. As a result, the dielectric multilayer guide can be modelled by an equivalent transmission line network for which analysis techniques are well established. The method involves replacing each dielectric layer by a transmission line element as in Figure 6.2 .

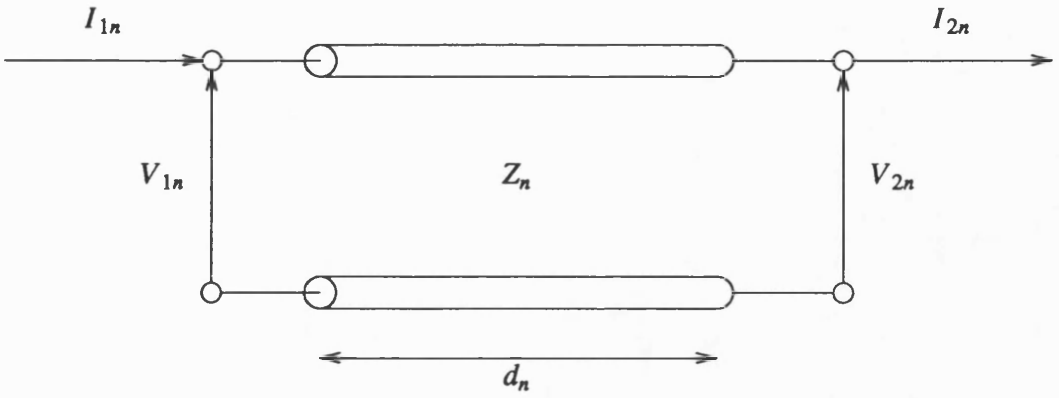

Figure 6.2 Transmission Line Element

The characteristic impedances are given for the TE mode as:

$$Z_n = \frac{\omega\mu_0}{k_{xn}}, \tag{6.5}$$

and by analogy

$$V(x) = E_y(x), \quad I(x) = H_z(x), \quad Z(x) = \frac{V(x)}{I(x)} = \frac{E_y(x)}{H_z(x)}. \tag{6.6}$$

The solution method relies on the ability to relate the input and output impedances via the following relationship (Whinnery and Van Duzer, 1984):

$$\frac{V_{1n}}{I_{1n}} = Z_n \frac{\dfrac{V_{2n}}{I_{2n}} - i\, Z_n \tan(k_{xn} d_n)}{Z_n - \dfrac{V_{2n}}{I_{2n}} \tan(k_{xn} d_n)}, \tag{6.7}$$

or more conveniently

$$\begin{bmatrix} V_{1n} \\ I_{1n} \end{bmatrix} = [T_n] \begin{bmatrix} V_{2n} \\ I_{2n} \end{bmatrix}, \tag{6.8}$$

where

$$[T_n] = \begin{bmatrix} \cos\theta_n & iZ_n \sin\theta_n \\ i\dfrac{1}{Z_n}\sin\theta_n & \cos\theta_n \end{bmatrix}, \tag{6.9}$$

and

$$\theta_n = k_x d_n . \tag{6.10}$$

The matrix T_n is known as the transmission or ABCD matrix for the circuit element. It simply relates the the input and output voltages and currents (E_y and H_z) for the circuit element of the network. A transmission matrix for the whole network is formed by multiplying all the constituent matrices for each element. The final equivalent circuit is now represented by Figure 6.3 where:

$$\begin{bmatrix} V_{11} \\ I_{11} \end{bmatrix} = [T_n] \begin{bmatrix} V_{2N} \\ I_{2N} \end{bmatrix}, \tag{6.11}$$

$$\text{and } [T] = \prod_{n=1}^{N} [T_n] . \tag{6.12}$$

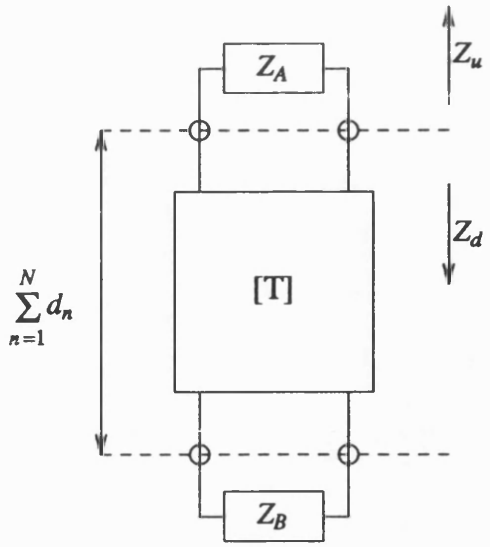

Figure 6.3 The Lumped Equivalent Transmission Line.

Suppose that the input impedance of the dielectric in region $x > d$ on the surface $x = 0$ is Z_u, and that for the region $x < d$ it is Z_d. The principle of transverse resonance then states that the condition,

$$Z_u + Z_d = 0\,, \tag{6.13}$$

is necessary for a guided mode to exist (Collin, 1960). Since $Z_u = Z_A$ and Z_d is given by Eq. 6.11 the resonance will produce the following eigen value equation:

$$T_{11} + \frac{T_{12}}{Z_B} + Z_A(T_{21} + \frac{T_{22}}{Z_B}) = 0\,. \tag{6.14}$$

As in the case of the single slab guide, a guided mode will be exponentially decaying in the substrates and so Z_A and Z_B will be purely imaginary. The solution technique is based on the a-priori knowledge of the form of these fields. For a given k_z the method involves testing the continuity of one of the fields across a chosen interface given that all the fields have been matched at all the other boundaries. The transverse resonance technique was used to solve the multilayer guides arising from the analysis of nonlinear two dimensional structures treated in chapter five.

6.3 Nonlinear Multilayer Structures

The problem of a Kerr-type nonlinearity occurring arbitrarily in a multilayer system was first addressed by Trutschel et al (1988). They considered layers,

either linear or nonlinear, sandwiched between two linear bounding media. Their method of solution is, in essentials, identical to that outlined for the all-linear guide described above. It relies on the ability to construct a transmission matrix that relates the transverse components of a field at one interface of a layer to the components at the other. For a TE mode the components are E_y and H_z, or equivalently E_y and $\dot{E}_y$, where the derivative is with respect to x. The major difference from the linear analysis is that the matrix elements A, B, C, and D will themselves be functions of the interface fields, and will be described by Jacobi elliptic functions. As expected the mode solutions in the nonlinear case will therefore be power dependent.

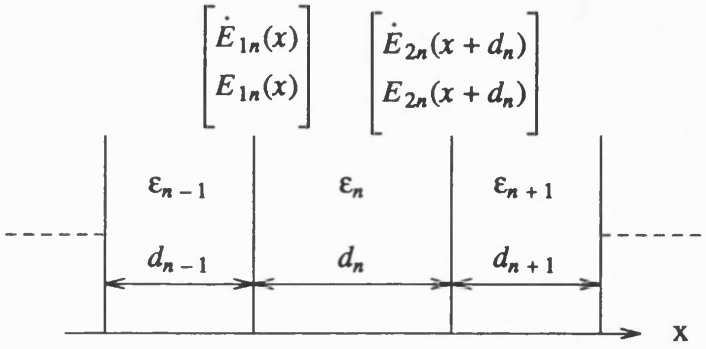

Figure 6.4 The n'th Nonlinear Layer

Consider the n'th layer in a stack shown in Figure 6.4 . It is assumed to be characterised by the following Kerr-type nonlinearity:

$$\varepsilon_{nl}(x) = \varepsilon_n + \alpha_{nl} \mid E \mid^2 , \tag{6.15}$$

with a background linear dielectric constant of ε_n. The field inside the layer is assumed to vary as:

$$E_n(X_n) = P_n \, cn(q_n(X_n - X_{0n}), m_n) , \tag{6.16}$$

where $X_n = k_0 x$. The relationships of $P_n(k_{xn})$, $q_n(k_{xn})$, and $m_n(k_{xn})$ to each other have already been established in the treatment of the nonlinear planar guide and are given by Eqs. 4.32 - 4.34 . The fields inside the layer are then related to the input fields by:

$$\begin{bmatrix} E_n(X_n) \\ \dot{E}_n(X_n) \end{bmatrix} = \begin{bmatrix} A_n & B_n \\ C_n & D_n \end{bmatrix} \begin{bmatrix} E_{n0} \\ \dot{E}_{n0} \end{bmatrix}, \tag{6.17}$$

where

$$A_n = \frac{1}{R_n(X_n)} cn(q_n X_n, m_n), \tag{6.18}$$

$$B_n = \frac{1}{q_n R_n(X_n)} sn(q_n X_n, m_n)\, dn(q_n X_n, m_n), \tag{6.19}$$

$$C_n = \frac{q_n S_n(X_n)}{R_n^2(X_n)} sn(q_n X_n, m_n)\, dn(q_n X_n, m_n), \tag{6.20}$$

$$D_n = \frac{T_n(X_n)}{R_n^2(X_n)} cn(q_n X_n, m_n), \tag{6.21}$$

and use has been made of the following abbreviations:

$$R_n(X_n) = 1 - m_n(1 - \frac{E_{0n}^2}{P_n^2})\, sn^2(q_n X_n, m_n), \tag{6.22}$$

$$S_n(X_n) = 1 - m_n(1 - \frac{E_{0n}^2}{P_n^2})\, [1 + cn^2(q_n X_n, m_n)], \tag{6.23}$$

$$T_n(X_n) = 1 - m_n(1 + \frac{E_{0n}^2}{P_n^2})\, sn^2(q_n X_n, m_n). \tag{6.24}$$

As in the linear multilayer guide, the solution technique requires an a-priori knowledge of the fields in the substrates. These are taken as exponential for a guided mode. For a given electric field value at a substrate boundary, say $E(x=0)$, then $\dot{E}(x=0)$ is automatically determined by a k_z and the restriction of an exponential decay. The transmission matrix can then be used to move consecutively across the remainder of the guide to the opposite half-space boundary. Here the output field and derivative can be tested for consistency with the assumption of exponential decay in this region. Any linear layers within the stack will also be adequately treated by the transmission matrix since in the linear limit the moduli of the elliptic functions will become zero and the matrix will reduce to that given in section 6.2 .

6.4 Periodic Structures

A comprehensive theory of electromagnetic propagation in periodic stratified media was first presented by Yeh (1977). It has a strong formal similarity to the quantum theory of electrons in crystals and hence makes use of the concepts, familiar in the study of transmission lines, of Bloch modes and forbidden gaps (Brillouin, 1953). Here the subject will be introduced via a less rigorous ray optics approach using the idea of Bragg scattering and the Bragg condition.

6.4.1 Bragg Reflection

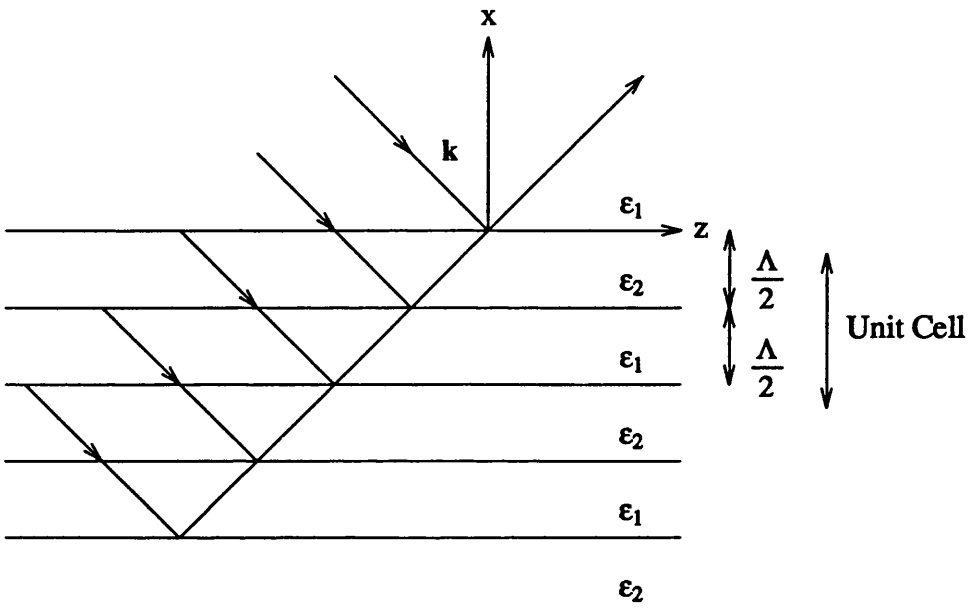

Figure 6.5 The Bragg Condition

Consider a plane wave incident upon a stack of periodic dielectric layers at an angle θ_i as shown in Figure 6.5 . It is further assumed that the fractional difference between ε_1 and ε_2 is small. Under these circumstances ray optics can be applied to determine the angle of incidence for a strong reflection. The restriction on the dielectric constants means transmission changes in propagation angle can be ignored, but at each boundary a fraction of the incident power will be reflected due to the discontinuity. For a strong reflection these contributions must add in phase so that:

$$k_x 2 \frac{\Lambda}{2} = 2\pi m . \tag{6.25}$$

The solution for $m = 1$ is called the first order Bragg condition and is given by

$k \sin(\theta_B) = 2\pi/\Lambda$, where θ_B is the Bragg angle.

From this analysis two points can be made. Firstly, for the Bragg condition the amount of transmitted energy will be a decreasing function of the number of layers and for an infinite stack the reflection will be total. Secondly, the fields in the stratified medium will decay away from the $x = 0$ interface. In fact the fields in this region will be described by Floquet's theorem giving an electric field of the form:

$$E_K(x, z) = E_K(x) \exp(iKx) \exp(ik_z z), \tag{6.26}$$

where $E_K(x)$ is periodic with a period Λ, ie:

$$E_K(x + \Lambda) = E_K(x). \tag{6.27}$$

The constant K is known as the Bloch wave number. For the decaying fields associated with Bragg reflection K must therefore be complex. Values of k_z and ω for which this is true are said to lie in the " forbidden " bands of the periodic medium. In general, the unit cell will consist of layers of unequal thickness and the 2π phase change will accumulate over each cell, as opposed to each individual layer, so the real part of the Bloch wave number can be written down immediately as:

$$2K_r\Lambda = m2\pi \quad \text{or} \quad K_r = \frac{m\pi}{\Lambda}, \tag{6.28}$$

where

$$K = K_r + iK_i. \tag{6.29}$$

In the theory of Yeh (1977) the restriction of a small dielectric step is lifted, as is the restriction of equal width on the unit cell layers. It is shown that the phase factor $\exp(-iKx)$ is the eigenvalue for the ABCD transmission matrix for the system. This matrix relates the complex amplitudes of the incident and reflected plane waves in one layer of a unit cell to those of the equivalent layer in the next unit cell. It may be derived for either TE or TM modes.

6.5 Bragg Reflection Waveguides

The dielectric slab waveguide relies on total internal reflection to confine energy to a high index region. In the previous section it has been established that periodic media can also behave as efficient reflectors. It is therefore feasible that light can be guided by the mechanism of Bragg reflection or by Bragg reflection in

combination with total internal reflection. In principle, such Bragg reflection waveguides (BRW's) enable lossless propagation in a low index slab, even though the indices of the periodic media might be higher than that of the slab. The BRW relies on simultaneously satisfying the Bragg condition in the reflectors and the resonant 2π phase change in the guiding layer. As a result, such a structure should display strong discrimination against higher order transverse modes since if the waveguide is designed to meet these conditions for a certain mode, they will not be satisfied by others except accidentally.

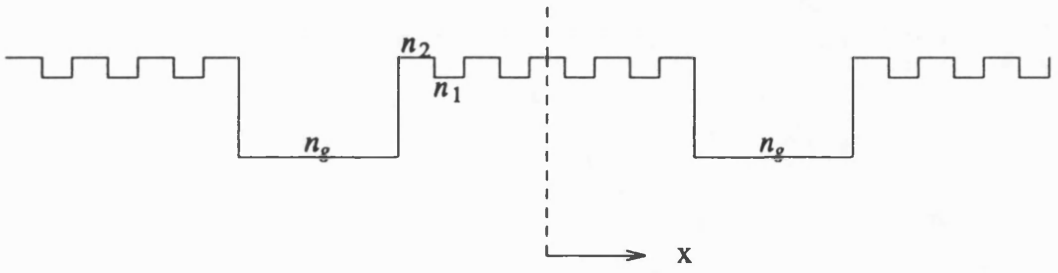

Figure 6.6 The refractive index profile for a BRW directional coupler.

The analysis of BRW's by Yeh (1977) was successfully followed by a number of experimental demonstrations (Cho, 1977), (Yeh, 1978), and (Ng, 1978). Salzman and Lenz (1989) have pointed out that the lack of subsequent interest may have been a result of fabrication difficulties concerning multilayer structures. Present technology has largely overcome these with epitaxially grown layers tightly controlled in index and thickness. Consequently, there has been a certain amount of renewed interest. Dods (1989) has recently given an exact solution for a BRW with continuous periodic variation in refractive index. The impedance for this region was established by solving a scattering problem and then used to find the transverse resonant condition. Salzman and Lenz (1989) have studied the BRW directional coupler illustrated in Figure 6.6 . Here two BRW's are brought into close proximity enabling coupling in the shared reflector. Using the Bloch function formalism the nearly-degenerate symmetric and antisymmetric modes of the composite structure were found. These characterise the coupling coefficient. It was shown that the coupling is a sensitive function of the indices in the layered media. A 100% change in coupling coefficient could be obtained by a 1% change in index. This prompted the proposal of a directional coupler switch where the required index modulations might be induced electro-optically. This sensitivity to refractive index changes also makes the BRW a promising structure in relation to variations obtained through a band filling nonlinearity. In the next section this

idea is investigated and results presented for a nonlinear Bragg reflection waveguide (NLBRW).

6.6 Nonlinear Bragg Reflectors

The theory of Floquet makes fundamental use of the property of linearity and so cannot be applied to the periodicity problem of nonlinear waveguides. The analysis of a NLBRW must use an alternative approach. An obvious solution would be to use the theory developed by Trutschel (1988) and apply it to a finite structure with a large number of layers. However, there are problems associated with this. Consider a typical finite BRW shown in Figure 6.7 .

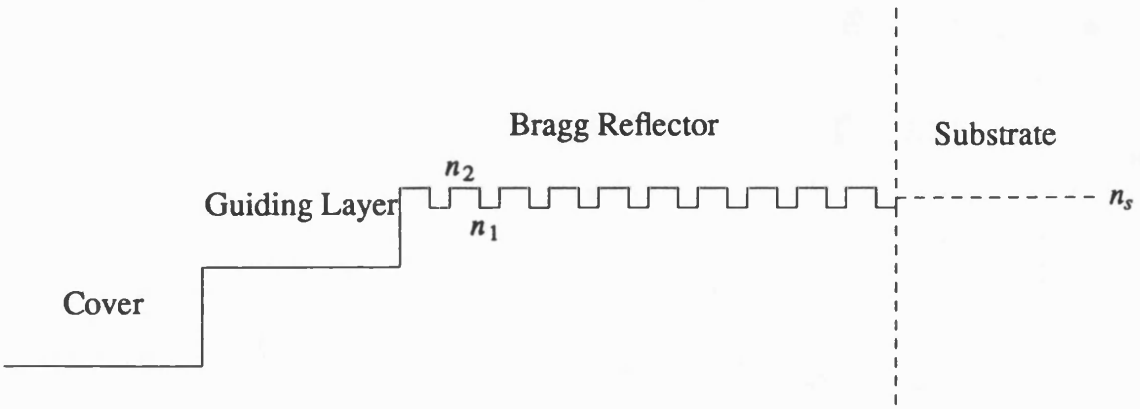

Figure 6.7. Index Profile of a Finite Bragg Waveguide

The question is how the periodic medium at the right hand boundary is to be terminated. If a substrate index n_s is used such that $n_s < n_2$ the structure will represent a wide asymmetric guide that will support many modes by total internal reflection. If $n_s = n_2$ no conventional modes can exist, but confinement from satisfying the Bragg condition may be possible. The finite number of layers means that reflections cannot be total and energy will be lost to the substrate as the mode propagates. The structure is thus lossy even in the absence of material loss. Since the field propagation is of the form $\exp(-ik_z z)$, the attenuation can be described by a complex wavenumber $k_z = k_{zr} - i \mid k_{zi} \mid$. The conservation equation Eq. 6.30,

$$k_z^2 + k_{xs}^2 = \varepsilon_s k_0^2 \,, \tag{6.30}$$

in which the s denotes substrate, will then dictate the nature of the field in the substrate. Since there is no material loss $\varepsilon_s k_0^2$ will be real and so k_{xs} must be complex: $k_{xs} = k_{xsr} + ik_{xsi}$. The transverse field in the substrate will be of the form

$\exp(i(k_{xsr} + i \mid k_{xsi} \mid)$, that is, exponentially growing. This does not strictly satisfy the definition of a guided mode that requires the field to decay to zero at $x = \pm\infty$. If ε_s is allowed to become complex, an exponential decay in both the longitudinal and transverse directions will be possible. This is equivalent to introducing material loss in the substrate. The loss is introduced purely as an artifice to account for the finite nature of the guide. The effect of the substrates can be made arbitrarily small by increasing the number of periodic layers considered.

The use of complex propagating constants in the nonlinear wave equation has a number of consequences. For a given nonlinear layer the wave equation will be:

$$\frac{d^2E_y}{dx^2} + k_x^2 + \alpha_{nl} \mid E_y \mid^2 E_y = 0 . \tag{6.31}$$

For real k_z the field E_y will be real and hence Eq. 6.31 reduces to:

$$\frac{d^2E_y}{dx^2} + k_x^2 + \alpha_{nl} E_y^3 = 0 , \tag{6.32}$$

whose solutions are defined in terms of elliptic Jacobi functions. For complex k_z the field will be complex and the reduction to Eq. 6.32 will not be strictly possible. However, for almost lossless modes it is justifiable to approximate $\alpha_{nl} \mid E_y \mid^2$ by $\alpha_{nl} E_y^2$ and make use of the analytic solutions. The other consequence of a complex propagation constant is that both argument and moduli of the elliptic functions will also be complex. There evaluation must be in terms of a Fourier expansion as outlined in chapter two.

6.6.1 Method of Calculation

A computer code has been developed to solve for a finite nonlinear Bragg reflector structure in terms of complex elliptic functions. A Muller search routine was written to search for appropriate bound mode solutions in the complex k_z plane utilising the matrix formalism (Trutschel, 1989) for the nonlinear multilayer waveguide geometry indicated above. In order to test the code, a comparison was made between an evaluation of a linear BRW using the present technique and the Bloch function approach described by Yeh (1977). The guide analysed in the comparison is shown in Figure 6.8 except that the periodic multilayer regions were now considered to be semi-infinite for the Yeh analysis. Calculations made using that approach (Fisher, 1990) were compared with the predictions of the present treatment. For example, calculated propagation constants were: 12.98145 cm^{-1} for an infinite periodic structure; 12.98147 cm^{-1} for a finite structure in

which the core is bounded by two 10 period reflector structures and for which a substrate absorption loss of 0.81 cm^{-1} was assumed. This very close agreement gave confidence in the theoretical approach adopted for the finite structure and was also taken to validate the computer codes developed for numerical work. In the next section, computational results obtained using the method described here are given for both linear and nonlinear finite BRWs.

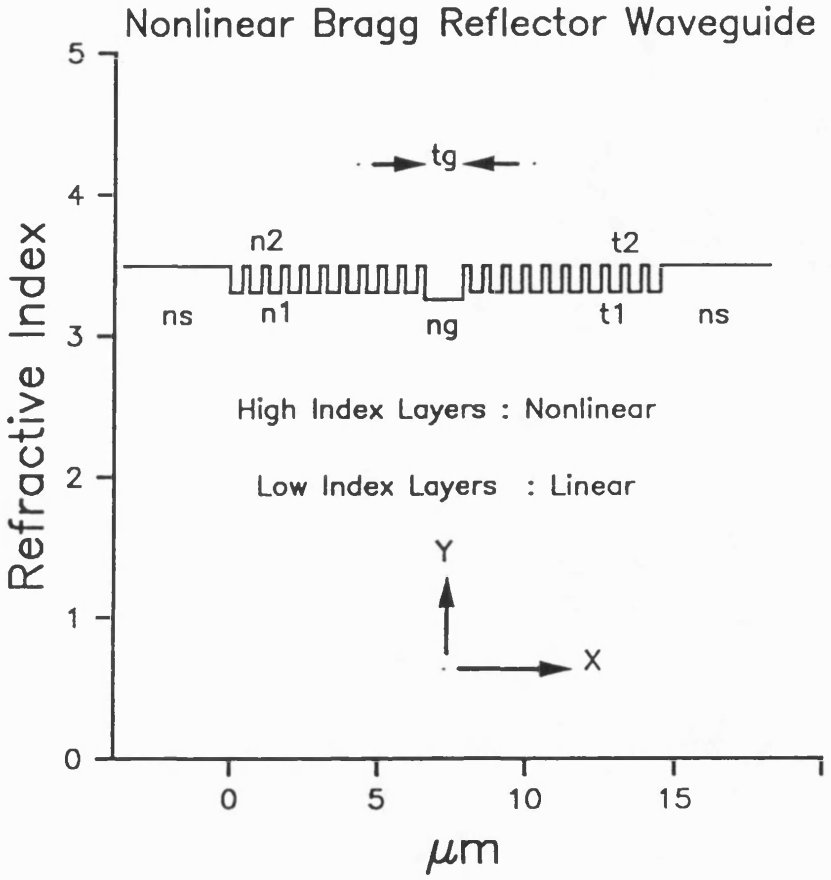

Figure 6.8 Finite Bragg Reflection Waveguide structure. Calculations have been performed for the following: $n_g = 3.250$, $n_1 = 3.304$, $n_2 = 3.490$, linear substrates $n_s = (3.490 - i\,10^{-4})$ $t_1 = 0.40\ \mu m$, $t_2 = 0.26\ \mu m$.

6.7 Results

6.7.1 Finite Linear BRW Properties

Analysis of the finite linear BRW's was first performed in order to identify regimes of operation where nonlinear effects could be expected to be significant. The parameter values used in the calculations are specified in Figure 6.8. Attention is centred on the parameter dependence of bound modes of the structure shown in Figure 6.8. As noted in section 6.6 such modes may be identified from the imaginary parts of the longitudinal and transverse propagation constants.

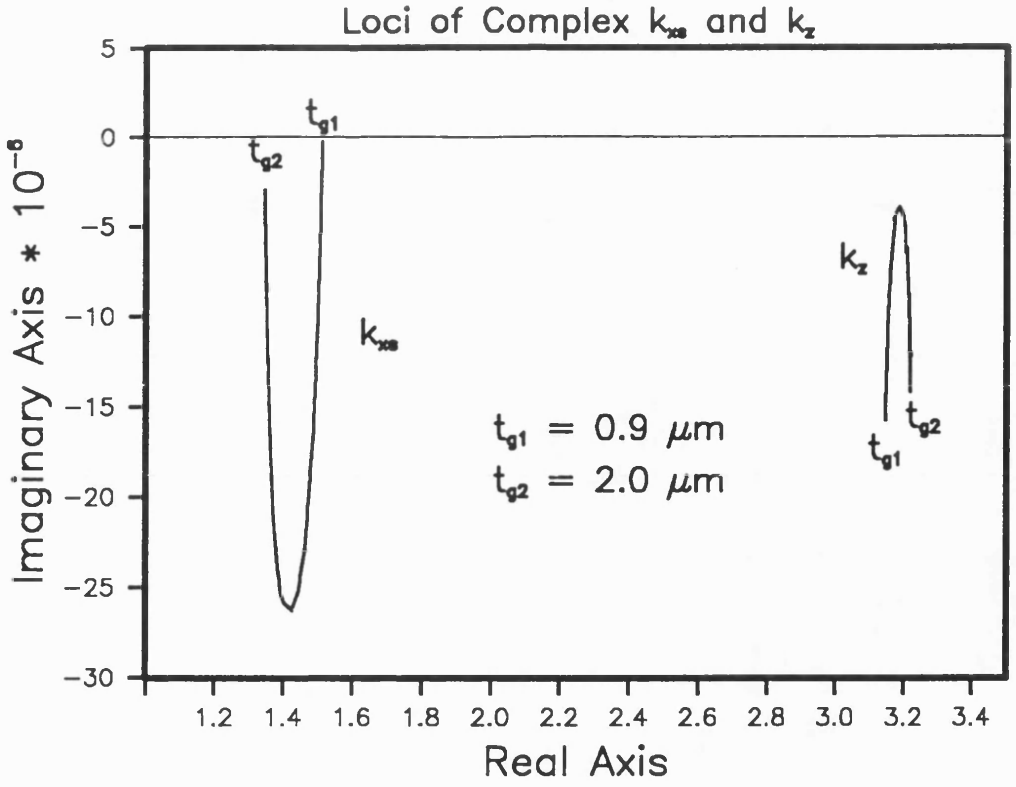

Figure 6.9 Loci of complex propagation constants as core layer thickness t_g is varied between $t_{g1} = 0.9\mu m$ and $t_{g2} = 2.0\mu m$.

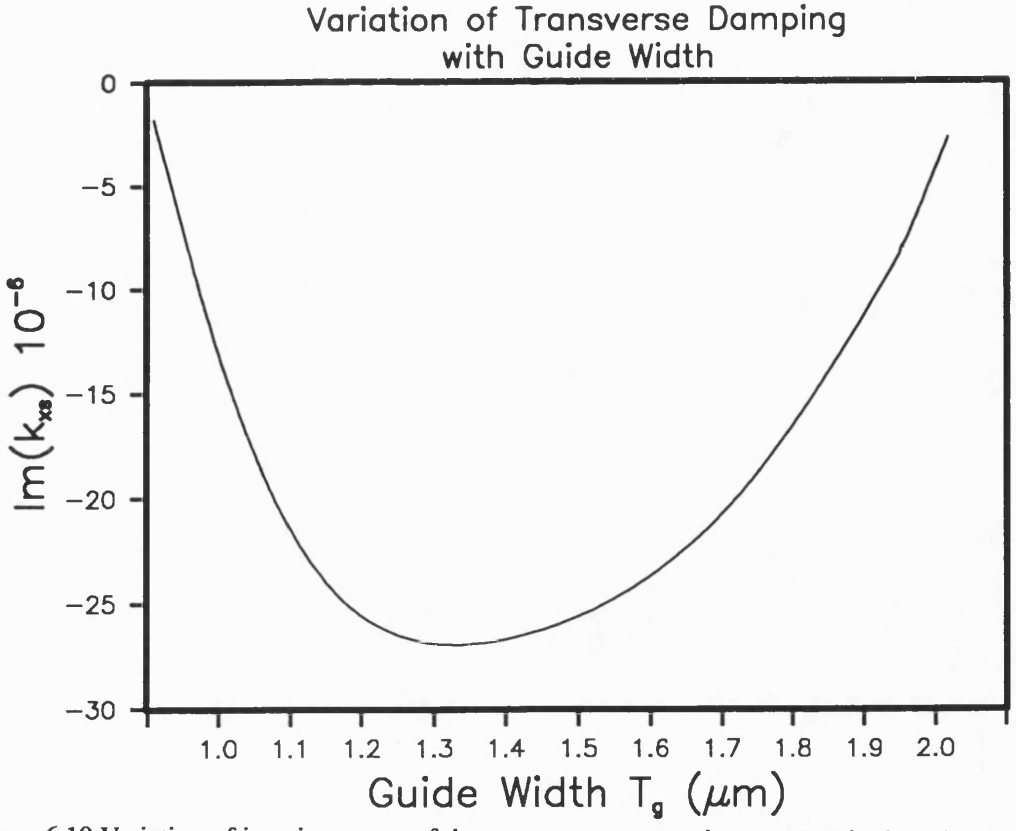

Figure 6.10 Variation of imaginary part of the transverse propagation constant in the substrate k_{xs} versus core layer thickness t_g.

Figure 6.9 shows the loci of the longitudinal propagation constant k_z and the substrate transverse propagation constant k_{xs} as the width of the core layer t_g is varied. For the present calculations a small absorption has been assumed in the substrate only. It is seen that guided wave solutions are only obtained if the core layer thickness, t_g, falls within the limits $t_{g1} < t_g < t_{g2}$ where $t_{g1} = 0.9\,\mu m$ and $t_{g2} = 2.0\,\mu m$. A quite pronounced resonance in the propagation constants occurs corresponding to a matching of the transverse resonance of the guide layer to the Bragg reflectors.

The propagation constant resonance for varying t_g is again shown in Figure 6.10 . Here the minimum on the $Im(k_{xs})$ curve indicates the point of greatest transverse damping and hence the point of maximum field confinement. It also represents the point of least propagation loss. A typical intensity distribution is given in Figure 6.11 for the structure close to resonance, corresponding to a core layer thickness of $1.3\mu m$. The index profile is also indicated in Figure 6.11 and it is clearly seen that the field profile oscillations have vanished after the first few periods of the multilayer structure away from the guiding layer. It should also be noted that the intensity maxima occupy the high index layers in this region.

6.7.2 Nonlinear Bragg Reflector Waveguides

In accordance with the general arguments outlined in chapter two, a nonlinear BRW should be constructed such that the nonlinear portions (ie. those layers with an intensity dependent refractive index) of the multilayer structure are the layers of highest refractive index. The low index layers and the core layer sandwiched by the periodic structures would be assumed to be linear. The substrates may additionally be considered linear since in most cases of interest the field intensity of the guided modes is negligible in the substrate regions. Such an approach has already been described in regard to a single reflector structure (Lambkin and Shore, 1990) where the effects of the nonlinearity on the mode profile were examined.

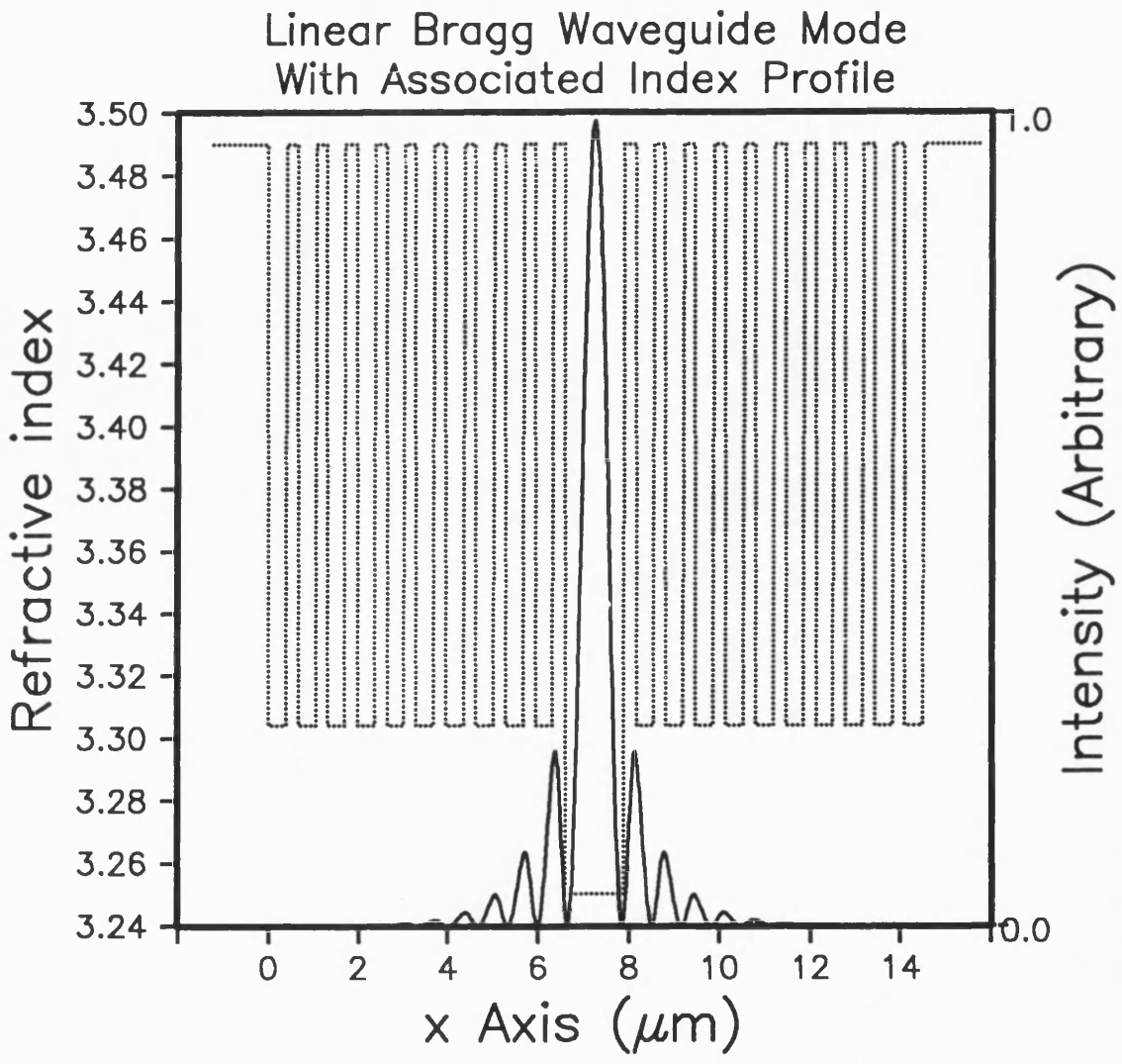

Figure 6.11 Mode and refractive index profiles for a linear Bragg reflection waveguide at the optimum guide width $t_g = 1.3\mu m$.

On the basis of the preceding calculations of the linear BRW it is seen that the thickness of the core layer will be expected to play an important role in determining the properties of nonlinear BRWs. Calculations have shown, in particular, that the core layer thickness below the resonant limit, $t_g < t_{g1}$, gives rise to interesting effects. Here, therefore, this case is considered and it will be shown that certain structures, which in the linear case have no bound modes, may be brought into the Bragg resonance by means of the nonlinearity and hence capable of supporting guided waves.

In the linear regime no guided modes exist for core thicknesses less than $t_g = t_{g1} = 0.9\,\mu m$. In contrast, the nonlinear guide will support guided modes at sufficiently high powers. This is clearly shown in Figure 6.12 . Here the absorption associated with guides of various core thicknesses is plotted as a function of increasing power. The solutions become physically meaningful at critical powers labeled A, B, and C above which a propagation loss is present - in contrast to the gain implied by the negative absorption at low powers. Also plotted is the curve for the optimum thickness of $t_g = 1.3\,\mu m$. Since this value lies within the resonant limits a solution still exists at zero power. The critical power for a given t_g is plotted in Figure 6.13 and shows, as would be expected, that the power required for a guided mode increases as the core thickness is detuned. The maximum detuning from the resonant limit considered here is $t_g = 0.7\,\mu m$. In that case with a significant change in power (about 500W/m) the real part of k_z changes by only $1.3.10^{-5}$ and hence the guide seems to be operating almost linearly. This is due to the combination of a number of factors. Consideration of this high optical power mode in relation to its index profile, shown in Figure 6.14, gives some explanation for this behaviour. Firstly, it is noted that the nonlinear perturbation of the index profile is very slight. The striking difference between this mode and that of the linear case is the increased oscillatory behaviour near the substrates. More significantly, the intensity maxima now lie in regions of low index which are of course linear. It is thus clear why the nonlinear perturbation of the permittivity is so slight.

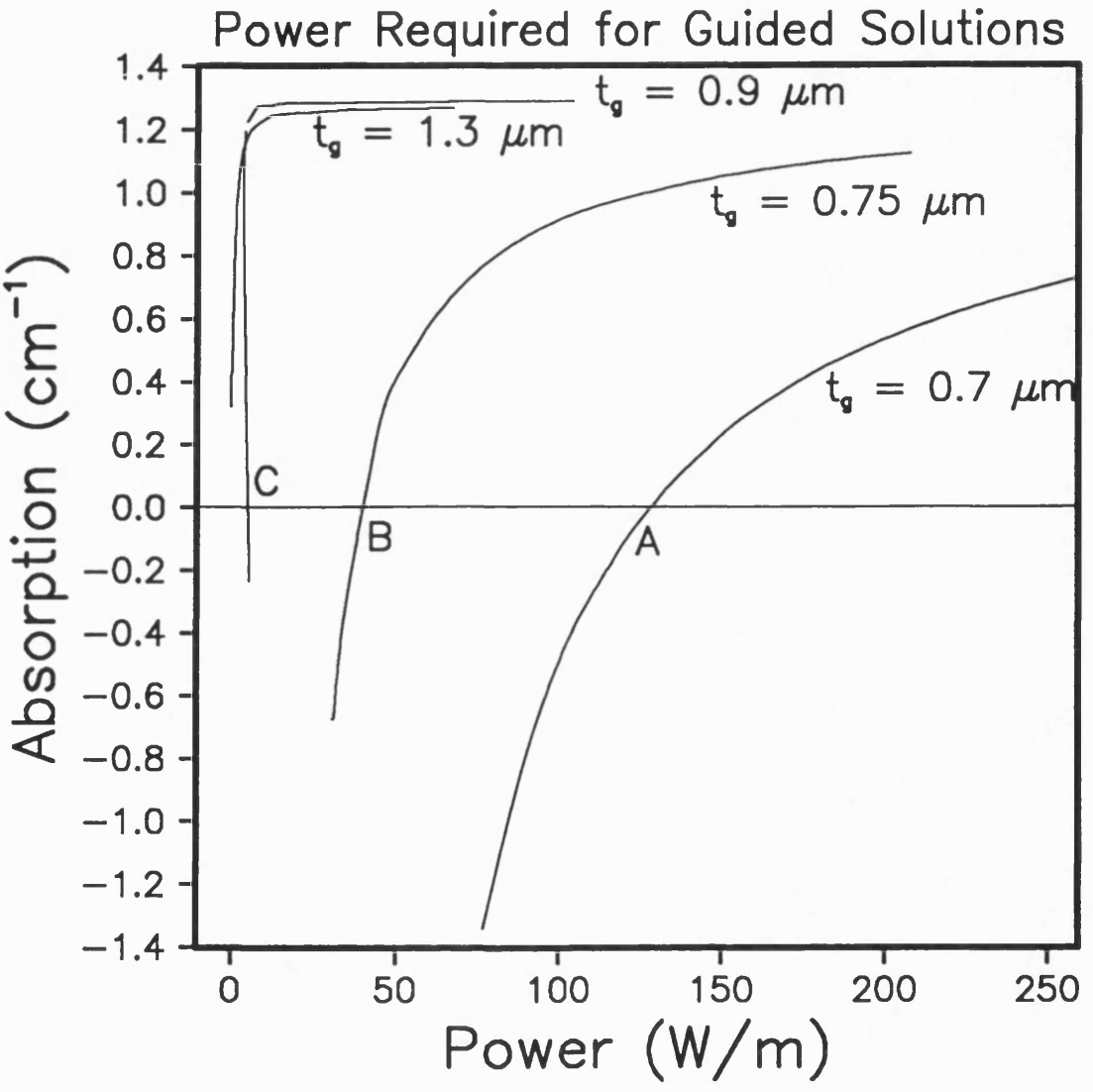

Figure 6.12 The dependence of absorption on power indicating the points A, B, C at which guided mode solutions are obtained. Curves are associated with different core layer thicknesses t_g.

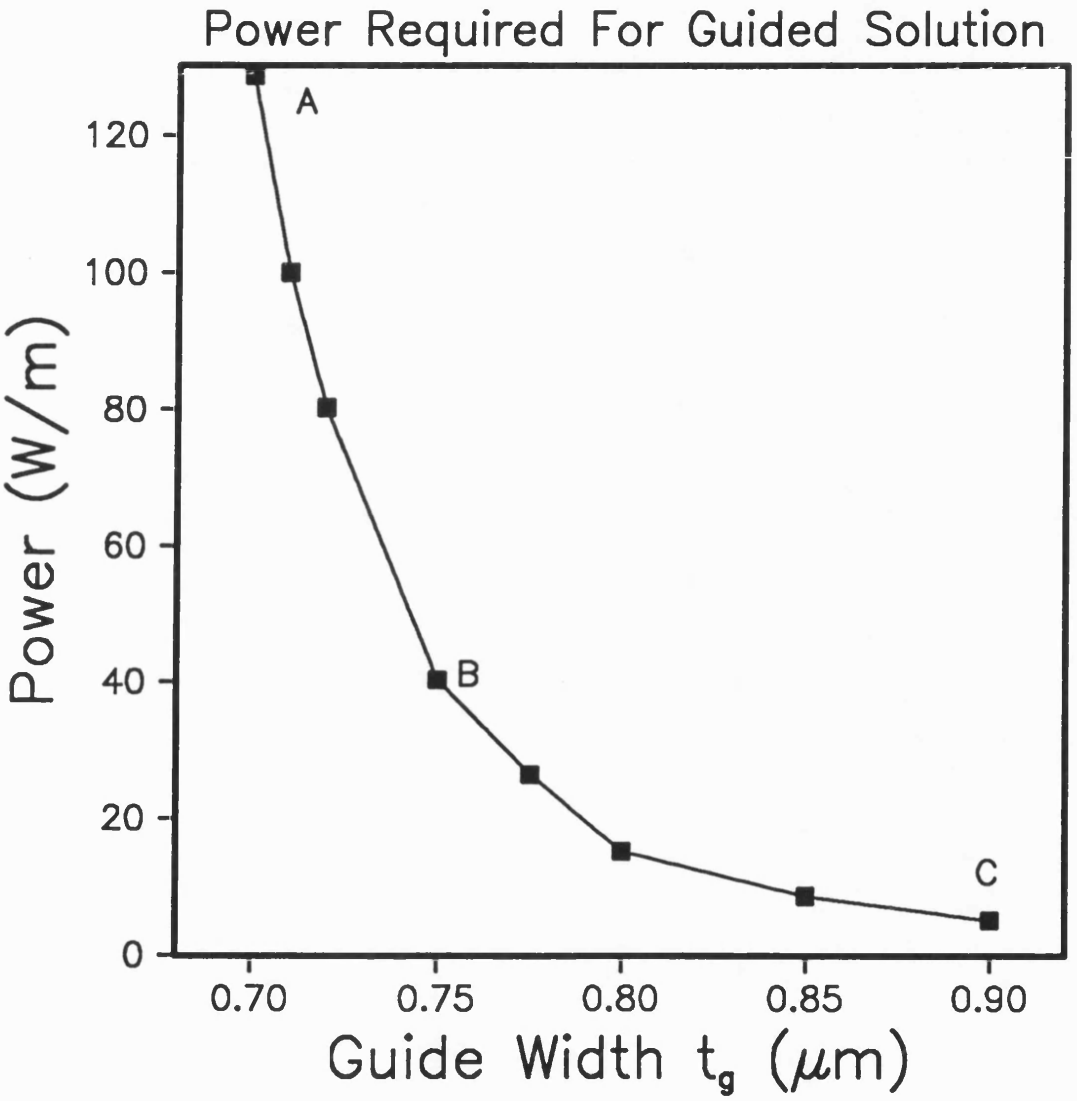

Figure 6.13 Threshold optical power for guided modes as a function of core layer thickness t_g.

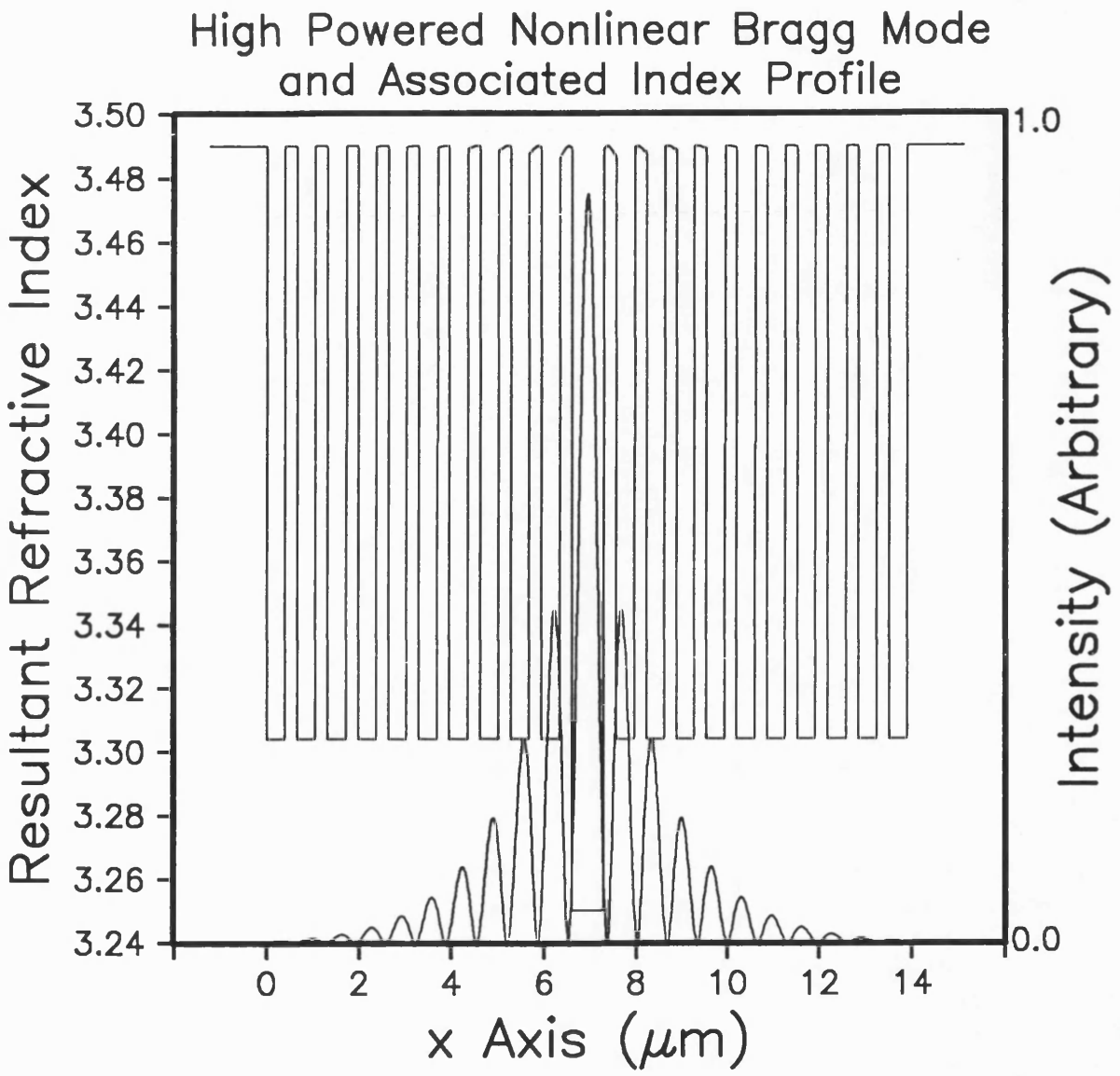

Figure 6.14 High power mode and refractive index profiles for nonlinear Bragg reflection waveguide. Core layer thickness $t_g = 0.7\mu m$ and total power $P = 500\ W/m$.

The high powers associated with the nonlinear mode is a result of the decreasing transverse damping in the substrates ie. $Im(k_{xs}) \rightarrow 0$ as the longitudinal propagation constant takes up the material loss available from the substrates. It is very relevant, therefore, to compute the power confined between the substrates, that is the power in the core and periodic layers. Figure 6.15 shows (for the case $t_g = 0.7\mu m$) that although the overall optical power carried by the guide is increasing, the power associated with the guiding region actually decreases to a minimum. Any excess power is then leaked to the substrates. In this sense the device is behaving as an optical limiter. Nevertheless, a finite power is required to obtain solutions that satisfy the guided mode criteria $Im(k_z, k_{xs}) < 0$.

6.8 Conclusions

The waveguiding properties of finite Bragg Reflection Waveguides have been investigated in both linear and nonlinear regimes. The guiding properties of both linear and nonlinear BRWs have been shown to depend quite sensitively upon the core layer dimension. A feature of the analysis of the nonlinear case has been the use of Jacobian elliptic functions of complex modulus and argument to give an analytic prescription of the optical field. With structures incorporating a defocusing nonlinearity it has been shown that BRWs may be optical-intensity tuned to support bound modes. For optical nonlinearities typical of III-V semiconductors the threshold optical powers required to access guided bound modes can be provided by diode lasers. The effects described here are therefore amenable to comparatively straightforward experimental demonstration and practical exploitation.

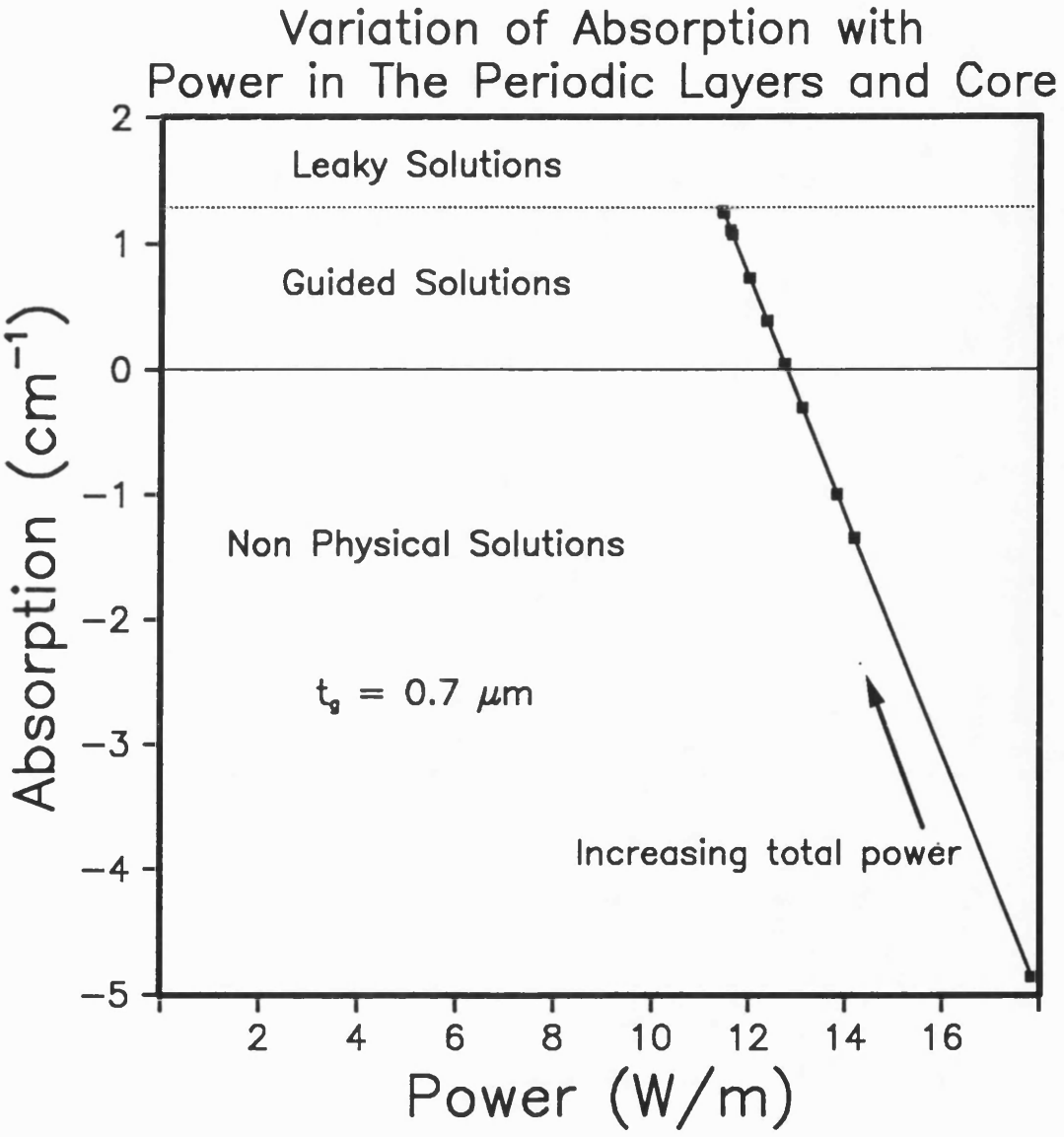

Figure 6.15 Absorption versus optical power confined between the substrates. As the total power carried by the guide increases, power confined to the core and periodic layers decreases.

6.9 References

L.Brillouin,'' *Wave Propagation in Periodic Structures,''* Dover Publications, New York, (1953).

A. Y. Cho, A. Yariv and P.Yeh,''Observation of confined propagation in Bragg waveguides,'' Appl. Phys. Lett., vol 30, pp. 471 - 472, (1977).

R. E. Collin, '' *Field Theory of Guided Waves,''* McGraw-Hill, New York, (1960).

S. Dodds, ''Bragg reflection waveguide, ''J. Opt. Soc America A6, pp. 1465-1476, (1989).

M. A. Fisher, private communication, (1990).

A. Ghatak and K. Thyagarajan, '' *Optical Electronics,''* Cambridge University Press, (1989).

P.M.Lambkin and K.A.Shore, ''Novel waveguiding phenomena in nonlinear semiconductor Bragg reflector structures'', Proceedings of the OSA/LEOS topical meeting on Integrated Photonic Research 1990, Technical Digest Series vol.5, Hilton Head, South Carolina, 92-93, (1990).

G. Lenz and J. Salzman,''Bragg reflection waveguide composite structures,'' IEEE. J. Quantum Electron., vol. 26, pp. 519 - 531, (1990).

W. Ng, P. Yeh, P. C. Chen and A. Yariv, ''Optical surface waves in periodic layered medium grown by liquid phase epitaxy,'' Appl. Phys. Lett., vol. 32, pp. 370 - 371, (1978).

S. Ramo, J. R. Whinnery and T. Van Duzer, '' *Fields and Waves in Communication Electronics,''* John Willey & Sons, 2nd Edition, (1984).

J.Salzman and G.Lenz, ''The Bragg reflection waveguide directional coupler, '' IEEE Phot. Tech. Lett., 1, pp. 319-322, (1989).

U.Trutschel, F.Lederer and M.Golz, "Nonlinear guided waves in Multilayer systems," IEEE J. Quantum Electron., QE-25, pp. 194-200, (1989).

P. Yeh, A.Yariv and C.S.Hong, "Electromagnetic propagation in periodic stratified media I : General Theory, " J. Opt. Soc. Amer., vol. 67, pp. 423-438, (1976).

P. Yeh, A. Yariv and A. Y. Cho, "Optical surface waves in periodic layered media, " Appl. Phys. Lett., vol. 32, pp. 104 - 105, (1978).

Chapter Seven

Conclusions

7.1 Introduction

This thesis has been concerned with the possible applications of intensity dependent nonlinearities in semiconductor optical waveguide devices. The origin and nature of the semiconductor band-filling nonlinearity was first discussed and was shown to be described by a nonlinear, Kerr-like permittivity. Elliptic Jacobi functions were then introduced as the solution to a nonlinear differential equation. This equation was subsequently derived as the governing wave equation for a medium characterised by a Kerr-like permittivity. A detailed nonlinear modal analysis of the important planar waveguide geometry was then presented. This analysis was then applied to two dimensional waveguides and an optical limiting action was demonstrated. Finally, nonlinear effects in periodic structures were considered. It was shown how guided wave solutions could be obtained above a certain power threshold for a suitably designed Bragg reflection waveguide (BRW).

The modal analysis of nonlinear waveguides adopted in this thesis involves solving a boundary value problem. An alternative approach to the study of wave guiding involves solving an initial value problem thereby investigating the propagation and evolution of input fields by numerical techniques. The remainder of this chapter is concerned with placing the present work in this context and concludes with some remarks regarding the role of theoretical investigations of semiconductor nonlinear devices.

7.2 Modal Interactions

Nonlinearity precludes the field in a guide being represented as a linear combination of the modes of the structure. Whilst this does not present a problem for initial value techniques (eg. beam propagation method) it does represent a restriction on a modal treatment. This restriction is not as limiting as might first be thought. Often in integrated optics single mode operation is a prerequisite in order to avoid dispersive effects. This has been true of the guides considered in

this thesis and especially true of BRW's which show strong discrimination against higher order modes. However, if a guide is multi-moded, such as the nonlinear directional coupler, an analysis of stationary solutions can still be applied. In previous analysis of nonlinear directional couplers, coupled mode theory has been used, but recently Cada (1990) has used an alternative approach considering vertical couplers. Firstly, the symmetric and anti-symmetric modes are determined in terms of Jacobi functions assuming they propagate independently. These are then nonlinearly combined by calculating the interaction between the modes as a perturbation series. The problem of TE and TM mode interaction has also been recently addressed in the context of waves guided by an interface of a semi-infinite medium and characterised by an intrinsic nonlinearity (Boardman and Twardowski, 1989).

7.3 Material Effects

A potentially more serious shortcoming of analytic solutions of nonlinear waveguides is the inability to adequately treat absorption, saturation or diffusion. It has been observed that if these are included in numerical simulations (Caglioti, 1988), (Gubbels, 1987), profound differences from the ideal Kerr-like behaviour can be found. This has prompted Wright (1989) to develop a general numerical methodology for investigating nonlinear guided wave phenomena in semiconductors. It relies on a macroscopic field evolution utilising the beam-propagating method (BPM) with the microscopic semiconductor response obtained from the plasma theory of Banyai and Koch (1986). The BPM is a well established Fourier transform technique for obtaining solutions of parabolic wave equations (Feit and Fleck, 1978), but the finite element method could equally well be employed. The Wright (1989) approach is essentially similar to that used by Gibbons and Sarid (1987) for the analysis of the GaAs limiters discussed in chapter four. The cost of including absorption, saturation and diffusion, is that the method is computationally very intensive even for simple planar structures. The extension to two dimensional channel or strip loaded waveguides would involve a prohibitive increase in the computational effort required. Problems can also be encountered with respect to numerical stability and the generation of spurious solutions. Nevertheless, if absorption, saturation and diffusion are likely to be significant then, at present, there is no satisfactory alternative to a numerical investigation. Conversely, if these effects are small, an analytic solution can give an adequate description of a nonlinear guide. This was demonstrated in chapter four when the results presented for a GaAs limiter (Gibbons and Sarid, 1987) were

successfully reproduced using elliptic Jacobi functions in a straightforward manner and with modest computational effort.

7.4 The Theoretical Treatment of Semiconductor Nonlinear Optical Waveguides

It is clear that there are advantages and disadvantages associated with treating nonlinear guiding phenomena either as initial or boundary value problems. In this respect the approaches should be treated as complementary. The calculations presented in this thesis have shown that under the right circumstances a modal analysis gives a valid description of a planar guide. With confidence gained from that work, and with an understanding of the method's limitations, it has been shown that a modal analysis approach can be applied to more complex structures such as channel waveguides and Bragg reflection waveguides. In this way a realistic initial investigation can be performed that will highlight the important characteristics of a structure. A more detailed, numerically intensive approach can then be undertaken when, for example, interesting device effects have been found. It is in this manner that the full potential of nonlinear semiconductor waveguides might be investigated.

Up to now, experimental interest in semiconductor nonlinearities has been largely motivated by the directional coupler. This thesis has shown that Bragg structures also provide suitably sensitive environments for such phenomena. The evolution of this field of research will, to a great extent, rely on the perceived applications for these novel effects occurring in nonlinear optical waveguides.

7.5 References

A. D. Boardman and T. Twardowski, "Transverse-electric and transverse-magnetic waves in nonlinear isotropic waveguides," Phys. Rev. A., vol. 39, pp. 2481-2492, (1989).

L. Banyai and S. W. Koch, "A simple theory for the effects of plasma screening on the optical spectra of highly excited semiconductors," Z. Phys. B, vol. 63, pp. 283-291 (1986).

M. Cada and J. D. Begin, "An analysis of a planar optical directional coupler with a lossless Kerr-like coupling medium," IEEE J. Quantum. Electron., vol. QE-26, pp. 361-371, (1990).

E. Caglioti, S. Trillo, and S. Wabnitz, G. I. Stegeman,"Limitations to all-optical switching using nonlinear coupler in the presence of linear and nonlinear absorption and saturation," J. Opt. Soc. Am. B, vol. 5, pp. 472-482,(1988).

M.D. Feit and J. A. Fleck, "Light propagation in graded-index optical fibers," Appl. Opt., vol. 17, pp. 3990-3998, (1978).

W. M. Gibbons and D. Sarid, "Effect of carrier diffusion on the nonlinear response of optical waveguides," Opt. Lett., vol. 12, pp. 564-566, (1987).

M. Gubbels, E. M. Wright, G. I. Stegeman, C. T. Seaton and J. V. Moloney," Effects of absorption on TE_0 nonlinear guided waves," Opt. Commun., vol. 61, pp. 357-362, (1987).

E. M. Wright, G. I. Stegeman, and S. W. Koch, "Numerical simulation of guided wave phenomena in semiconductors," J. Opt. Soc. Am. B., vol. 6, pp. 1598-1606, (1989).

Appendix 1

TM Planar Analysis

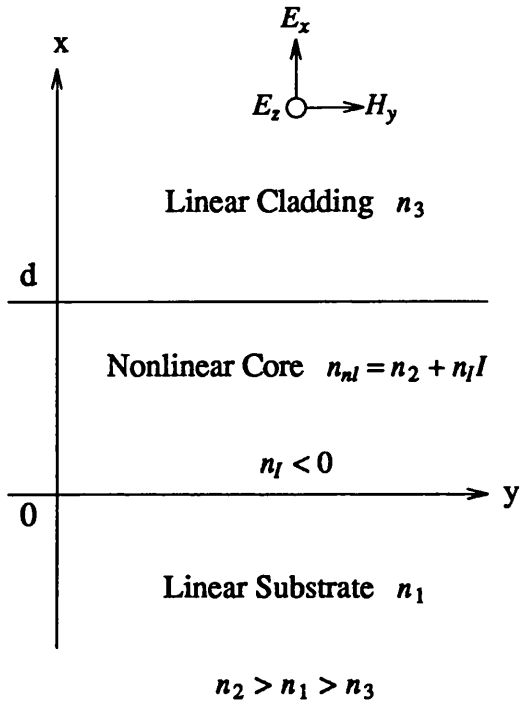

Figure A.1 Planar nonlinear optical waveguide. The propagation constants are defined as $k_i^2 = k_0^2 \varepsilon_i - k_z^2$ $i = 1, 2, 3$.

TM Nonlinear Refractive Index

The structure under consideration is shown in Figure A.1 and consists of a core, characterised by a defocusing nonlinearity, bounded by linear semi-infinite regions. A TM mode analysis is presented. The nonlinear refractive index is written as:

$$n = n_0 + n_I I \,. \tag{A1.1}$$

For the TM mode the intensity will be given by:

$$I = \frac{k_z}{2\omega \varepsilon_{nl} \varepsilon_0} \mid H_y \mid^2. \tag{A1.2}$$

Using Eq. A.1 and neglecting $n_I^2 I^2$ the nonlinear permittivity is:

$$\varepsilon_{nl} = \varepsilon_2 + \frac{k_z n_2}{k_0 \varepsilon_{nl}} \frac{k_0 n_I}{\omega \varepsilon_0} | H_y |^2 , \qquad \text{(A1.3)}$$

but $\frac{k_z n_2}{k_0 \varepsilon_{nl}} \approx 1$, so:

$$\varepsilon_{nl} \approx \varepsilon_2 + \frac{k_0 n_I}{\omega \varepsilon_0} | H_y |^2 = \varepsilon_2 + \alpha_{nl} | H_y |^2, \qquad \text{(A1.4)}$$

where

$$\alpha_{nl} = \frac{k_0 n_I}{\omega \varepsilon_0}. \qquad \text{(A1.5)}$$

Interface Intensity Relationship

Following the TE modal analysis for a planar guide, a relationship between field amplitudes at each interface $H_0 = H_y(x=0)$ and $H_d = H_y(x=d)$ can be found. First the permittivities at the interfaces are defined as:

$$\begin{aligned} \varepsilon_{nl}(0) &= \varepsilon_2 + \alpha_{nl} H_0^2, \\ \varepsilon_{nl}(d) &= \varepsilon_2 + \alpha_{nl} H_d^2. \end{aligned} \qquad \text{(A1.6)}$$

The relationship can then be written as:

$$\frac{k_1^2 H_0^2}{(\omega \varepsilon_1)^2} - (k_2^2 + k_0^2 \frac{\alpha_{nl} H_0^2}{2}) \frac{H_0^2}{(\omega \varepsilon_{nl}(0))^2} = -\frac{C}{(\omega \varepsilon_{nl}(0))^2}, \qquad \text{(A1.7)}$$

$$\frac{k_3^2 H_d^2}{(\omega \varepsilon_3)^2} - (k_2^2 + k_0^2 \frac{\alpha_{nl} H_d^2}{2}) \frac{H_d^2}{(\omega \varepsilon_{nl}(d))^2} = -\frac{C}{(\omega \varepsilon_{nl}(d))^2}, \qquad \text{(A1.8)}$$

where C is an integration constant.

Dispersion Equation

The field in the core is described by the *cn* Jacobi function:

$$H_y = P\, cn(\, q(x + x_0), m\,), \qquad \text{(A1.9)}$$

with parametric relations given by:

$$q = (k_2^4 + 2\alpha_{nl} k_0^2 C)^{\frac{1}{4}} \quad \text{and} \quad m^2 = \frac{q^2 - k_2^2}{2q^2}, \qquad \text{(A1.10)}$$

and x_0 is an integration constant. An eigen-value equation can then be obtained as:

$$cn(qd) = \frac{2H_0H_d\left(q^2 + k_1k_3\dfrac{\varepsilon_{nl}(0)\varepsilon_{nl}(d)}{\varepsilon_1\varepsilon_3}\right)}{-\left(\dfrac{\varepsilon_{nl}(0)k^1H^0}{\varepsilon_1}\right)^2-\left(\dfrac{\varepsilon_{nl}(d)k^3H^d}{\varepsilon_3}\right)^2 + q^2(H_0^2 + H_d^2) + \dfrac{\alpha_{nl}k_0^2}{2}(H_0^2 - H_d^2)^2}. \quad \text{(A1.11)}$$

Reduction to the Linear Limit

In the linear limit $\alpha_{nl} = 0$, $q^2 = k_2^2$ and $cn(u, 0) = \cos(u)$. The dispersion relation and the hyperbolic relations immediately reduce to:

$$\cos(k_2d) = \frac{2H_0H_d\left(k_2^2 - k_1k_3\dfrac{\varepsilon_2^2}{\varepsilon_1\varepsilon_3}\right)}{-(\varepsilon_2/\varepsilon_1)^2k_1^2H_0^2 - (\varepsilon_2/\varepsilon_3)^2k_3^2H_d^2 + k_2^2(H_0^2 + H_d^2)}, \quad \text{(A1.12)}$$

and

$$H_d^2 = H_0^2\,a^2 \quad \text{where} \quad a^2 = \frac{\varepsilon_3^2(k_2^2\varepsilon_1^2 - \varepsilon_2^2k_1^2)}{\varepsilon_1^2(k_2^2\varepsilon_3^2 - \varepsilon_2^2k_3^2)}. \quad \text{(A1.13)}$$

Making the substitution for H_d removes any field dependence and gives:

$$\cos(k_2d) = \frac{\varepsilon_1^2a\left(k_2^2 - \dfrac{k_1k_3\varepsilon_2^2}{\varepsilon_1\varepsilon_3}\right)}{k_2^2\varepsilon_1^2 - k_1^2\varepsilon_2^2}. \quad \text{(A1.14)}$$

Inverting and squaring yields:

$$sec^2(k_2d) = \frac{(k_2^2\varepsilon_1^2 - k_1^2\varepsilon_2^2)^2}{\varepsilon_1^4a^2\left(k_2^2 - \dfrac{k_1k_3\varepsilon_2^2}{\varepsilon_1\varepsilon_3}\right)^2}. \quad \text{(A1.15)}$$

Expanding and subtracting 1 from each side gives:

$$sec^2(k_2d) - 1 = \frac{-\varepsilon_2^2(k_2^2k_3^2\varepsilon_1^2\varepsilon_2^2 - 2k_2^2\varepsilon_2^2k_1k_3\varepsilon_1\varepsilon_3 + k_2^2k_1^2\varepsilon_3^2\varepsilon_2^2)}{(k_2^2\varepsilon_1\varepsilon_3 - k_1k_3\varepsilon_2^2)^2}, \quad \text{(A1.16)}$$

or

$$\tan^2(k_2d) = \frac{-\varepsilon_2^2(k_2k_3\varepsilon_1\varepsilon_2 - k_2k_1\varepsilon_3\varepsilon_2)^2}{(k_2^2\varepsilon_1\varepsilon_3 - k_1k_3\varepsilon_2^2)^2}, \quad \text{(A1.17)}$$

so finally:

$$\tan(k_2 d) = \frac{i\,\varepsilon_2^2 k_2^2\,(k_3\varepsilon_1 - k_1\varepsilon_3)}{k_2^2\varepsilon_1\varepsilon_3 - k_1 k_3 \varepsilon_2^2}, \qquad \text{(A1.18)}$$

which is the TM dispersion relation familiar from linear analysis.

Appendix 2

A Comparison Between Analytical and Numerical Results For A Nonlinear Rib Waveguide.

Introduction

In this appendix a comparison is made between results from the semi-analytical method for solving nonlinear rib guides presented in chapter 5 and results from the 2D Beam Propagation Method (BPM). The BPM is a well established Fourier transform technique for obtaining solutions of parabolic wave equations. The method relies on replacing a guide by an equivalent array of infinitesimally thin lenses in a homogeneous medium and propagating an input field using the Fresnel lens equation. The programme used to perform the BPM calculations was written by Mr. C. H. Chong of Bath University and his assistance is gratefully acknowledged.

Linear Comparison

The rib guide under consideration is that treated in chapter 5, namely a guide with a shoulder thickness of 1.0 μm whilst the rib is 3 μm wide and 1.3 μm high. The permittivities of the substrate, core and cladding are 11.42, 11.76 and 1.0 respectively. Initially the guide is considered to be entirely linear. The intensity distributions for such a guide, generated by each method, are shown in Figure A2.1 and A2.2. The input field for the BPM was a plane wave. Since the guide is linear the distribution in Figure A2.1 is that obtained by the Effective Index (EI) method. The close agreement with the BPM result indicates that the guide dimensions are such that the EI gives a valid representation of the structure.

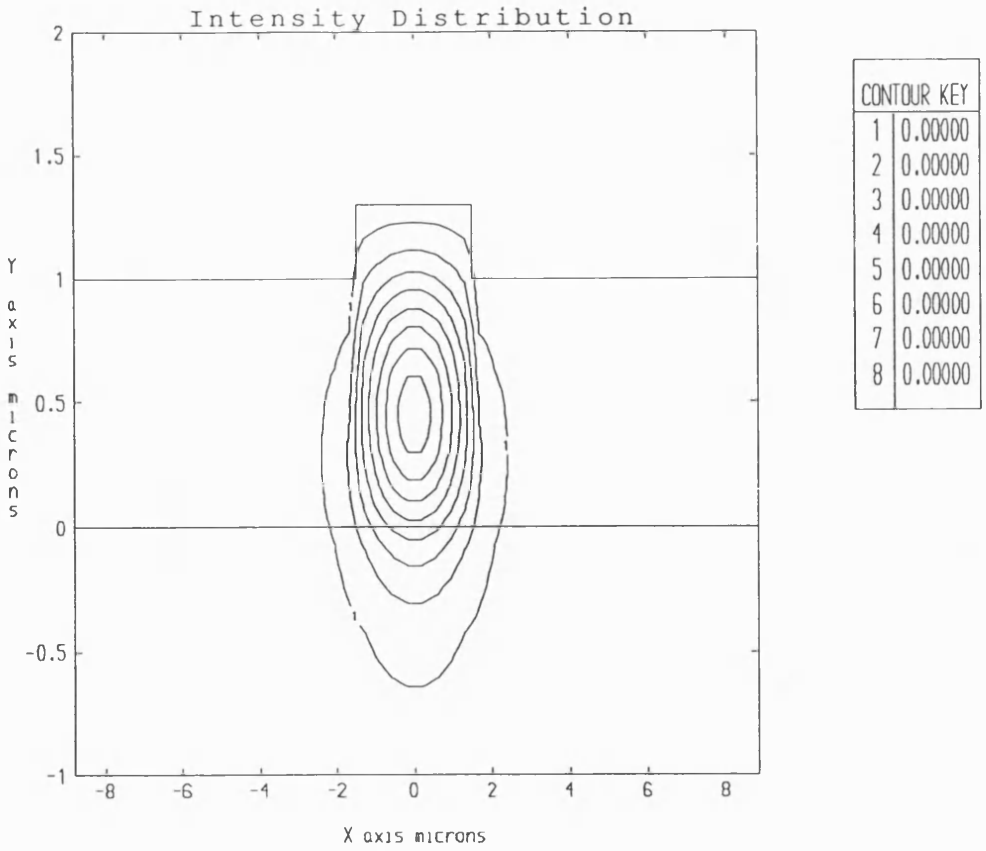

Figure A2.1 Intensity distribution for a linear rib waveguide calculated by the EI method.

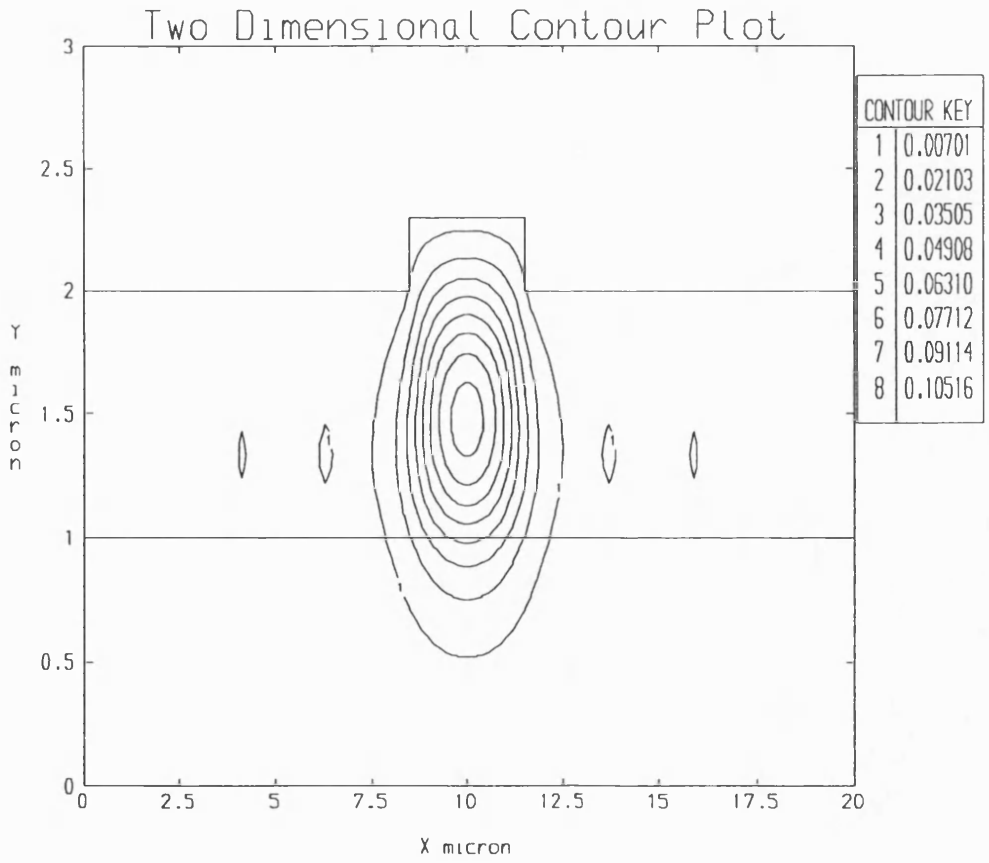

Figure A2.2 Intensity distribution for a linear rib waveguide calculated by the Beam Propagation Method.

Nonlinear Rib Guides

Using the linear result as an input for the BPM, the distribution was propagated for 100 μm under the influence of a defocusing nonlinearity in the core. The resulting output is shown in Figure A2.3 where the contours join points having equal values of $\alpha \mid E_y \mid^2$. The lateral spreading due to the suppressed index in the core is clearly shown.

Calculations using the semi-analytical method are based on the value of $\frac{\alpha \mid E_0 \mid^2}{2}$, ie the intensity at the substrate/core interface midway under the rib. In the co-ordinate system of Figure A2.3 $\frac{\alpha \mid E_0 \mid^2}{2} = \frac{\alpha \mid E(10.0,1.0) \mid^2}{2} = 1.757\ 10^{-2}$. Using this value, the $\alpha \mid E_y \mid^2$ distribution derived using the Jacobi function formalism is shown in Figure A2.4 . Whilst the field discontinuities suggest the EI method is becoming inaccurate, there is qualatative agreement with the BPM results with respect to the degree of lateral field spreading. This close agreement demonstrates the integrity of the semi-analytical method and shows that the high power nonlinear results are valid. Furthermore, the semi-analytical results have been obtained after only seconds of CPU time in contrast to the BPM which requires hours.

Finally, the stability of the convergence of the semi-analytical method has been tested by using an alternative initial condition to that of the scheme outlined in chapter 5. There the first ''guess'' for the $E_y(x=0,y)$ distribution was based on the result of an EI approximation assuming a totally linear guide. Calculations have been performed in which $E_y(x=0,y)$ is set to a constant value depending on the prescribed value of $\frac{\alpha \mid E_0 \mid^2}{2}$. The difference between results for the two initial conditions are minimal with only the fifth decimal place of the propagation constant being effected.

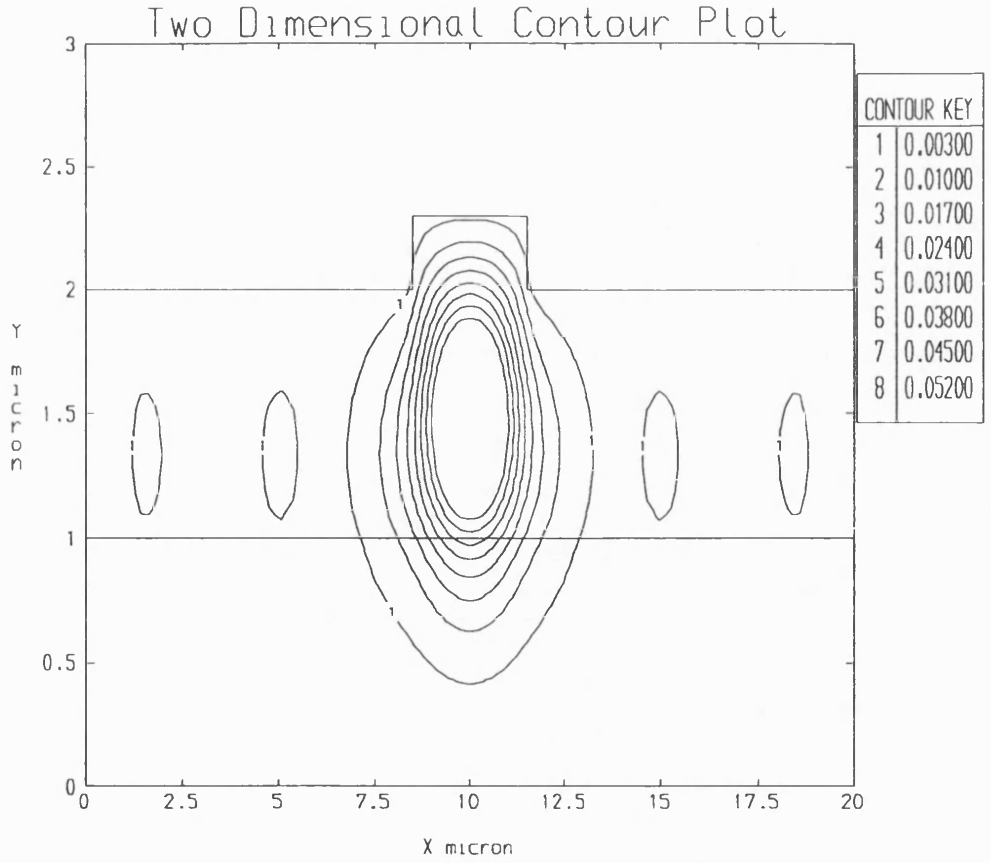

Figure A2.3 Intensity distribution for a nonlinear rib waveguide calculated by the BPM method.

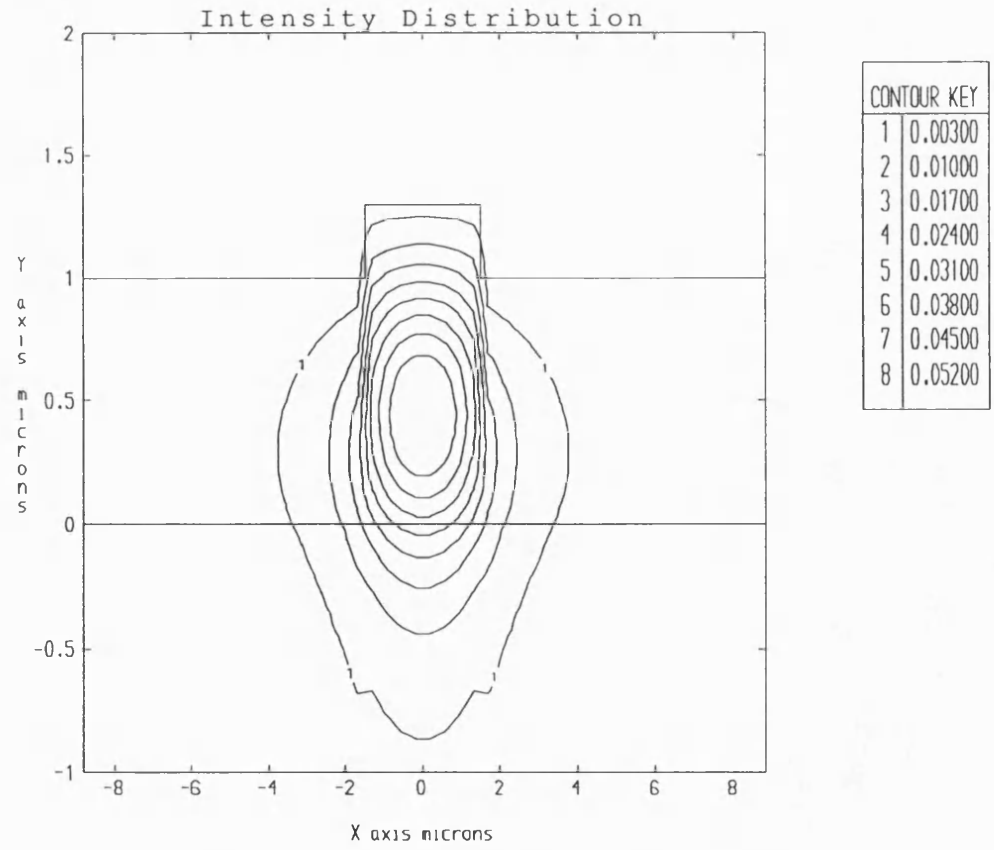

Figure A2.3 Intensity distribution for a linear rib waveguide calculated by the semi-analytical method described in chapter 5.

Publications

The following presentations have been made based on the work presented in this thesis:

P. M. Lambkin and K. A. Shore, "Non-linear semiconductor ridge waveguides," in IEE *Colloquium on Nonlinear Optical Waveguides* (Institution of Electrical Engineers, London, 1988), paper 12, (1988).

P. Lambkin and K. A. Shore, "Non-linear optical waveguiding in semiconductors," Journal de Physique, Colloque C2, Supplement au no.6, Tome 49, juin 1988.

P.M.Lambkin and K.A.Shore, "Novel waveguiding phenomena in nonlinear semiconductor Bragg reflector structures", Proceedings of the OSA/LEOS topical meeting on Integrated Photonic Research 1990, Technical Digest Series vol.5, Hilton Head, South Carolina, 92-93, (1990).

P.M.Lambkin and K.A.Shore, "Novel waveguiding phenomena in nonlinear semiconductor Bragg reflector structures", Proceedings of the CLEO/IQEC '90 conference on Lasers and Electro-Optics, International Quantum Electronics Conference, Anaheim, California, May 21-25, 1990, CTuH69.

The following papers have also been published:

P. M. Lambkin and K. A. Shore, "Analysis of an optical rib waveguide with a nonlinear substrate," J. Opt. Soc. Soc. Am. B, vol. 6, pp. 669 - 674, (1989).

P. M. Lambkin and K. A. Shore, " Asymmetric semiconductor waveguide with defocusing nonlinearity," IEEE J. Quantum. Electron., vol. 24, pp. 2046-2051, (1988).

J-QE/24/10//22675

Asymmetric Semiconductor Waveguide with Defocusing Nonlinearity

Paul M. Lambkin
K. Alan Shore

Reprinted from
IEEE JOURNAL OF QUANTUM ELECTRONICS
Vol. 24, No. 10, October 1988

Asymmetric Semiconductor Waveguide with Defocusing Nonlinearity

PAUL M. LAMBKIN AND K. ALAN SHORE

Abstract—**The properties of a waveguide designed to exploit the nonlinearity associated with the fundamental absorption edge of semiconductor material is analyzed for the first time. Power and frequency dependence of the field are found and a form of optical limiter action is theoretically predicted.**

I. Introduction

With the recent recognition of the applications potential of nonlinear optical waveguides [1], attention has been given to a number of waveguide structures. In particular, three-layer planar (slab) guides have been investigated in several combinations of linear and nonlinear layers. The case of a nonlinear medium bounded by linear media has been treated for both self-focusing and defocusing nonlinearities [2], [3]. Practical device implementations of the properties of nonlinear waveguides have been considered in relation to semiconductor waveguides, notably for directional couplers [4], [5].

In the present work, we consider optical waveguides whose properties depend upon the defocusing nonlinearity associated with the fundamental absorption edge of semiconductor material. The large change in absorption which occurs for wavelengths tuned close to the bandgap of the semiconductor gives rise, via the Kramers–Kronig relations, to a strong refractive index nonlinearity. The proposal here is to utilize that effect in a semiconductor structure for which the refractive index of the guiding layer may be tailored to meet specific requirements. It is proposed that the waveguide be implemented in multiquantum well (MQW) material which, compared to quaternary material, allows easier fabrication of prescribed waveguide structures. By appropriate choice of the materials and thicknesses of the well and barrier layers, the refractive index of the MQW layer can be engineered in accordance with the needs of the guide design. Also, since the choice of material determines the absorption edge (at which the nonlinearity is effective), this approach provides means for developing guiding structures which are nonlinear at chosen wavelengths.

Manuscript received March 1, 1988; revised May 30, 1988. The work of P. M Lambkin was supported by a UK SERC CASE Award with British Telecom Research Laboratories, Martelsham Heath.

The authors are with the School of Electrical Engineering, University of Bath, Claverton Down, Bath BA2 7AY, England.

IEEE Log Number 8822675.

It is important to emphasize that although MQW material is considered in this work, no reliance is made on excitonic effects for obtaining the nonlinearity.

Use of the material absorption edge to obtain the nonlinearity has an important implication for the design of the guiding structure. It becomes apparent that the waveguide configuration must consist of a nonlinear layer bounded by linear layers. The argument for this is straightforward. The core guiding layer must have a higher refractive index than the cladding layers, and hence must be composed of material of smaller bandgap than the cladding layers. When the guide is excited by light of energy slightly below the bandgap of the core region (to obtain the nonlinear effect with small absorption), the cladding layers will be nonabsorptive and thus linear. These considerations should also apply to other proposed structures [6], [7] which have been analyzed assuming a nonlinear substrate supporting a linear guiding layer. The implementation of these latter structures would then appear to be prevented by rather fundamental difficulties.

In this paper, we are proposing a novel structure capable of practical realization. The use of multiquantum well material offers considerable flexibility in waveguide design and implies that the resulting nonlinear waveguide can be extremely versatile. It is thus foreseen that a wide range of operating conditions and applications will arise for the exploitation of the structure. In this paper, we give the first analysis of a nonlinear waveguide based upon the above concept.

We develop a theory appropriate to TE modes in the general case of an asymmetric planar (slab) waveguide. The treatment allows comparison to be made to results obtained in the analysis of other nonlinear waveguide structures for the cases of both self-focusing and self-defocusing nonlinearities. The theory is developed in Section II. The solution technique together with a discussion of its accuracy is described in Section III. Results obtained from the analysis are then given in Section IV.

II. Theory

The nonlinear dielectric slab structure to be analyzed is shown in Fig. 1. The material in regions 1 and 3 ($x < 0$ and $x > 0$), respectively, are assumed to be linear with dielectric constants ϵ_1 and ϵ_3 such that the nonlinear region ($0 < x < d$) is guiding. The theory is developed

0018-9197/88/1000-2046$01.00 © 1988 IEEE

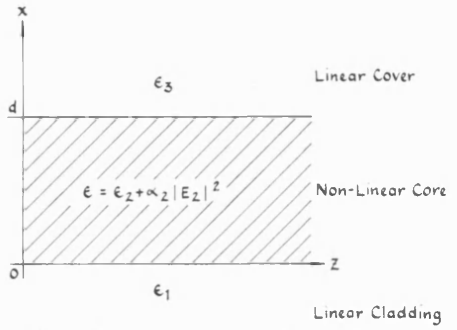

Fig. 1. Asymmetric nonlinear waveguide with nonlinear core and linear cladding layers.

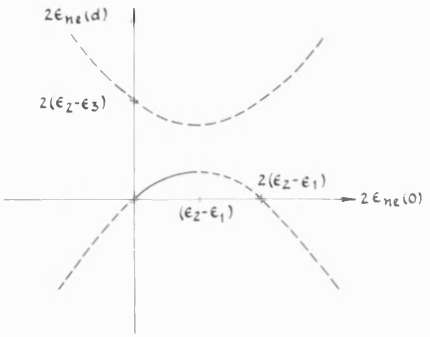

Fig. 2. Nonlinear dielectric constant change at core-cover interface ($2\epsilon_{nl}(d)$) versus nonlinear dielectric constant change at core-cladding interface ($2\epsilon_{nl}(0)$).

for TE modes propagating as

$$\exp\left(j(\beta z - \omega t)\right)$$

where $j = \sqrt{-1}$.

In the linear regions, exponentially decaying fields are taken:

$$E_1 = E_0 \exp(k_1 x) \tag{1}$$

$$E_2 = E_d \exp(k_3 x) \tag{2}$$

where

$$k_i^2 = \beta^2 - k_0^2 \epsilon_i, \qquad i = 1 \text{ and } 3 \tag{3}$$

and

$$k_0 = 2\pi/\lambda$$

is the wavenumber for light of free-space wavelength λ.

E_0 is the field amplitude at the interface between the nonlinear core (region 2) and the linear cladding (region 1); E_d is the field amplitude at the interface between the nonlinear core region and the linear cover (region 3).

In the nonlinear region, the wave equation takes the form

$$\frac{d^2E_2}{dx^2} + (k_2^2 + k_0^2\alpha_2 E_2^2)E_2 = 0. \tag{4}$$

It is convenient to represent the field intensities in terms of the nonlinear dielectric constant change at the interfaces. For this purpose, we introduce the notation

$$\epsilon_{nl}(x) = \tfrac{1}{2}\alpha_2 E^2(x) \tag{5}$$

So that

$$\epsilon_{nl}(0) = \tfrac{1}{2}\alpha_2 E_0^2 \tag{6a}$$

and

$$\epsilon_{nl}(d) = \tfrac{1}{2}\alpha_2 E_d^2. \tag{6b}$$

Use will also be made of a normalized waveguide frequency D defined by

$$D = k_0 d. \tag{7}$$

Following Boardman and Egan [8], a first integral of (4) is obtained as

$$\left(\frac{dE_2}{dx}\right)^2 + \left(k_2^2 + \frac{1}{2}k_0^2\alpha_2 E_2^2\right)E_2^2 = C_2 \tag{8}$$

where the constant of integration is

$$C_2 = k_0^2 E_0^2(\epsilon_2 - \epsilon_1 + \epsilon_{nl}(0)) \tag{9a}$$

$$= k_0^2 E_d^2(\epsilon_2 - \epsilon_3 + \epsilon_{nl}(d)). \tag{9b}$$

Equations (9a) and (9b) define a hyperbolic relationship between the boundary field intensities as shown in Fig. 2. For the guiding structure of interest with a defocusing nonlinearity ($\alpha_2 < 0$), appropriate values of the boundary field intensities lie on the solid portion of Fig. 2. For those values, the integration constant $C2$ is positive, and hence the field in the guiding layer is given by

$$E_2 = pcn(q(x + x_0), m). \tag{10}$$

Here cn is a Jacobian elliptic cosine function of modulus m; x_0 is an integration constant. We also have

$$m^2 = \frac{q^2 - k_2^2}{2q^2} \tag{11}$$

and

$$p^2 = \frac{q^2 - k_2^2}{k_0^2\alpha_2} \tag{12}$$

with

$$q = (2k_0^2\alpha_2 C_2 + k_2^4)^{1/4}. \tag{13}$$

Using (1), (2), and (4), an eigenvalue equation is obtained as

$$cn(qd, m) = \frac{2E_0E_d(q^2 - k_1k_3)}{\left\{k_1^2E_0^2 + k_3^2E_d^2 + q^2[E_0^2 + E_d^2] + \dfrac{\alpha_2k_0^2}{2}[E_0^2 - E_d^2]^2\right\}}. \tag{14}$$

In the limit $\alpha_2 \to 0$ under which the nonlinearity is removed, the above equation assumes the form appropriate to a linear asymmetric slab waveguide [9].

III. Solution Technique

Equations (9a) and (9b) prescribe the relationship between the boundary field intensities E_0^2 and E_d^2. Even and odd order solutions to the eigenvalue equation may be generated by appropriate choice of sign of the amplitudes. Setting E_0 positive, even order modes arise when E_d is taken positive, while odd order modes are obtained with E_d negative. Then for a specified E_0, the propagation constant may be found from (14). Hence, the electric field may be evaluated by the use of (1), (2), and (10). An explicit form for E_2 may also be obtained as

$$E_2 = \frac{qE_0\{qcn(qx) + k_1 sn(qx)\, dn(qx)\}}{\{q^2 dn^2(qx) + k_0^2 \epsilon_{nl}(0)\, sn^2(qx)\}}. \quad (15)$$

In the above, *sn* and *dn* are Jacobian elliptic functions (with modulus *m* suppressed).

In order to perform numerical evaluation of the Jacobian function *cn* in (15), some standard function transformations are useful. With α_2 negative, it is found that the modulus defined by (11) is imaginary. It is convenient therefore to utilize an imaginary function transformation [10] to give

$$cn(qd, jm) = cd(qd\sqrt{1 + m^2}, m_1) \quad (16)$$

where

$$j = \sqrt{-1}$$

and

$$cd(u) = \frac{cn(u)}{dn(u)} \quad (17)$$

and

$$m_1 = \frac{m}{\sqrt{1 + m^2}}. \quad (18)$$

Having obtained the electric field, the total power P in the waveguide can be calculated using

$$\frac{P}{P_0} = \beta\left\{\frac{1}{k_1}\epsilon_{nl}(0) + \frac{1}{k_3}\epsilon_{nl}(d) + 2\epsilon_{nl}(0)\int_0^d E_2^2\, dx\right\} \quad (19)$$

where

$$P_0 = \left(\frac{\epsilon_0}{\mu_0}\right)^{1/2} \frac{1}{\alpha_2 k_0}. \quad (20)$$

In addition, the far-field pattern of the waveguide may be found by taking the Fourier transformation of the near field.

A computer program was written to perform the above computations. A validation of the program was effected by reproducing results obtained in other studies of TE mode propagation in nonlinear waveguide structures. This validation procedure both confirms the reliability of the program and also points up its flexibility in accommodating a range of nonlinear waveguide structures. Specific comparison was made to work reported earlier by Boardman [8] and Ogusu [11], and we also have been able to make a comparison to the results obtained very recently by Al-badah [12]. The first and last of these authors deals with structures containing self-focusing nonlinearities, while Ogusu considers both self-focusing and self-defocusing nonlinearities.

Results shown in [8, Fig. 4] were reproduced with a precision limited only by the ability to obtain numerical values from the published graphs. Any error is certainly much less than 0.01 percent. In order to make a comparison to results applicable to a defocusing nonlinearity, the appropriate graphs appearing in [11, Fig. 3(a) and (b)] were computed and agreement to the accuracy noted above was again obtained. The recent results of Al-badah and Jamid [12] contain in Table I numerical values obtained by two methods. We were able to obtain these results to within the accuracy claimed by the authors, that is to say, with an error less than 0.01 percent.

In the confidence provided by this confirmation of the reliability of the program and the solution technique, attention was turned to modeling the new structure. The appropriate results are detailed in the next section.

IV. Results

Calculations have been performed for a waveguide fabricated in GaInAs/AlInAs MQW material lattice matched to InP. The core guiding layer was assumed to consist of 120 A GaInAs wells and 30 A AlInAs barriers, the cladding layer was taken to be formed with 60 A GaInAs wells and 30 A AlInAs wells. The structure is designed so that the band edge nonlinearity is obtained at an operating wavelength of 1.55 μm.

The dielectric constant of the core layer at this wavelength was estimated, using a weighted mean [13] of the dielectric constants of the constituent ternary materials [14], [15], to be 11.76. Similarly, the dielectric constant of the cladding layer was established to be 11.42. The capping layer is assumed to be air so that its dielectric constant is unity. The resulting waveguide structure is thus strongly asymmetric.

Results are presented for two general cases of interest. First, the power dependence of the optical field profile is found for a structure with fixed normalized frequency D.

In Figs. 3 and 4, we give the near fields and far fields for a guide with the value of D taken as 4.05. This corresponds to the case of an operating wavelength of 1.55 μm and a core guiding layer thickness of 1 μm.

For the asymmetric waveguide under consideration, the fundamental mode is at cutoff when the core–cladding dielectric step is less than about 0.09. With a low-power dielectric constant step between the core and the substrate of 0.34, it is thus expected that guiding action at the core–

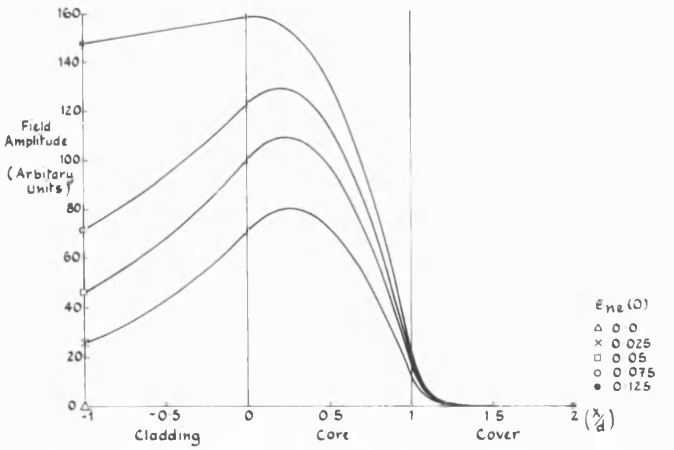

Fig. 3. Waveguide near field profile dependence upon $\epsilon_{nl}(0)$.

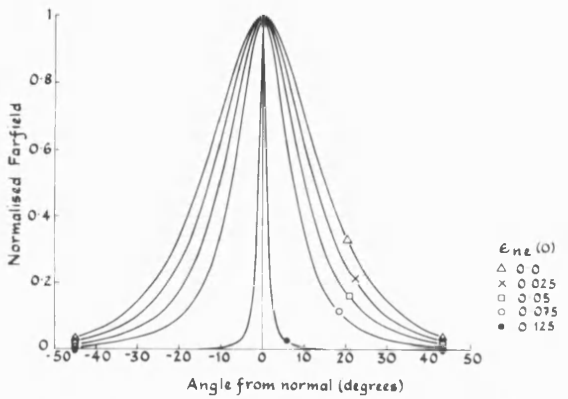

Fig. 4. Normalized far-field dependence upon $\epsilon_{nl}(0)$.

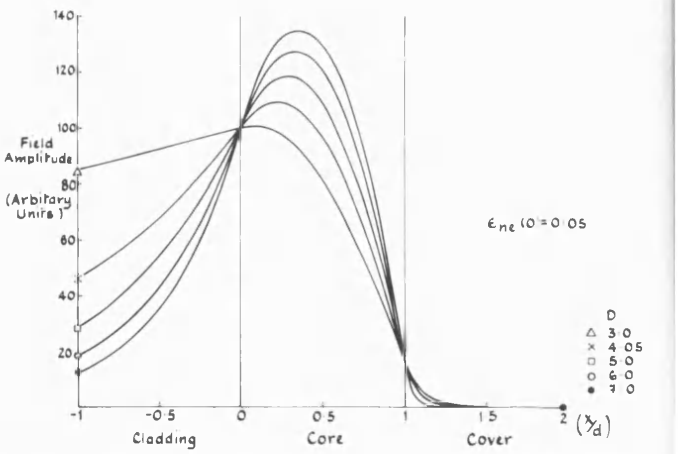

Fig. 5. Waveguide near field dependence upon normalized frequency D.

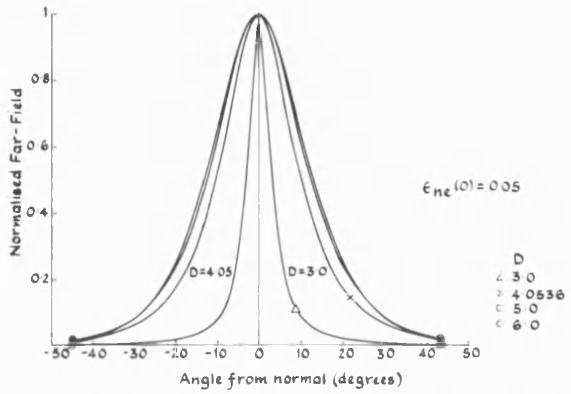

Fig. 6. Normalized far-field dependence upon normalized frequency D.

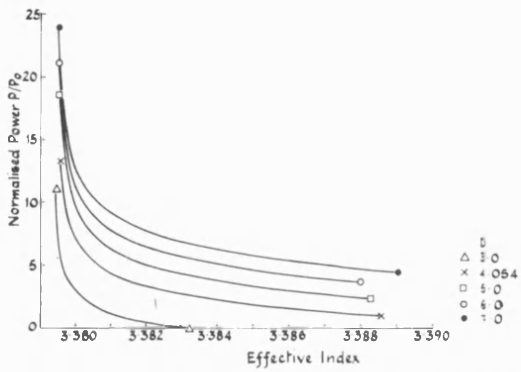

Fig. 7. Normalized power (P/P_0) versus effective index (β/k_0) for various values of the normalized frequency D.

cladding interface will be lost when $2\epsilon_{nl}(0)$ approaches 0.25. This is seen in Fig. 3 where optical fields are shown for $\epsilon_{nl}(0)$ values up to 0.125. Beyond this value, no bound mode solutions were found.

The breakdown in guiding action shown in Fig. 3 indicates that the present structure may be used as an optical limiter. An estimate of the optical power levels at which this behavior may be expected can be made by using a representative value of the nonlinearity factor (α_2) of 10^{-5} cm^2/W [16], [17]. With the optical field focused in a spot of area 1 μm^2, a launched optical power of a few hundred μW will eradicate the guiding action. It is noted that in order to establish the optical limiting properties of the device, it is necessary to perform a calculation of the device behavior beyond the waveguide cutoff found above.

The dependence of the field profile on the normalized frequency D is also of interest. In this case, the optical power at the interfaces are held constant so that the nonlinear dielectric constant steps at the interfaces are also held fixed. In Figs. 5 and 6, $\epsilon_{nl}(0)$ is fixed at 0.1 and D is varied. The resulting field profile of Fig. 5 may be interpreted as being either due to a change of the core layer dimension or else to a change of the operating wavelength. Using the latter interpretation, it should be appreciated that the results given here are appropriate to a large class of structures wherein material composition is chosen to obtain the nonlinear effect at the appropriate wavelength. The corresponding far-field patterns are given in Fig. 6.

Finally, in Fig. 7, the power dependence of the propagation constant for differing normalized frequencies is given. These curves are again of wide application and should be useful as design guides for a class of structures.

V. Conclusions and Discussion

A novel nonlinear waveguide structure capable of implementation in multiquantum well material has been analyzed for the first time. It has been shown that the defocusing nonlinearity associated with the fundamental

absorption edge of semiconductor material imposes a basic design requirement upon the waveguide structure. The results for a specific structure designed for operation at a wavelength of 1.55 μm show a form of optical limiter action which, for representative values of the semiconductor nonlinearity, is found to be operative at about 100 μW of launched optical power.

Practical device implementation of the effects described in this paper will require consideration of the tradeoff which arises between attainable optical nonlinearity and acceptable optical absorption in the structure. In this work, it has been assumed that the operating wavelength is tuned near to but below the material bandgap, with the objective of maximizing the former while minimizing the latter. In circumstances where it is found that constraints on absorption imply that the achievable nonlinearity is relatively small—so that relatively large optical powers are needed to effect the necessary changes in dielectric constant—the implications of the saturation of the nonlinearity would also require consideration.

The requirement of taking into account carrier-density dependence of absorption effects in nonlinear semiconductor waveguides has been stressed by Sarid who has also taken into account diffusion effects [5], [18] and thermal effects [19]. In performing his calculations, Sarid utilized the plasma theory of Banyai and Koch [20] which provides a theoretical framework for performing the required calculations of absorption and nonlinearity. Nevertheless, it seems that some caution may be necessary in developing this approach to obtain precise quantitative estimates of the above tradeoff for the situation assumed in our analysis. We note that it is only very recently that a systematic experimental study of optical nonlinearities in multiquantum-well material been undertaken [21]. Use of the theoretical model has been successfully made to compare to some experiments [22], but a wider comparison would be desirable giving attention, in particular, to effects in the near bandgap range. With that caveat, it is possible to make further calculations of the practical operating conditions of the structure analyzed in the present paper using [20] as the theoretical basis coupled, ideally, with experimental results performed on structures fabricated in the relevant material system.

With respect to saturation effects, there is a requirement to undertake a basic reformulation of the analysis, and in particular to perform more extensive computational studies of optical wave propagation in the structure (also taking into account absorption effects). Such calculations have been reported for waveguides with self-focusing nonlinearities [23] and have been applied in particular to directional couplers [24]. The model for saturation used in these papers has been either that for two-level atomic systems or else a model chosen for mathematical rather than physical reasons [25]. To the best of our knowledge, however, there has been no attempt to include a realistic model of saturation in the theory of a semiconductor waveguide with defocusing nonlinearity.

As with absorption effects, there is a need to obtain relevant experimental results on the basic saturation effect in the material under examination if it is wished to proceed with confidence (with the committment of quite substantial computer resources) to evaluate the effects of saturation (and absorption) on the waveguiding properties. From the device design viewpoint, the use of qualitative models of these effects is of very limited benefit. Rather, there is a need to utilize quantitative data obtained with some precision. It appears that such data are not available at the moment. Since doubts about the basic physical parameters would seriously undermine the value of any computational results in the provision of useful device design criteria, it is not considered appropriate to undertake such large-scale computations. In contrast, within the present paper, we have obtained the waveguiding properties of a novel nonlinear semiconductor waveguide structure with modest computational effort.

Acknowledgment

The authors thank Dr. M. J. Adams and Dr. D. Mace of BTRL for discussions on the work and for detailed comments on the present paper.

References

[1] G. I. Stegeman and C. T. Seaton, "Non-linear integrated optics," *J. Appl. Phys.*, vol. 58, pp. R57–R78, 1986.

[2] V. K. Fedyakin and D. Mihalache, "P-polarised nonlinear surface polaritons in layered structures," *Zeit. Phys. B*, vol. 47, pp. 167–173, 1982.

[3] N. N. Akhmediev, K. O. Boltar, and V. M. Eleonskii, "Dielectric optical waveguide with non-linear susceptibility. Asymmetric refractive index profile," *Opt. Spectrosc. (USSR)*, vol. 53, pp. 654–658, 1982.

[4] P. Li Kam Wa *et al.*, "All-optical multiple quantum well waveguide switch," *Electron. Lett.*, vol. 21, pp. 26–28, 1985.

[5] W. M. Gibbons and D. Sarid, "Model of a non-linear directional coupler in gallium arsenide," *Appl. Phys. Lett.*, vol. 51, pp. 403–405, 1987.

[6] M. Cada, R. C. Gauthier, B. E. Paton, and J. Chrostowski, "Nonlinear guided waves coupled non-linearly in a planar GaAs/GaAlAs multiple quantum well structure," *Appl. Phys. Lett.*, vol. 49, pp. 755–757, 1986.

[7] M. Cada, R. C. Gauthier, B. E. Paton, and J. M. Glinski, "Multiple quantum well coupling element with losses," *Appl. Phys. Lett.*, vol. 51, pp. 713–715, 1987.

[8] A. D. Boardman and P. Egan, "Optically nonlinear waves in thin films," *IEEE J. Quantum Electron.*, vol. QE-22, pp. 319–324, 1986.

[9] See, e.g., R. G. Hunsperger, *Integrated Optics: Theory and Technology*. New York: Springer-Verlag, 1985.

[10] P. F. Byrd and M. D. Friedman, *Handbook of Elliptic Integrals for Engineers and Scientists*. New York: Springer, 1954.

[11] K. Ogusu, "TE waves in a symmetric dielectric slab waveguide with a Kerr-like non-linear permittivity," *Opt. Quantum Electron.*, vol. 19, pp. 65–72, 1987.

[12] S. J. Al-badah and H. A. Jamid, "Guided waves in nonlinear saturable self-focusing thin films," *IEEE J. Quantum Electron.*, vol. QE-23, pp. 1947–1955, 1987.

[13] W. Streifer, D. R. Scifres, and R. D. Burnham, "Optical analysis of multiple-quantum-well lasers," *Appl. Opt.*, vol. 18, pp. 3547–3548, 1979.

[14] M. A. Afromowitz, "Refractive index of $Ga_{1-x}Al_xAs$," *Solid-State Commun.*, vol. 15, pp. 59–63, 1974.

[15] B. Broberg and S. Lindgren, "Refractive index of $In_{1-x}Ga_xAs_yP_{1-y}$ layers and InP in the transparent wavelength region," *J. Appl. Phys.*, vol. 55, pp. 3376–3381, 1984.

[16] A. M. Fox, A. C. Maciel, J. F. Ryan, and M. D. Scott, "Nonlinear optical absorption in bulk GaInAs/InP at room temperature," *Appl. Phys. Lett.*, vol. 50, pp. 398–400, 1987.

[17] D. S. Chemla, D. A. B. Miller, P. W. Smith, A. C. Gossard, and

W. Wiegmann, "Room temperature excitonic nonlinear absorption and refraction in GaAs/AlGaAs multiple quantum well structures," *IEEE J. Quantum Electron.*, vol. QE-20, pp. 265–275, 1984.

[18] W. M. Gibbons and D. Sarid, "Effect of carrier diffusion on the nonlinear response of optical waveguides," *Opt. Lett.*, vol. 12, pp. 564–566, 1987.

[19] D. Sarid and W. M. Gibbons, "Model of a nonlinear guided-wave Mach-Zehnder interferometer in GaAs," presented at Optical Bistability IV, Aussois, France, Mar. 1988, paper FB5.

[20] L. Banyai and S. W. Koch, "A simple theory for the effects of plasma screening on the optical spectra of highly excited semiconductors," *Zeit. Phys. B*, vol. 63, pp. 293–291, 1986.

[21] S. H. Park *et al.*, "Measurements of room temperature band-gap-resonant optical nonlinearities of GaAs/AlGaAs multiple quantum wells and bulk GaAs," *Appl. Phys. Lett.*, vol. 52, pp. 1201–1203, 1988.

[22] S. W. Koch, N. Peyghambarian, and H. M. Gibbs, "Band edge nonlinearities in direct gap semiconductors and their application to optical bistability and optical computing," *J. Appl. Phys.*, vol. 63, pp. R1–R11, 1988.

[23] U. Langbein, F. Lederer, T. Peschel, and H.-E. Ponath, "Nonlinear guided waves in saturable nonlinear media," *Opt. Lett.*, vol. 10, pp. 571–573, 1985; see also E. Caglioti, S. Trillo, S. Wabnitz, and G. I. Stegeman, "Limitations to all-optical switching using nonlinear couplers in the presence of linear and nonlinear absorption and saturation," *J. Opt. Soc. Amer. B*, vol. 5, pp. 472–482, 1988.

[24] G. I. Stegeman, E. Caglioti, S. Trillo, and S. Wabnitz, "Parameter trade-offs in nonlinear directional coplers: Two-level saturable nonlinear media," *Opt. Commun.*, vol. 63, pp. 281–284, 1987.

[25] M. Romangoli and G. I. Stegeman, "Saturation of guided wave index with power in nonlinear planar waveguides," *Opt. Commun.*, vol. 64, pp. 343–346, 1987.

Paul M. Lambkin received the B.Sc. degree in mathematical engineering from Loughborough University of Technology in 1986.

He is currently working towards the Ph.D. degree in the School of Electrical Engineering, University of Bath. His research is concerned with the properties of nonlinear semiconductor optical waveguides.

K. Alan Shore was born in New Tredegar, Wales, on June 11, 1950. He received the B.A. degree in mathematics from Oxford University, England, in 1971 and the Ph.D. degree in applied mathematics from University College, Cardiff, Wales, in 1975. His thesis was concerned with a self-consistent computer model of the double-heterostructure laser.

He spent a year as a Post Doctoral Research Assistant at the Department of Applied Physics and Electronics, UWIST, Cardiff before moving to the Department of Computing there. In 1979 he was appointed as Lecturer in the Department of Electrical Engineering and Electronics, University of Liverpool, England. In October 1983 he became a Lecturer in the School of Electrical Engineering, University of Bath, Bath, where he is now a Senior Lecturer. His research interests have involved semiconductor laser modeling, and in particular, the characterization of twin-stripe lasers. His work has examined the potential of the devices for optical logic, high-speed switching, and optically controlled beam scanning functions. Currently he is concerned with utilizing nonlinear properties of semiconductor lasers for novel device applications of static and dynamic bifurcation phenomena, and also to provide insight into the behavior of nonlinear dynamical systems. He has an active research interest in the design of compact optical spatial switches for optoelectronic integrated circuits and optical interconnects. He is also involved in investigations of the properties of nonlinear waveguides and high-power laser diodes.

Analysis of a nonlinear rib-structure semiconductor optical waveguide

P. M. Lambkin and K. A. Shore

School of Electrical Engineering, University of Bath, Bath BA2 7AY, UK

Received October 11, 1988; accepted December 28, 1988

We report on a technique for the analysis of the modal properties of channel-structure nonlinear-optical waveguides. The method is used to provide the first calculations of semiconductor-based rib-geometry waveguides with defocusing nonlinearity in the core region.

1. INTRODUCTION

With the recognition of the applications potential of nonlinear-optical waveguides,[1] attention has been given to a number of waveguide structures. In particular, three-layer planar (slab) guides have been investigated in several combinations of linear and nonlinear layers. The case of a nonlinear medium bounded by linear media has been treated for both self-focusing and defocusing nonlinearities.[2,3] Practical device implementations of the properties of nonlinear waveguides have been considered in relation to semiconductor waveguides, most notably for directional couplers.[4,5]

In recent work[6,7] we gave consideration to optical waveguides whose properties depend on the defocusing nonlinearity associated with the fundamental absorption edge of semiconductor materials. The large change in absorption that occurs for wavelengths tuned close to the band gap of the semiconductor gives rise, through the Kramers–Kronig relations, to a strong refractive-index nonlinearity. The proposal here is to utilize that effect in a semiconductor structure for which the refractive index of the guiding layer may be tailored to meet specific requirements. It is proposed that the waveguide be implemented in multi-quantum-well (MQW) materials, which, compared with quaternary materials, allow for easier fabrication of prescribed waveguide structures. By appropriate choice of the materials and thicknesses of the well and barrier layers, the refractive index of the MQW layer can be engineered in accordance with the needs of the guide design. Also, because the choice of material determines the absorption edge (at which the nonlinearity is effective), this approach provides the means for developing guiding structures that are nonlinear at chosen wavelengths. It is important to emphasize that although MQW material is considered in this paper, no reliance is made on excitonic effects for obtaining the nonlinearity.

It has been shown[6,7] that a suitable waveguide structure for exploiting the band-edge nonlinearity would be a nonlinear guiding layer bounded by cladding layers that are nonabsorbing and hence linear at the operating wavelength. An analysis of TE modes in a planar waveguide structure on the basis of the above concept was given recently.[7] In this paper the analysis is extended to provide the first reported description of two-dimensional guiding action in such a nonlinear waveguide. The technique of analysis used is of quite general application but is applied here to a rib-guide structure. The choice of this structure is motivated by practical considerations and, in particular, with regard to ease of fabrication.

Practical device implementation of the effects described in this paper will require consideration of the trade-off that arises between attainable optical nonlinearity and acceptable optical absorption in the structure. In this paper we assume that the operating wavelength is tuned to, but below, the material band gap with the objective of maximizing the former while minimizing the latter. In circumstances under which we find that constraints on absorption imply that the achievable nonlinearity is relatively small—so that relatively large optical powers are needed to effect the necessary changes in dielectric constant—the implications of the saturation of the nonlinearity would also require consideration.

The requirement of taking into account carrier-density dependence of absorption effects in nonlinear semiconductor waveguides has been stressed by Sarid, who has also taken into account diffusion effects[5,8] and thermal effects.[9] In performing his calculations, Sarid utilized the plasma theory of Banyai and Koch,[10] which provides a theoretical framework for performing the required calculations of absorption and nonlinearity. Nevertheless it seems that some caution may be necessary in developing this approach to obtain precise quantitative estimates of the above trade-off for the situation assumed in our analysis. We note that it was only recently that a systematic experimental study of optical nonlinearities in MQW materials was undertaken.[11] The theoretical model has been used successfully to compare with some experiments,[12] but a more general comparison would be desirable, giving attention, in particular, to effects in the near band-gap range. With that caveat it is possible to make further calculations of the practical operating conditions of the structure analyzed in the present paper by using Ref. 10 as the theoretical basis, coupled, ideally, with experimental results performed on structures fabricated in the relevant material system.

In respect to saturation effects, there is a requirement to undertake a basic reformulation of the analysis and, in particular, to perform more extensive computational studies of optical wave propagation in the structure (also taking into account absorption effects). Such calculations have been reported for waveguides with self-focusing nonlinearities[13]

0740-3224/89/040669-06$02.00

and have been applied in particular to directional couplers.[14] The model for saturation used in these papers has been either that for two-level atomic systems or that for a model chosen for mathematical rather than physical reasons.[15] To the best of our knowledge, however, there has been no attempt to include a realistic model of saturation in the theory of a semiconductor waveguide with defocusing nonlinearity.

As with absorption effects, there is a need to obtain relevant experimental results on the basic saturation effect in the material under examination if we wish to proceed with confidence (with the commitment of substantial computer resources) to evaluate the effects of saturation (and absorption) on the waveguiding properties. From the device design viewpoint, the use of qualitative models of these effects is of limited benefit. Rather, there is a need to utilize quantitative data that are obtained with some precision. It appears that such data are not available at the moment. Because doubts about the basic physical parameters would seriously undermine the value of any computational results in the provision of useful device design criteria, it is not considered appropriate to undertake such large-scale computations. In contrast, our approach has been to obtain the waveguiding properties of nonlinear semiconductor waveguide structures with modest computational effort.

2. ANALYSIS

In this section we describe a technique for the modal analysis of channel-structure optical waveguides with a nonlinear core region and linear cladding layers. The only previous consideration of two-dimensional guiding behavior in rectangular-geometry nonlinear waveguides, to our knowledge, has been concerned with a structure with a nonlinear substrate.[16,17] The rib-guide geometry, considered as a specific example in our research, is illustrated in Fig. 1, where coordinate axes and guide dimensions are defined. In the calculations described here the waveguide dimensions are chosen to ensure (low-power) monomode operation at the operating wavelength. For a given rib width w and fixed shoulder thickness d, the maximum rib height, t, that is compatible with monomode operation is chosen to provide the strongest possible channel-guide action. We note that the defocusing nature of the nonlinearity provides a natural fabricational tolerance in this respect: the preferential reduction of the effective index under the rib with increased optical power, in fact, permits wider rib structures to remain monomode.

It is well known that the solution of rectangular geometry waveguides is difficult and that, even in the linear case, approximate methods are required.[18] For nonlinear waveguides it is, *ipso facto*, to be expected that such approximate techniques must be adopted. The essence of the present method is the combination of solutions of a y-direction nonlinear guide and an x-direction linear guide within an effective index approximation to the two-dimensional guiding behavior.

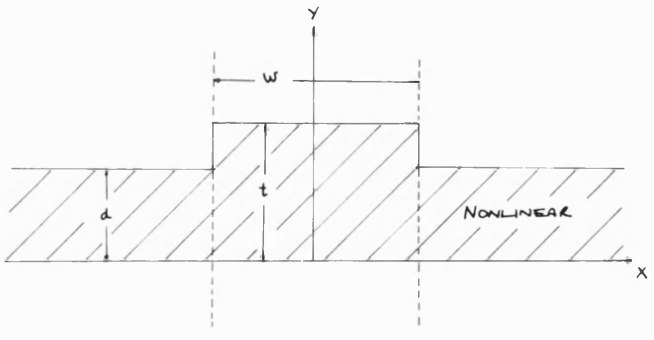

Fig. 1. Rib-guide structure.

In the spirit of the effective index approximation, solutions to the y-direction guide with nonlinear core and linear substrate and cover layers are first obtained for a number of regions along the x direction. The calculated effective indices of these regions are then used to define a *linear* x-direction waveguide whose solution may easily be obtained.

The theory is developed for modes propagating as $\exp[j(\beta z - \omega t)]$, where $j = \sqrt{-1}$.

In the solution of the (nonlinear) y-direction waveguide, exponentially decaying (bound-mode) fields are assumed in the cladding layers. In the nonlinear core the optical field is found from a wave equation in the form

$$\frac{d^2E}{dx^2} + [k^2 + (k_0^2\alpha E^2)]E = 0. \tag{1}$$

Here

$$k^2 = \beta^2 - k_0^2\epsilon, \tag{2}$$

with β the longitudinal propagation constant, k_0 the free-space wave number, and ϵ the (low-power) dielectric constant in the nonlinear region.

Use will also be made of a normalized waveguide dimension T defined by

$$T = k_0 t. \tag{3}$$

Following Boardman and Egan,[19] a first integral of Eq. (1) is obtained as

$$(dE/dx)^2 + (k^2 + \tfrac{1}{2}k_0^2\alpha E^2)E^2 = C_2. \tag{4}$$

For the guiding structure of interest, with a defocusing nonlinearity ($\alpha < 0$), appropriate values of the boundary field intensities imply that the integration constant C_2 is positive, and hence the field in the guiding layer is given by

$$E = p\ \mathrm{cn}[q(x + x_0), m]. \tag{5}$$

Here cn is a Jacobian elliptic cosine function of modulus m, and x_0 is an integration constant. We also have

$$m^2 = (q^2 - k^2)/2q^2 \tag{6}$$

and

$$p^2 = (q^2 - k^2)/k_0^2\alpha, \tag{7}$$

with

$$q = (2k_0^2\alpha C_2 + k^4)^{1/4}. \tag{8}$$

An eigenvalue equation for the modal solution may thus be derived and, with the aid of transformations, can be solved easily by a semianalytical method.[6,7,19]

A convenient representation of the results may be made in terms of a normalized optical power P_0, defined in terms of the nonlinear dielectric constant change: $P_0 = \alpha|E_0|^2/2$. Here E_0 is the field amplitude at the interface between the linear substrate and the nonlinear guiding layer.

3. SELF-CONSISTENT CALCULATIONS

In nonlinear guides it is, of course, necessary to specify the optical-field intensity at which solutions are being sought. In planar structures it is sufficient to define the optical field by using the optical intensity at the interface between the nonlinear core and the linear substrate cladding.[19] In analyzing channel-guide structures it is necessary to prescribe the intensity in a self-consistent fashion. Here this is done by using the effective index analysis to calculate the x-direction optical-field distribution.

The basis for this approach may be seen from a three-region model for the x-direction with nonlinear (y-direction) guides taken in the rib and two shoulder regions. As noted above, the waveguide is considered to be linear in the x direction. Therefore it is a straightforward matter to calculate the proportion of the optical intensity confined to any of the three regions. The proportion confined in the region under the rib is conventionally termed the confinement factor.[18] Because the structure considered here is a two-dimensional waveguide, we use the terminology x-direction optical confinement factor to identify this quantity unambiguously. To calculate the y dependence of the optical field, we perform an integration of the nonlinear wave equation in each of the three x-direction regions. For this purpose it is necessary to prescribe the optical intensity at one linear–nonlinear interface. The interface between the linear substrate and the nonlinear guiding layer is a convenient place to make the required prescription of the optical-field intensity. The actual values of the interface optical intensities in the three regions may in a first iteration be weighted in accordance with the x-direction optical confinement factor found by assuming that the structure is linear. In subsequent iterations the effective modal indices found in the nonlinear regions are used to define a (symmetric) three-layer linear (x-direction) guide, for which the confinement factor may easily be found. The computed confinement factors are then used to weight the interface optical-field intensities required for a recalculation of the (y-direction) nonlinear guiding properties of the rib and shoulder regions. These calculations yield revised values of the effective modal indices of the three regions, which, when used in the solution of the linear x-direction three-layer waveguide, in turn produce a revised value of the x-direction confinement factor. These calculations are iterated until convergence to a self-consistent solution is obtained.

The more general method adopted here is to extend the above self-consistent calculations to the N-layer x-direction model shown in Fig. 2. For this method the interface optical intensities in the N layers are obtained directly from the x-direction optical intensity distribution rather than from the confinement factor. In the N layers the y-direction nonlinear waveguides are solved in a semianalytical way, as indicated in Section 2; hence an efficient computer code is obtained. A typical run time is 2 sec on a Cifer Club personal computer.

The technique described here is capable of straightforward extension to multilayer structures in the y direction (including the possibility of other nonlinear layers) and also of taking into account polarization effects.

Because of the defocusing nature of the nonlinearity in the semiconductor waveguides under consideration, guiding action may be eradicated for optical power beyond a characteristic threshold value. The issue of loss of guiding in the transverse direction (y direction) has been treated elsewhere.[6,7] In channel-guide structures the possibility of breakdown of the guide in the lateral direction (x direction) also arises, and in this respect it is important to obtain a measure of the effectiveness of the lateral guide. For the particular structure under examination here we use the x-direction optical-field confinement factor under the rib as a measure of the strength of the lateral guide and also as a benchmark of the accuracy of the solution technique.

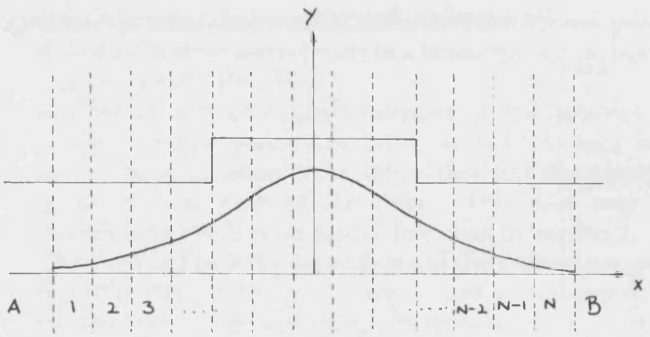

Fig. 2. Self-consistent multilayer (N-layer model).

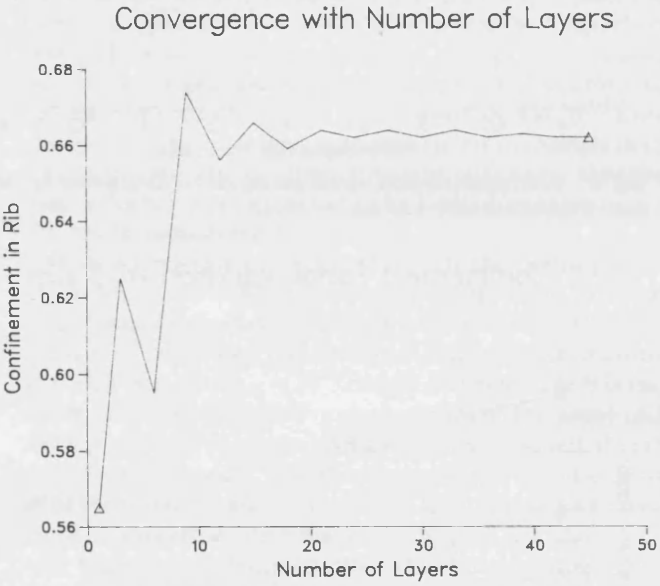

Fig. 3. Optical confinement factor versus layer number (N).

As a means of assessing the accuracy of the technique, we show in Fig. 3 how, at fixed optical power, computed values of the confinement factor depend on the number of x-direction layers (defined by the integer N) used in the analysis. It can be seen that a 10% fluctuation in the calculated value occurs for small numbers of layers ($N < 10$), and then convergence is obtained for $N > 30$. Thus care must be taken to ensure that an appropriate value of N is used in the simulations.

4. RESULTS

Calculations have been performed for a waveguide fabricated in GaInAs/AlInAs MQW material lattice matched to InP. The core guiding layer was assumed to consist of 120-Å

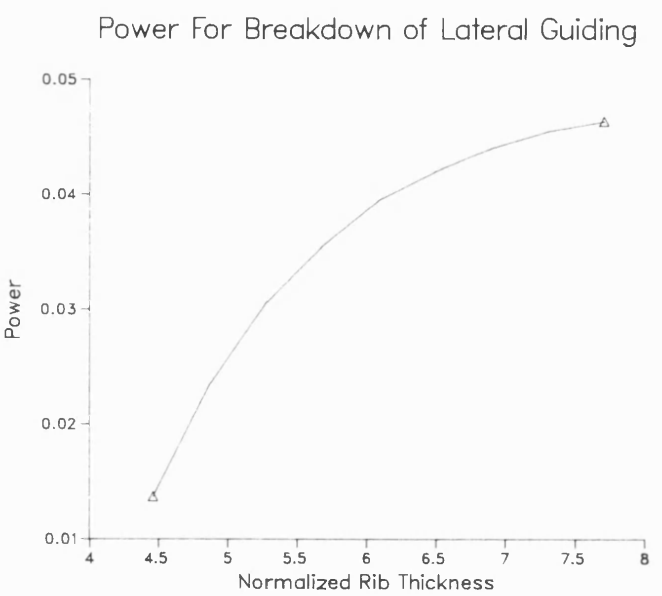

Fig. 4. Confinement factor versus normalized optical power for the case of linear shoulder regions.

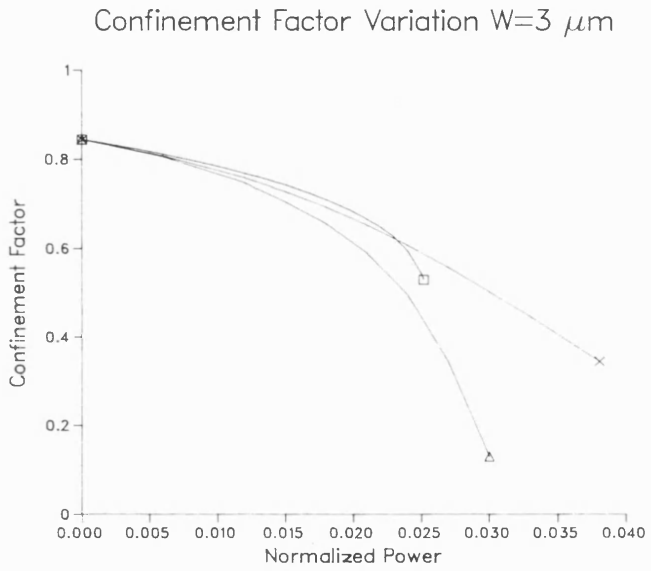

Fig. 5. Confinement factor versus normalized optical power for 3-μm-wide rib, calculated by using (Δ) $N = 1$, ($\times$) $N = 3$, ($\square$) $N = 45$.

GaInAs wells and 30-Å AlInAs barriers; the cladding layer was taken to be formed with 60-Å GaInAs wells and 30-Å AlInAs wells. The structure is designed so that the band-edge nonlinearity is obtained at an operating wavelength of 1.55 μm.

The dielectric constant of the core layer at this wavelength was estimated, using a weighted mean of the dielectric constants of the constituent ternary materials,[20,21] to be 11.76.[7] Similarly, the dielectric constant of the cladding layer was estimated to be 11.42. The capping layer is assumed to be air, so that its dielectric constant is unity. The resulting waveguide structure is thus strongly asymmetric in the y direction.

With the above solution technique available, it is now possible to address the optical power dependence of the modal properties of the structure. In particular, it is possible to attempt to make an estimate of the threshold optical power that may cause eradication of the lateral (x-direction) guiding action.

The simplest method is to consider rib-guide structures for which at low optical powers the field is laterally well confined to the waveguide channel under the rib (one-layer model).[22] In these circumstances, only the change of the effective index under the rib needs to be taken into account. Such a model would also apply in the case of a rib structure with linear shoulder regions. As the ridge thickness t is increased, the effective index under the ridge tends to the refractive index of the guiding layer; consequently the threshold optical power required to eradicate the lateral guiding saturates. This effect is shown in Fig. 4, where the normalized threshold optical power is given as a function of normalized ridge thickness (T). For typical semiconductor

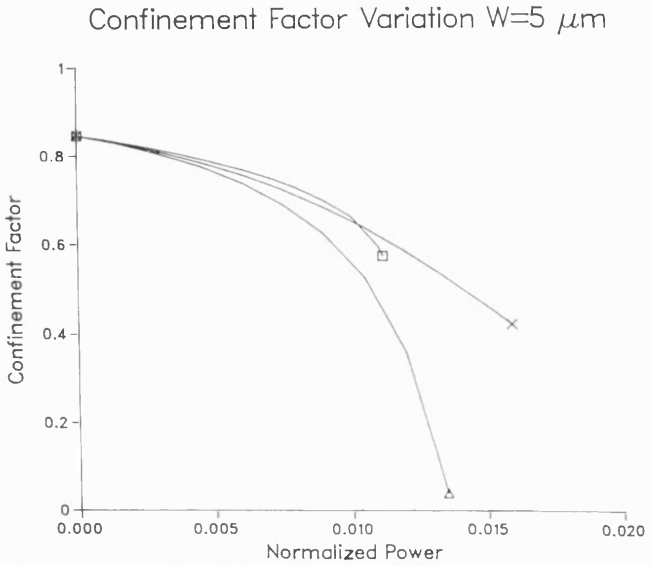

Fig. 6. Confinement factor versus normalized optical power for 5-μm-wide rib, calculated by using (Δ) $N = 1$, ($\times$) $N = 3$, ($\square$) $N = 45$.

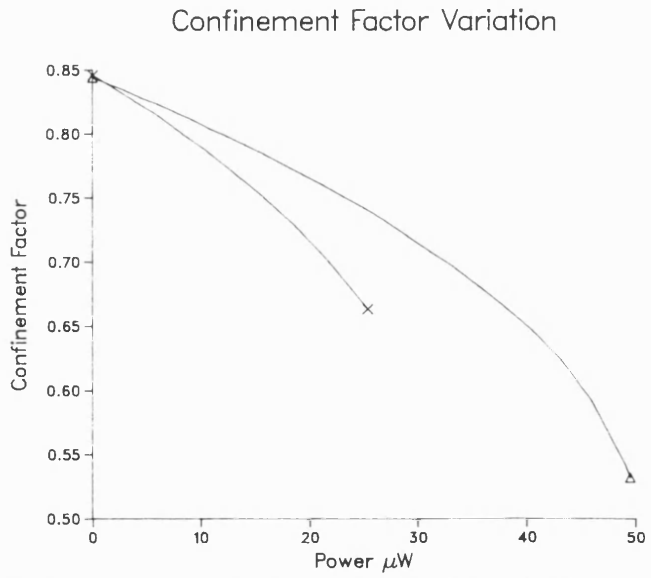

Fig. 7. Confinement factor versus total optical power for rib guides with widths of (Δ) 3 and ($\times$) 5 μm.

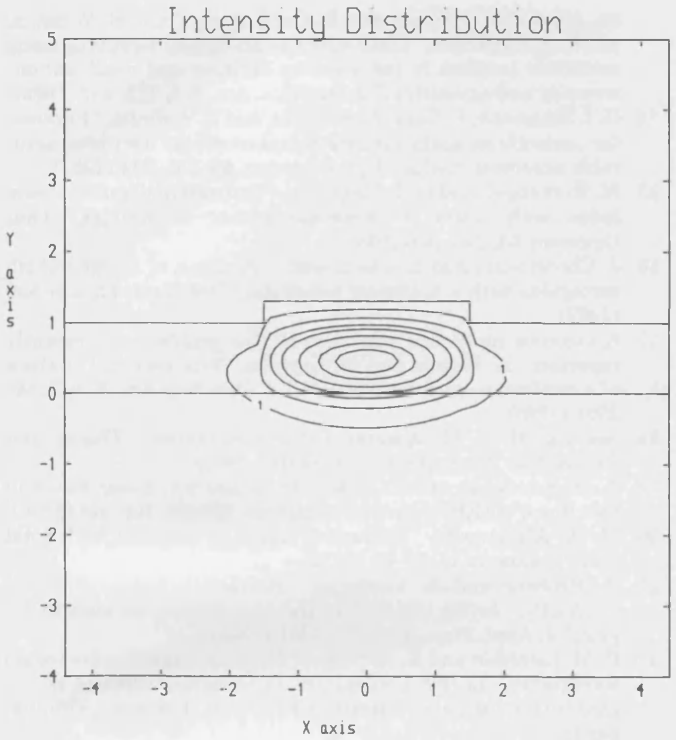

Fig. 8. Optical field intensity contours for 3-μm-wide rib guide. (The axis labels are in units of micrometers.) The intensities are normalized to that at the midpoint of the lower interface ($x = 0; y = 0$). The total optical power in the guide is 0.35 μW.

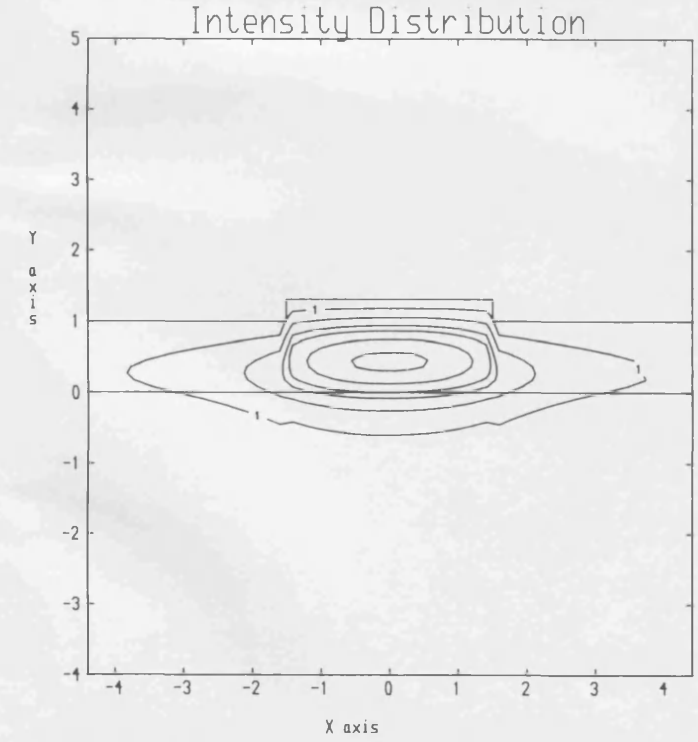

Fig. 9. Optical field intensity contours for 3-μm-wide rib guide. (The axis labels are in units of micrometers.) The intensities are normalized to that at the midpoint of the lower interface ($x = 0; y = 0$). The total optical power in the guide is 49 μW.

nonlinearity parameters,[23,24] the threshold optical-power value at saturation corresponds to a launched optical power of approximately 100 μW.

To obtain a more realistic estimate of the behavior of nonlinear channel-guide structures, we need to take into account the penetration of the optical field into the shoulder regions on both sides of the ridge. This then may be achieved with the N-layer model described in Section 3.

We show in Fig. 5 the dependence of the x-direction optical confinement factor on the normalized optical power, as computed for a 3-μm-wide rib-guide structure by using $N = 1$, $N = 3$, and $N = 45$. The penetration of the optical field into the shoulder regions is seen to change the behavior of the structure markedly. As the ridge width w increases, low-power monomode operation implies a smaller ridge thickness and hence a weaker x-direction guide. Thus it is expected that lower optical powers are required to affect the optical confinement. This is apparent in Fig. 6. These changes in optical confinement correspond to changes in the dielectric constant of approximately 0.03, and therefore these effects are not expected to be limited by saturation of the optical nonlinearity.

Of direct relevance to applications are the results given in Fig. 7, which show the optical confinement factor as a function of total integrated power in the waveguide. Calculation of the total integrated power requires the use of an appropriate value of α. Here $\alpha = 10^{-5}$ cm^2/W is taken. For this case, we can see that launched optical powers of the order of 10 μW are required to bring about a significant reduction in the optical confinement. The greater sensitivity to optical power of the wider rib structure follows from the weaker lateral guide in this structure (smaller rib height), which is necessary to meet the design criterion of low-power single-mode operation. Contour plots of the optical field intensity are given for low optical power in Fig. 8 and for a launched optical power of $\sim$50 μW in Fig. 9. The change in the field profile with increasing power is clearly seen.

CONCLUSION

In summary, a technique for the analysis of channel-structure nonlinear-optical waveguides has been successfully applied to semiconductor rib-guide structures. The results obtained serve to underline the importance of a careful formulation of solution techniques for such waveguides. In future research the analysis of other channel-guide structures will be considered by using the method described here.

ACKNOWLEDGMENTS

This research was carried out under a United Kingdom Science and Engineering Research Council Co-operative Award in Science and Engineering with British Telecom Research Laboratories. We thank M. J. Adams and D. Mace for helpful discussions on the research. We also thank D. Mihalache (Bucharest, Romania) for bringing Ref. 24 to our attention.

REFERENCES

1. G. I. Stegeman and C. T. Seaton, "Non-linear integrated optics," J. Appl. Phys. **58**, R57–R78 (1986).

2. V. K. Fedyakin and D. Mihalache, "*P*-polarized nonlinear surface polarizations in layered structures," Z. Phys. B **47,** 167–173 (1982).
3. N. N. Akhmediev, K. O. Boltar, and V. M. Eleonskii, "Dielectric optical waveguide with non-linear susceptibility. Asymmetric refractive index profile," Opt. Spectrosc. (USSR) **53,** 654–658 (1982).
4. P. Li Kam Wa, J. E. Stitch, N. J. Mason, J. S. Roberts, and P. N. Robson, "All-optical multiple quantum well waveguide switch," Electron. Lett. **21,** 26–28 (1985).
5. W. M. Gibbons and D. Sarid, "Model of a non-linear directional coupler in gallium arsenide," Appl. Phys. Lett. **51,** 403–405 (1987).
6. P. Lambkin and K. A. Shore, "Non-linear optical waveguiding in semiconductors," in *Optical Bistability IV,* W. Firth, N. Peyghambarian, and A. Tallet, eds., J. Phys. (Paris) **49,** 293–296 (1988).
7. P. M. Lambkin and K. A. Shore, "Asymmetric semiconductor waveguide with defocussing nonlinearity," IEEE J. Quantum Electron. **QE-24,** 2046–2051 (1988).
8. W. M. Gibbons and D. Sarid, "Effect of carrier diffusion on the nonlinear response of optical waveguides," Opt. Lett. **12,** 564–566 (1987).
9. D. Sarid and W. M. Gibbons, "Model of a nonlinear guided-wave Mach–Zehnder interferometer in GaAs," in *Optical Bistability IV,* W. Firth, N. Peyghambarian, and A. Tallet, eds. J. Phys. (Paris) **49,** 297–300 (1988).
10. L. Banyai and S. W. Koch, "A simple theory for the effects of plasma screening on the optical spectra of highly excited semiconductors," Z. Phys. B **63,** 283–291 (1986).
11. S. H. Park, J. F. Morhange, A. D. Jeffery, R. A. Morgan, A. Chavez-Pirson, H. M. Gibbs, S. W. Koch, N. Peyghambarian, M. Derstine, A. C. Gossard, J. H. English, and W. Wiegmann, "Measurement of room temperature band-gap-resonant optical nonlinearities of GaAs/AlGaAs multiple quantum wells and bulk GaAs," Appl. Phys. Lett. **52,** 1201–1203 (1988).
12. S. W. Koch, N. Peyghambarian, and H. M. Gibbs, "Band edge nonlinearities in direct gap semiconductors and their application to optical bistability and optical computing," J. Appl. Phys. **63,** R1–R11 (1988).
13. U. Langbein, F. Lederer, T. Peschel, and H.-E. Ponath, "Nonlinear guided waves in saturable nonlinear media," Opt. Lett. **10,** 571–573 (1985); see also E. Caglioti, S. Trillo, S. Wabnitz, and G. I. Stegeman, "Limitations to all-optical switching using nonlinear couplers in the presence of linear and nonlinear absorption and saturation," J. Opt. Soc. Am. B **5,** 472–482 (1988).
14. G. I. Stegeman, E. Caglioti, S. Trillo, and S. Wabnitz, "Parameter tradeoffs in nonlinear directional couplers: two-level saturable nonlinear media," Opt. Commun. **63,** 281–284 (1987).
15. M. Romangoli and G. I. Stegeman, "Saturation of guided wave index with power in nonlinear planar waveguides," Opt. Commun. **64,** 343–346 (1987).
16. J. Chrostowski and S. Chelkowski, "Analysis of an optical rib waveguide with a nonlinear substrate," Opt. Lett. **12,** 538–530 (1987).
17. A vigorous numerical approach to this problem was recently reported: K. Hayata and M. Koshiba, "Full vectorial analysis of a nonlinear-optical waveguide," J. Opt. Soc. Am. B **5,** 2494–2501 (1988).
18. See, e.g., R. G. Hunsperger, *Integrated Optics: Theory and Technology* (Springer-Verlag, Berlin, 1985).
19. A. D. Boardman and P. Egan, "Optically non-linear waves in thin films," IEEE J. Quantum Electron. **QE-22,** 319–324 (1986).
20. M. A. Afromowitz, "Refractive index of $Ga_{1-x}Al_xAs$," Solid State Commun. **15,** 59–63 (1974).
21. B. Broberg and S. Lindgren, "Refractive index of $In_{1-x}Ga_xAs_yP_{1-y}$ layers and InP in the transparent wavelength region," J. Appl. Phys. **55,** 3376–3381 (1984).
22. P. M. Lambkin and K. A. Shore, "Nonlinear semiconductor rib waveguides," in *IEE Colloquium on Nonlinear Optical Waveguides* (Institution of Electrical Engineers, London, 1988), paper 12.
23. A. M. Fox, A. C. Maciel, J. F. Ryan, and M. D. Scott, "Nonlinear optical absorption in bulk GaInAs/InP at room temperature," Appl. Phys. Lett. **50,** 398–400 (1987).
24. D. S. Chemla, D. A. B. Miller, P. W. Smith, A. C. Gossard, and W. Wiegmann, "Room temperature excitonic non-linear absorption and refraction in GaAs/AlGaAs multiple quantum well structures," IEEE J. Quantum Electron. **QE-20,** 265–275 (1984).
25. N. N. Akhmediev, R. F. Nabiev, and Yu. M. Popov, "Stripe nonlinear surface waves," Solid State Commun. **66,** 981–985 (1988).